PUBLS. INST. GEOPHYS. POL. ACAD. SC., D-73 (412), 2009

Editorial Note

The present publication contains the contributions presented during the Jubilee Session organized to commemorate the ninetieth birthday of Stanisław Michnowski, many-year leader of the atmospheric electricity group at the Institute of Geophysics, the pioneer of atmospheric electricity and thunderstorm research in Poland, and world-renown expert in this field. The Jubilee Session was held in Warsaw on November 20, 2008.

The publication consists of two parts. The first, introductory part is thematically related to the Jubilee and contains addresses and recollections of people engaged in scientific collaboration with Stanisław Michnowski. This is followed by a set of papers presenting new developments in atmospheric electricity achieved by the scientists from the Institute of Geophysics and other institutions. Stanisław Michnowski himself is a co-author of one of the papers, and his inspiration and advice had an impact on many other.

Stanisław Michnowski during the Jubilee Ceremony at the Institute of Geophysics.

PUBLS. INST. GEOPHYS. POL. ACAD. SC., D-73 (412), 2009

Preface

Roman TEISSEYRE

Institute of Geophysics, Polish Academy of Sciences
Księcia Janusza 64, 01-452, Warszawa, Poland

The present monographic volume is a consecutive collection of papers dealing with atmospheric electricity that has been published, along with the 60-year Świder Observatory Atmospheric Electricity Yearbooks, in the frame of the Publications of the Institute of Geophysics, Polish Academy of Sciences.

Our new monograph related to atmospheric electricity has a specific character, as it is an output of the Jubilee Session to commemorate the ninetieth birthday of Stanisław Michnowski – the pioneer and leader of modern research in some branches of atmospheric electricity and lightning investigations. He organized the atmospheric electricity laboratory of our Institute over 60 years ago, and was its many-year head. He is well know in the scientific world and highly appreciated by the international community of atmospheric electricity researchers.

Professor Stanisław Michnowski during his 90th Birthday Ceremony, in a discussion with Professors Andrzej Wernik and Zbigniew Kłos from the Space Research Center, Polish Academy of Sciences.

His scientific results were very important and innovative, as documented by over 100 publications, a significant part in journals of high standard. Let me quote Professor Lothar Ruhnke, former President of the International Commission on Atmospheric Electricity: "Michnowski has significantly contributed to the study of the effect of solar wind and magnetic variations on the global circuit. He also wrote a significant paper on initiation of lightning in clouds."

I would like to especially point out a number of papers related to his research in the frame of our scientific expedition to Vietnam during the International Geophysical Year 1957-58; Stanisław Michnowski has organized continuous observations and recordings of the electric field at the stations Cha-Pa and Phu-Lien established there in a frame of cooperative Polish-Vietnamese geophysical program. He has continued this scientific cooperation with the Vietnamese researchers during almost 50 years!

Many of his results were presented at important international meetings over the world. He organized the International Workshop on Global Atmospheric Electricity Measurements held in Poland in 1989, and contributed to organization of the International Conference on Atmospheric Electricity in St. Petersburg, Russia. He was also a pioneer of researches on the electric atmospheric precursors of earthquakes in our Institute.

Last but not least, I have to point out his important personal contribution to the resistance against the Nazis occupation of Poland during the II World War.

In spite of his ninety years of age, he is a very active and hard working scientist, full of plans and ideas for future research, so we are looking forward to his next contributions.

PUBLS. INST. GEOPHYS. POL. ACAD. SC., D-73 (412), 2009

Recollections, Congratulations and Wishes on the Occasion of Stanisław Michnowski's Jubilee

Address at the Jubilee Ceremony

Zdobysław FLISOWSKI

Warsaw University of Technology,
Department of High Voltage Engineering and Electrical Apparatus
Koszykowa 75, 00-662 Warsaw, Poland

Dear Mr. Stanislaus, Dear Mr. Director, Dear Sirs!

Please accept my sincere thankfulness for the invitation to this nice and very important ceremony. I am extremely honoured and very glad to be here. It is not only my great pleasure, but also a best opportunity for me to extend my warmest congratulations on such splendid 90th anniversary of the birth and to express the best wishes for a happy future, good health and great satisfaction to you, Mr. Stanislaus. I join you with all my heart. Acting in accordance with the practice of jubilee ceremonies I try to reach for some recollections concerning your very rich past and interesting experiences. Some events and facts connected mainly with your patriotic and scientific activity have been kept strongly in my mind.

From the very beginning of our acquaintance, the silhouette of Mr. Stanislaus Michnowski has been associated in my consciousness with his unusual patriotism on the one hand and with his great professional activity on the other.

During the Second World War he was strongly engaged into the conspiracy activity of the resistance movement. Together with future outstanding Professor S. Bernas he took part in many serious and successful actions against the occupation of our country.

After the war he came back to his studies undertaken previously in the Warsaw University of Technology. He majored in high voltage engineering and entered into close cooperation with famous Professor J.L. Jakubowski, locating his own scientific interest in the lightning phenomena and then in physics of the atmosphere.

The beginnings of our professional contacts go back to the sixties. They have been connected with registration of lightning discharges by means of the so-called

CIGRE counters. Thanks to foreign contacts of Professor Jakubowski, making it possible to take advantage of the concept and help of Swedish experts, and thanks to meaningful participation of Dr. S. Michnowski, the counters have been installed also in Poland. However, two essential scientific problems connected with their operational use had to be solved:

- the problem of sensitivity and functioning reach,
- the problem of selectivity in registration of cloud-to-ground discharges.

Dr. Michnowski engaged himself very seriously into solution of these problems.The opening of a new investigation centre in this time (it was the year 1965), namely the Central Geophysical Observatory in Belsk, was a favourable circumstance for such a task. Investigations have been performed both in this Observatory as well as in the Geophysical Observatory in Świder, where Dr. Michnowski conducted scientific activity in atmospheric electricity. The results of his investigations on CIGRE counters brought measurable effects, namely:

- the relation between the number of cloud-to-ground flashes and the entire number of lightning discharges has been established,
- the calibration of counters has been performed and their sensitivity together with functioning reach have been determined,
- the reliability of counting of lightning flashes has been obtained.

Some research related to these results has been connected with thesis of doctor student from Vietnam, Mr. Nguyen Manh Duc, who performed investigations under tutorial of Professor Manczarski and with a very effective help of Dr Michnowski.

His investigations from the area of atmospheric electricity have been concentrated, among other things, on the registration of changes of electric and magnetic fields as well as the currents at the ground level. They brought also meaningful effects. Achievements of the Researcher in this area are enormous and valuable, especially for the assessment of electromagnetic interferences originated in lightning discharges and for the improvement of our knowledge on characteristics describing the phenomena associated with these discharges.

Professor Michnowski has been involved in intense cooperation with other domestic and foreign scientific centres as well as their outstanding representatives, participated in numerous international seminars and symposiums, and organized domestic seminaries with participation of foreign experts.

Professor Michnowski is an active member of Polish Committee on Lightning Protection (PCLP) and one of its main upholders from very beginning of its existence. His participation in the PCLP activity is very priceless.

He contributed distinctly to the enrichment of knowledge on lightning discharges and to the credibility of their data for engineering applications and by it − to the development of entire lightning protection domain. Thank you for it Mr. Stanislaus and please accept our best wishes for the good health and great satisfaction in further creative scientific activity.

PUBLS. INST. GEOPHYS. POL. ACAD. SC., D-73 (412), 2009

Eighty Years of Fair-Weather Atmospheric Electricity Monitoring in Poland

Anna DZIEMBOWSKA

Institute of Geophysics, Polish Academy of Sciences
Księcia Janusza 64, 01-452, Warszawa, Poland

Abstract

The aim of this note is to draw greater attention to the fact that the Institute of Geophysics is in possession of atmospheric electricity measurement results from Świder for about 80-year period. The data are reliable and of good quality owing to the efforts of Stanisław Warzecha, head of the Świder Geophysical Observatory, and Stanisław Michnowski, head of the atmospheric electricity group at the Institute. With a view to the global climate changes, such materials may provide valuable background for various studies.

Systematic atmospheric electricity observations were begun in Poland already in the first half of the XX century. The electric field measurements at the Geophysical Observatory at Świder, presently named the S. Kalinowski Geophysical Observatory, have been carried out since 1929 until the outbreak of the Second World War. Even earlier, in 1924, an atmospheric-electricity station has been in operation at the Agricultural University in Poznań, but it also terminated its activity in 1939.

After the Second World War, Świder was the only place in Poland that resumed the atmospheric electricity observations. When the Institute of Geophysics, Polish Academy of Sciences, was established in 1952, the Świder Observatory became its main observational facility. Soon afterwards, works on updating the atmospheric electricity station were initiated by two young and energetic scientists, Stanisław Michnowski, and Stanisław Warzecha, who jointly organized the modern, as for those times, atmospheric electricity station. Stanisław Michnowski soon became head of the atmospheric electricity group at the Institute, while Stanisław Warzecha became the head of the Świder station and then of the whole observatory; he assembled and tested the necessary equipment, to a large extent of his own make. Owing to his diligence, thoroughness, and experimental talent, even the very early data are of excellent quality.

Fig. 1. Mrs Zofia Kalinowska, Stanisław Michnowski, and Stanisław Warzecha on the premises of the S. Kalinowski Geophysical Observatory at Świder in the 1960s.

The scope of measurements, which were initially restricted to the electric field and basic weather station, has soon expanded to include other parameters, such as air conductivity and the number of condensation nuclei. The nearby Atomic Energy Institute at Świerk provided the radioactivity monitoring. Up to now, the Świder Observatory has collected a unique, vast material concerning the potential gradient measurements since 1948, supplemented by meteorological observations. Some atmospheric electricity data are also available from the Central Geophysical Observatory at Belsk (measurements in the late 1960s).

The yearbooks with the results of Świder observations, covering the whole 60-year period, have been published and are still available from the Editorial Office of the Institute. In 2006, we resigned from publishing printed editions, making the data accessible from the Institute's webpage.

From the very beginning, the materials served as a basis for numerous studies on secular trends and effects of meteorological factors on atmospheric electricity parameters. Out of those early papers, we may quote, for example, the study of the effect of fallout (Gadomski 1964), or the effect of fog (Jaśkowska 1967). The first assessments of long-term variations in electric parameters in relation to natural (solar activity) and anthropogenic (aerosol, radioactive debris) factors, and statistical analyses of local and global trends have been made by Warzecha (1991b).

Of particular importance turned out to be the observations following the nuclear power plant incident at Chernobyl. Warzecha (1991a) describes the immediate response of atmospheric-electric parameters and noted that the electric conductivity measurements may serve as a relatively simple tool for radioactive hazard monitoring.

At present, the measurements at the Geophysical Observatory at Świder include: the electric field strength, electrical conductivity of both polarities, vertical current density, aerosol concentration, radioactive and chemical pollution, as well as meteorological observations of temperature, humidity, precipitation, wind, and cloudiness. A

comprehensive analysis of the atmospheric electricity parameters versus meteorological factors over the 35 year period (1965-2000) was made by Kubicki (2007). The latest evaluations of long-term variations of the electric field, electric conductivity of air and aerosol concentration at Świder observatory, until the year 2007 are shown in Fig. 4 (taken from Kubicki, 2008).

Fig. 2. Winter view on the atmospheric electricity sensors and meteorological station at Świder.

Fig. 3. Field-mill for the electric field strength measurement at Świder.

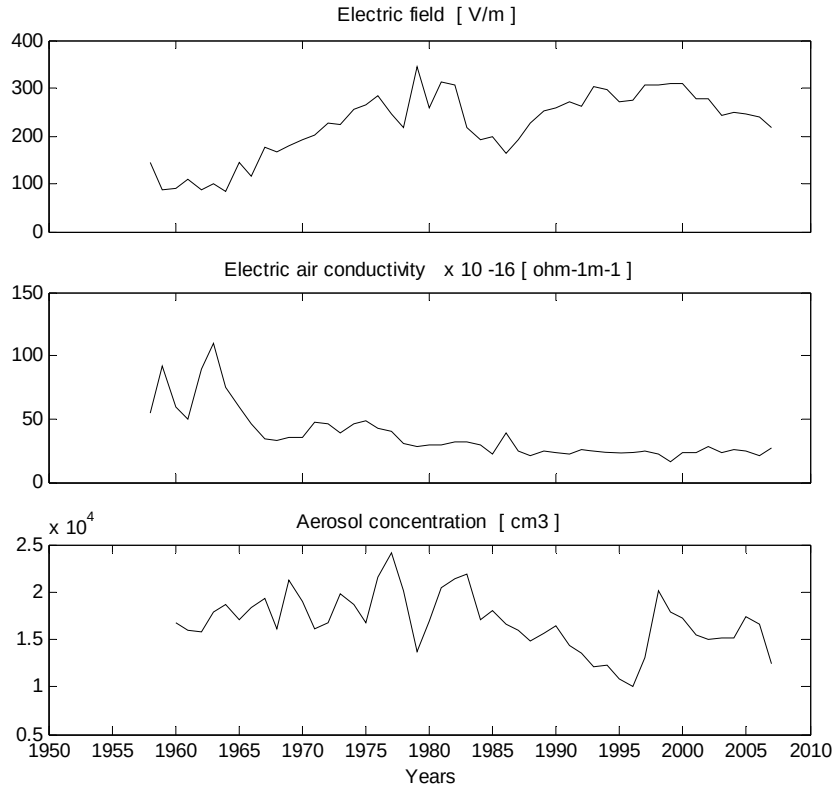

Fig. 4. Long-term variations of the electric field, electric conductivity of air and aerosol concentration at Świder Observatory.

Along with the Świder station, the Institute of Geophysics has put into operation an atmospheric electricity station in the arctic region. It is located in Hornsund, Spitsbergen, giving a good opportunity for studying the magnetosphere-ionosphere coupling. At present, the measurements carried out there include: electric field (see Fig. 5), meteorological data from a Vaisala automatic station, and ground-based geomagnetic and ionospheric recordings.

The scope of research based on the materials from both stations is now quite large. The fair-weather data, supplemented by global lightning activity and ionospheric investigations, have been used in the study of global electric circuit variations (Odzimek and Lester 2009). Extensive studies concerned the response of electric parameters in the lower atmosphere to solar wind-magnetosphere-ionosphere coupling (Nieckarz *et al.* 2007, Berliński *et al*. 2007, Kozyreva 2007, Kleimenova *et al*. 2009). Studied were also the effects of ion mixing in the atmospheric boundary layer (Kubicki 2009).

The papers quoted above are just a few examples of the present use of the vast experimental material that is available from the two Polish atmospheric electricity stations. With a view to the global climate changes, such long-lasting data as those from Świder are certainly an invaluable reference background for future research.

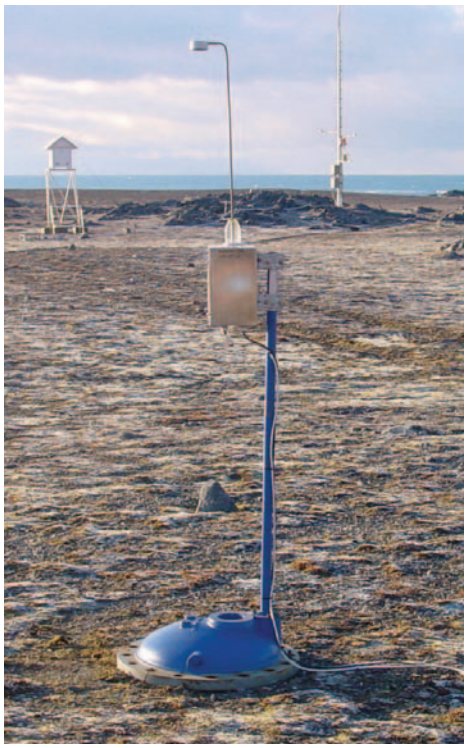

Fig. 5. The radioactive collector for electric field measurement at the Polish Polar Station Hornsund, Spitsbergen.

References

Berliński, J., G. Pankanin, and M. Kubicki (2007), Large scale monitoring of troposphere electric field. **In:** 13th International Conference on Atmospheric Electricity, August 13-17, 2007, Beijing, China, 124-125.

Gadomski, J. (1965), Effect of fallout on elements of atmospheric electricity, *Prz. Geof.* **9**, 17, 227-242.

Jaśkowska, A. (1967), Effect of fog on the elements of atmospheric electricity at Świder, *Acta Geophys. Polon*. **15**, 209-216.

Kleimenova, N., O. Kozyreva, M. Kubicki, and S. Michnowski (2009), Variations of the mid-latitude atmospheric electric field (*Ez*) associated with geomagnetic disturbances and Forbush decreases of cosmic rays, *Publs. Inst. Geophys. Pol. Acad. Sc*. **D-73 (412)**, this issue.

Kozyreva, O.V., .N.N. Nikiforova, N.G. Kleimenova, S. Michnowski, and M. Kubicki (2007), Electric air-earth vertical current pulsations at Hornsund during polar sub-storms: Case study. **In:** 13th International Conference on Atmospheric Electricity, August 13-17, 2007, Beijing, China, 29-32.

Kubicki, M. (2008), Atmospheric Electricity Research at the Institute of Geophysics in the Years 2006-2007, *Publs. Inst. Geophys. Pol. Acad. Sc*. **D-72(403)**, 105-110.

Kubicki, M. (2009), Preliminary assessment of ions distribution in the atmospheric mixed layer based on a single column model, *Publs. Inst. Geophys. Pol. Acad. Sc*. **D-73 (412)**, this issue.

Kubicki, M., S. Michnowski, and B. Mysłek-Laurikainen (2007), Seasonal and daily variations of atmospheric electricity parameters registered at the Geophysical Observatory at Świder (Poland) during 1965-2000. **In:** 13th International Conference on Atmospheric Electricity, August 13-17, 2007, Beijing, China, 50-54.

Michnowski, S., M. Kubicki, N. Kleimenova, N. Nikiforova, O. Kozyreva, and S. Israelsson (2007), The polar ground-level electric field and current variations in relation to solar wind changes. **In:** 13th International Conference on Atmospheric Electricity, August 13-17, 2007, Beijing, China, 9-12.

Nieckarz, Z., A. Kułak, M. Kubicki, S. Michnowski, and P. Barański (2007), Calculating glo-bar strom activity rate on the basis of Schumann reasonance background component. **In:** 13th International Conference on Atmospheric Electricity, August 13-17, 2007, Beijing, China, 72-75.

Odzimek, A., and M. Lester (2009), Modelling the Earth's Global Atmospheric Electric Circuit – Development, Challenges and Directions, *Publs. Inst. Geophys. Pol. Acad. Sc*. **D-73 (412)**, this issue.

Warzecha, S. (1991a), Long-lasting radioactive contamination at Świder and its effect on the atmospheric electricity parameters after the Chernobyl nuclear power plant accident, *Publs. Inst. Geophys. Pol. Acad. Sc*. **D-35 (238)**, 187-192.

Warzecha, S. (1991b), Variations of the Electric Field and Air Conductivity at Świder in the years 1958-1985, *Publs. Inst. Geophys. Pol. Acad. Sc*. **D-35(238)**, 193-198.

PUBLS. INST. GEOPHYS. POL. ACAD. SC., D-73 (412), 2009

Brief Outline of the Long History of Collaboration Between the Central Laboratory for Radiological Protection and the Atmospheric Electricity Laboratory of the Institute of Geophysics

Jerzy PEŃSKO

Central Laboratory for Radiological Protection
ul. Konwaliowa 7, 03-194 Warszawa, Poland

In the mid-1950s I graduated from the Applied Physics Faculty at the Warsaw University of Technology (Politechnika Warszawska), majoring in medical electrotechnology. Stanisław Michnowski graduated from the Electrical Engineering Faculty of the same University at about the same time, although somewhat earlier. The years of studying at the same College were a natural environment for many friendships, often giving rise to long-lasting relations. Such a friendship sustained between me and Staszek Michnowski, although soon after graduation our ways diverted. Staszek indulged into the atmospheric electricity research, while I became engaged in investigation of ionizing radiation and radioactive substances measurements at the Chair of Radiology of the Warsaw University of Technology, led by Professor Cezary Pawłowski. Then I was assigned a difficult task to organize an overall radiological protection system in Poland.

These were the early years of the second half of the last century. In Poland, preparations were under way not only for the development of nuclear physics research, but also for the application of radioactive isotopes and their future production. In industry, medicine, agriculture, and various branches of technology, there was a great need for implementing the artificial radioactive isotopes, that began to be in common use in various applications in Europe and elsewhere. In Poland, the term "radioactive isotope" started to be a token of progress, although some people have not really known what practically it meant. The isotope laboratories have been appearing widely, but nobody was aware what amounts of radioactive materials were admissible, and what were the safety measures to work with them were.

In the first half of the year 1956, the meeting was held in which the necessity was formulated to establish a state institution to manage the organization of all the aspects of the radiological protection in Poland. The meeting took place on the premises of the

Warsaw University of Technology, in the office of Professor Cezary Pawłowski a former student of Maria Skłodowska-Curie in parisien Radium Institute, and my boss at that time, in the presence of the well-known radiologist, Professor Witold Zawadowski. These actions have led to convene, on 13 July 1957, a new institution named the Central Laboratory for Radiological Protection. I was nominated the head of this institution and held this position for the next fourteen years.

The work began by collecting data on isotope laboratories all over Poland, evidencing the employees subject to radiation hazard, and evidencing the radioactive isotope sources. This gave grounds for enacting the periodic check-up actions of the equipment and methods used in these laboratories all over the country, and thus monitoring the hazard to which the workers could be exposed.

The late 1950s and early 1960s were dominated by the armament race, in particular in nuclear weapons. Test explosions of atomic bombs in the atmosphere injected to the stratosphere huge amounts of radioactive dust, including long-lived fission products of heavy atomic nucleus. These contaminated the hitherto contamination-free natural environment and also the inhabited areas in many countries, including Poland.

The Central Laboratory for Radiological Protection faced the necessity of dealing with the problem of monitoring and assessing the hazard of people exposed to this, hitherto unknown source of radiation. The team assigned with this task had to prepare itself to collecting various samples from the constituents of the medium with which population of our county had contact: soil, plants, water, air, and food. We had to measure the radioactivity of these constituents and their effects on people.

We were already aware of the major role the weather conditions, and notably air turbulence, have been playing in the process of dispersion of radioactive materials in the stratosphere and atmosphere. In our team, we lacked a specialist in this matter. It was Professor Teodor Kopcewicz, head of the Atmospheric Physics Chair of the University of Warsaw, who agreed to join us. We learned from him a lot.

We then drew our attention to the relationships that can occur between meteorological elements, atmospheric electricity, and the radioactivity present in the natural environment. It was the year 1967 when I resumed contacts with my old colleague from the Electrical Faculty of the Warsaw University of Technology, Stanisław Michnowski, who was doing research in atmospheric electricity at the Institute of Geophysics, Polish Academy of Sciences, located at that time at the Pasteur a Street in Warsaw. We began consultations on these problems, which gave rise to close scientific cooperation between our two institutions.

Since 1960, the Central Laboratory for Radiological Protection was already in possession of a mini-laboratory at the premises of the City Water and Sewage Plant in Warsaw. In the years 1960-1971, the research conducted there concerned relationships between natural ionization radiation from soil and atmosphere and various environmental factors that might have affected this radiation. Specifically, the following factors and correlations were measured:

1. Content of natural radioactive gas, radon-222, in soil air at various depths,
2. Exhalation of radon-222 from intact ground layer by the soil surface to the air,
3. Radon-222 content in the atmospheric air,

4. Dose rate of gamma background radiation originating from natural radionuclides of uranium-radium and thorium series and potassium-40 present in the ground.

These were accompanied by the following meteorological and environmental observations:

5. Air temperature,
6. Atmospheric pressure,
7. Precipitation,
8. Snow cover (in winter),
9. Soil temperature at various depths,
10. Soil humidity.

The results were described in some publications; see, e.g., Peńsko *et. al*. (1968). However, our mini-laboratory was not quite suitable for this kind of research, because of its location in the centre of Warsaw, where the shallow soil could have been subject to various modifications over the years.

That is why I turned to my old colleague Stanisław Michnowski with a proposition to initiate similar research at the premises of the Geophysical Observatory at Świder, taking additional advantage of the atmospheric electricity observations carried out there for many years. The location of Świder was very appropriate, and the friendly atmosphere of the staff and authorities was much favoring the whole enterprise.

Most of the first research on the natural background radiation focused on the changes in its intensity as a function of geographical location and geological properties of the studied regions. It has been known for a long time that the cosmic ray intensity grows with the altitude. The effect of geological formations on the gamma background level has also been well known. Less attention has been given to the temporal changes of gamma radiation in selected sites.

Observations of this kind were initiated, among other places, at the Physical Faculty, University of Leeds, England, in 1962. A special instrument was constructed, based on the principle of ionizing chambers, which made it possible to observe the terrestrial gamma radiation as well as soft and hard cosmic radiation, although it was unable to distinguish the artificial radioactive fallout (Burch *et al*. 1964).

I had a chance to get acquainted with this instrument during my monthly stay at the University of Leeds in 1964. This inspired me to construct something similar at the Central Laboratory for Radiological Protection. This was accomplished, although instead of ionizing chambers we used two large-size NaJ(TI) scintillation detectors placed in a special steel housing.

Some difficulty in constructing the steel housing, which had to be deprived of any trace of radioactive contamination, was overcome by buying steel slabs from the dismounted ship which had been built many years before the age of nuclear energy.

The tedious task of constructing the instrument was finally accomplished and the instrument was deployed at Świder (Fig. 1), where we found excellent conditions for this type of measurements. The details of design, calibration and operation have been described by Peńsko and Jagielak (1969), and Peńsko (1977).

Fig. 1. Housing of the gamma radiation detector made of a steel slab from the wrecked ship.

The whole arrangement began continuous operation in January 1970; the observations concerned the level and changes of gamma radiation background, which enabled a relatively easy and fast calculation of the following quantities:

1. Total dose rate of the gamma background radiation,
2. Dose rates from gamma radiation originating from the radionuclides contained in the ground and at its surface, discriminating between natural and artificial component (radioactive fallout from nuclear explosions),
3. Dose rates from the gamma radiation of the radionuclides contained in the over-ground layer of the atmosphere,
4. Identification of gamma-ray emitting isotopes (natural and artificial) with energies greater than 150 keV, present in the air and soil medium in the amount exceeding the instrument's detection threshold.

Moreover, owing to the atmospheric electricity measurements and meteorological observations carried out at the Świder Observatory for many years, it became possible to search for possible correlations between them and radiological quantities. The results were published by Peńsko *et al.* (1976).

Unfortunately, in this stage of investigations it turned out impossible to deploy at the Observatory the measurements of radon-222 concentrations in soil air at various depths, exhalation of radon-222 through the ground surface to the air, and concentrations of radon-222 and its daughter products in the atmospheric air. Such measurements would certainly expand the scope of the correlations we investigated. Out of the parameters that were routinely recorded at the Observatory we succeeded in implementing the snow cover thickness. The observations of ground temperature and ground humidity were not included.

In 1971 a symposium “Rapid Methods for Measuring Radioactivity in the Environment” was held in Neuherberg near Münich, Germany, organized by the International Atomic Energy Agency. I attended this symposium, presenting our joint contribution (Peńsko *et al*. 1971).

During this symposium, scientific staff of the Institut für Umweltforschung in Neuherberg presented a publication in which they described an instrument enabling to let a large amount of air through a 0.25 m^2 filter paper and a method of spectrometric measurement of concentration of gamma radioactive isotopes concentrations present in the air sample.

The method seemed very useful for the needs of dosimetric monitoring of natural environment in the period when the nuclear armament and vast development of nuclear technologies in energetic industry were still under way, producing a thread of uncontrolled emission of dangerous radioactive substances into the atmosphere in case the security systems fail.

A similar method was soon successfully applied for detection of trace concentrations of some radioactive isotopes in atmospheric air at the ground of the Nuclear Research Institute in Świerk (Peńsko and Tomczyńska 1979).

At this time, a lively cooperation between the three institutions, the Institute of Nuclear Research, Central Laboratory for Radiological Protection, and the Atmospheric Electricity Laboratory of the Institute of Geophysics, Polish Academy of Sciences, was under way. Figure 2 presents a photo of the staff and collaborators, who gathered in front of the museum building of the Świder Observatory on September 29, 1972.

Fig. 2. A photo of the staff and collaborators of the Atmospheric Electricity Laboratory of the Institute of Geophysics, taken on September 29, 1972, in front of the museum house of the Geophysical Observatory at Świder (Professor Stefan Manczarski, director of the Institute, is standing on the stairs, dressed in a coat and holding a hat in his hand; Zofia Kalinowska and Ewa Kalinowska-Widomska are standing next to him; Jerzy Peńsko – sevenths from the left, in the back row; Stanisław Michnowski – eleventh from the left).

In these circumstances, the idea came forward to build a second, similar instrument and install it at the premises of the Geophysical Observatory at Świder. The idea, warmly supported by Stanisław Michnowski, was accepted by the authorities of the Observatory. This expanded the scope of cooperation by including the Radiation Protection Division of the Institute of Nuclear Research at Świerk, where I was then engaged in some works dealing with the radiological protection of the area surrounding the Institute. Unfortunately, I could not take part in this enterprise long enough, since in January 1981 I left Poland for nearly 6 years to work as a visiting scientist at various institutes in Germany and Switzerland, while a martial law was imposed in Poland for some years.

Having returned to Poland in 1986 I learned that the Central Laboratory for Radiological Protection has much improved the initial system, establishing the network that is presently called "Network of High-Sensitivity Stations ASS-500", composed of 12 objects in various localities in Poland, including Świder.

The system still works there and is supervised by the personnel of the Central Laboratory for Radiological Protection and the Atomic Energy Institute at Świerk, who are also doing the processing and analyses of the collected materials (see, e.g., Mysłek-Laurikainen *et al*. 1998). It is to be noted, however, that now those investigations have different character and different aims than previously intended; they focus on warning against the onset of unexpected radioactive contamination due to failures in nuclear power plants situated in neighboring countries or against other unforeseen circumstances in the vicinity of the system.

The present studies do not try to seek for correlations between the radiation quantities and observations of other parameters that characterize the environment. It would be desirable to encourage the two institutions collaborating with the Świder Observatory to make use of their large experimental facilities and take advantage of the vast materials collected by the Observatory personnel in the area of atmospheric electricity and meteorological data, in order to look for deeper interrelations between these quantities. This might help to elucidate, to some extent, the phenomena governing the environmental factors.

The sole monitoring of trace concentrations of radionuclides of natural and artificial origin and those produced by cosmic rays, as presently done at Świder, does not carry much scientific value. This unusual place deserves to be used for radioactivity observations in much greater scale, to take advantage of all its abilities.

References

Burch, P.R.J., J.C. Duggleby, B. Oldroyd, and F.W. Spiers (1964), Studies of environmental radiation at a particular site with a static gamma-ray monitor. **In:** J.A.S. Adams, and W.M. Lowder (eds.), *The Natural Radiation Environment*, The University of Chicago Press, Chicago, 767-779.

Mystek-Laurikainen, B., M. Biernacka, M. Bysiek, E. Proste, and M. Matul (1998), Radionuclides in the ground-level air in Poland, *Nukleonika* **43**, 4, 439-448.

Peńsko, J. (1977), Pole ziemskiego tła promieniowania gamma i metody jego badań, Monografia, pp. 144, PWN Warszawa.

Peńsko, J., B. Gwiazdowski, J. Jagielak, M. Biernacka, and K. Mamont (1971), Combined environmental radioactivity measurements for rapid estimation of the gamma radiation field. **In:** *Rapid methods for measuring radioactivity in the environment*, IAEA Proceedings Series, International Atomic Energy Agency, Vienna, Austria, 443-458.

Peńsko, J., and J. Jagielak (1969), Static gamma background monitor for identification of contamination and dose rate in the case of dispersal radionuclides to the atmosphere, *Nukleonika* **14**, 831-842, PWN Warszawa.

Peńsko, J., S. Michnowski, S. Warzecha, and B. Gwiazdowski (1976), Pomiary radioaktywności; elektryczności atmosferycznej i elementów meteorologicznych na terenie obserwatorium geofizycznego w świdrze, *Przegląd Geofizyczny* XXI (XXIX), z. 4, 281-286, PWN Warszawa.

Peńsko, J., and J. Tomczyńska (1979), Metoda i pomiary śladowych stężeń niektórych izotopów promieniotwórczych w powietrzu atmosferycznym na terenie instytutu badań jądrowych w świerku, *Postępy Fizyki Medycznej* 14, 111-120, PZWL Warszawa.

Peńsko, J., T. Wardaszko, and M. Wochna (1968), Natural atmospheric radioactivity and its dependence on some geophysical factors, *Atompraxis* **14**, 255-258.

Received September 24, 2009

Translated from Polish by Anna Dziembowska

PUBLS. INST. GEOPHYS. POL. ACAD. SC., D-73 (412), 2009

The Response of Towers and Other Structures to Nearby Lightning

Lothar H. RUHNKE[1], Vladislav MAZUR[2], and Silvério VISACRO[3]

[1]University of Oklahoma, Norman, OK, USA
e-mail: LRuhnke@aol.com (corresponding author)

[2]National Severe Storms Laboratory, Norman, OK, USA

[3]Lightning Research Centre, Federal University of Minas Gerais, Belo Horizonte, Brazil

Abstract

This study describes an attempt to evaluate the potentially hazardous effects on tall structures from nearby cloud-to-ground flashes by conducting measurements of currents and ground potentials on structures during thunderstorms. The analysis of these measurements has shown that the layout of the elements of ground structures and their connections within a grounding grid of the installation have profound effects on magnitudes and polarities of induced currents and voltages. Understanding of the factors affecting the response of tall ground structures to nearby lightning flashes, and therefore correct interpretation of induced lightning effects on a particular installation is crucial for improving the design of grounding systems of the installations.

Key words: lightning, grounding, lightning hazards, induced effects, lightning measurements.

1. Introduction

Hazardous effects of lightning are usually attributed to the impulse phase of the return stroke current and continuing current that follows cloud-to-ground flashes during their attachment to a ground structure. There is, however, a significant percentage of reported lightning-related damage to structures that is not associated with direct lightning strikes (lightning attachments) (Diendorfer 1990). Among the possible causes for these instances of damage may be upward leaders from the structure, or induction currents, both as effects of nearby lightning flashes. It is expected that the upward leaders would start from the same protruding elements of the structure both in case of

lightning attachment and of lightning nearby. Therefore, if the upward leaders are hazardous, the damages to installations may be similar in both cases. The direct hazardous effects could be from upward leader current pulses of reported maximum values up to 23 kA (Miki *et al*. 2005).

Indirect lightning effects on tall grounded structures are not well researched, and therefore not considered a lightning protection issue. Evaluation of these effects is the subject of our investigation, which has been conducted in the United States and Brazil. In depicting our data we use the traditional sign convention in atmospheric electricity ($E = \text{grad}\ \varphi$), where E is an electric field and φ is the ambient electrical potential.

2. Instrumentation

A 60-meter tall tower insulated from the ground at the top of a mountain (elevation 1400 m ASL) called Morrro do Cachimbo (MCS), near Belo Horizonte, Brazil, a free-standing 90-meter tall tower on a flat ground near Dallas, Texas, and two radar towers, one in Florida and the other in New Mexico, were instrumented for this study (Fig. 1). The measured variables were: the current on a down conductor of the tower, the potential of the grounding system, and local electric field changes produced by lightning flashes. A sensor for slow changes in the electric field (dE) was connected to the input of an A/D converter and had an input time constant of several hundred milliseconds. A similar sensor for detecting fast changes of the electric field (dE/dt) had a time constant of 10 microseconds. dE/dt pulses served to trigger data recording of lightning events. An electric field mill was used at the MCS and Dallas sites for sensing the stationary electric field from clouds prior to and during the lightning event. A ground potential probe, about 100 meters away from the installation, was a part of the system for monitoring the voltage drop over the grounding impedance of the installation. A current clamp (with range of up to 2 kA) on the down conductor of a tower leg was used to measure the current from the tower into the grounding system.

We have used a PC-based data recording system that consists of an A/D converter with a sampling rate of 100,000 samples per second with a 16-bit resolution, and a GPS system that tags each event with one millisecond accuracy. The local LLS (Lightning Location System) in Brazil and the National Lightning Detection Network (NLDN) in the U.S.A. provided complementary data on cloud-to-ground flashes in the vicinities of our installations.

For studying the effects of lightning on a grounded structure, it is critical to determine the value of the impedance of the grounding system. This is not a trivial matter, especially for the extended grounding grid typical of radar sites. We found that an independent ground point for voltage measurements needed to determine the grounding impedance using a three point system may be located as far as a few hundreds meters away from the installation. For example, at the Morro do Cachimbo site the independent ground point was 150 meters away from the tower. At the three other sites in the United States, it was simply impractical to find the true independent ground due to the close proximity of other structures, so we settled for such points as far away from our installation as we could. Resulting from this compromise, the values of ground impedance at our U.S. installations probably underestimated the actual

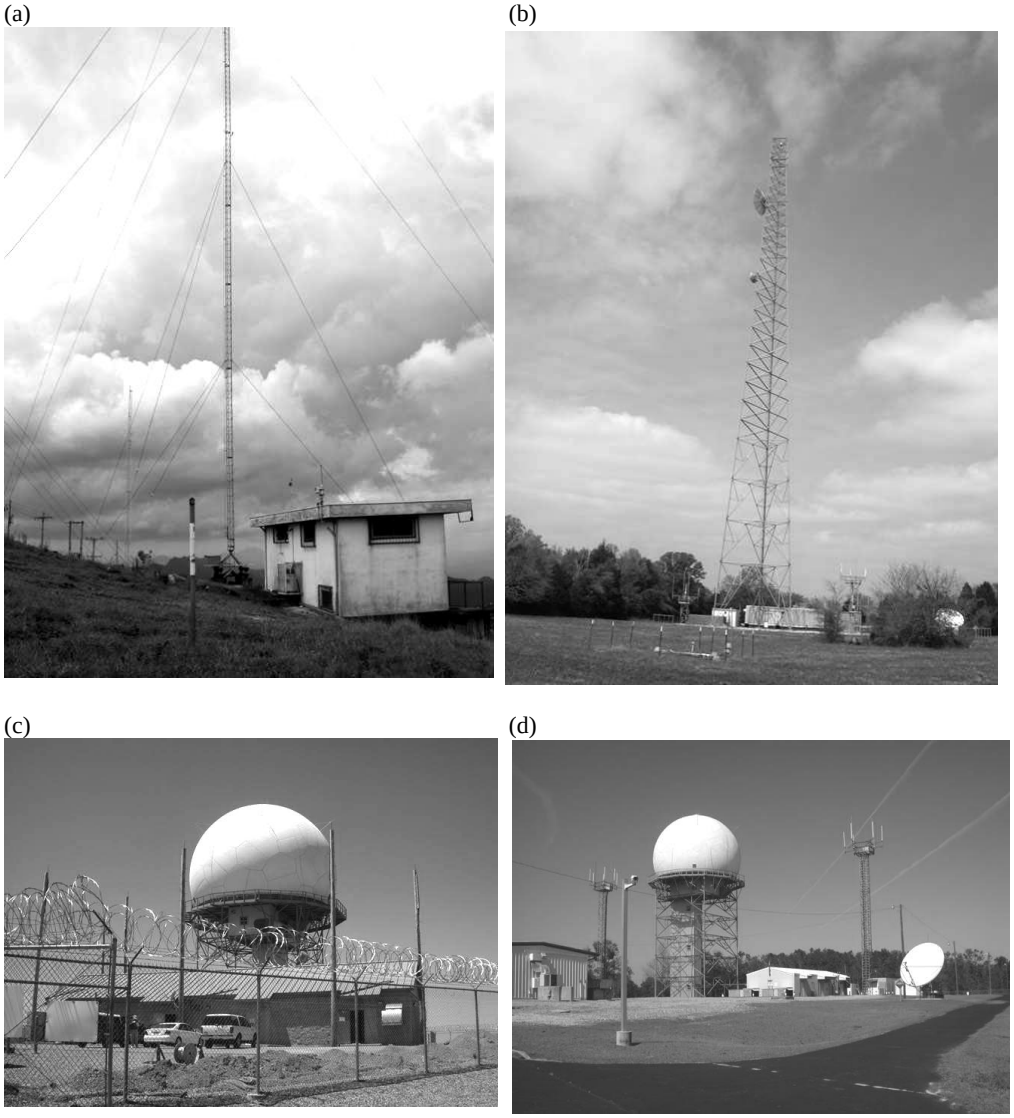

Fig. 1. Installations used for this study. (a) A tower set on insulators at the Morro do Cachimbo station, Brazil. (b) A free standing tower in Texas. (c) A radar site in New Mexico. (d) A radar site in Florida.

ones, because the voltages are lower for the ground points closer to the installations than for the points of the true independent ground.

There was another use of the independent ground point, namely for measurements of the potential of a structure affected by lightning. This potential (called here "the loop voltage") is the voltage between the ground grid of the installation and a ground not affected by the lightning striking the installation, i.e., an independent ground point. A coaxial cable buried in the ground connected the independent ground probe with the measuring system based on PC.

Figure 2 shows our initial set-up for measuring the ground potential change for the case of the induced upward leader emerging from the tower and the case of the direct lightning strike to the tower. In both cases the direction of the current is the same, i.e., positive charges are moving upward. The grounding system potential was $V = I_{RS} Z$ while the measured value of loop voltage on the PC was V/1000 where 1000 is the ratio of the resistor value at the remote probe to that at the entrance of the PC.

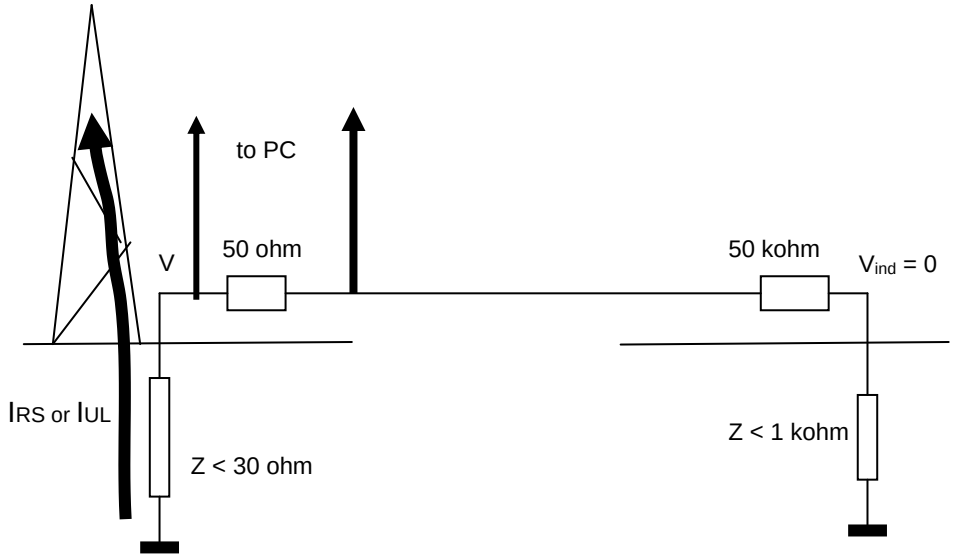

Fig. 2. Set-up for measuring a "loop voltage" during a direct lightning strike (return stroke current I_{RS}) or an upward leader (current I_{UL}) from the tower. Input resistor at the PC is 50 ohm, while the resistor on the other end of the coaxial line, at the independent ground point is 50 k ohm. V is a potential of the grounding system of the installation. The arrow shows the direction of positive charges flowing in the return stroke or upward leader.

The impedance Z of the grounding system was determined by injecting a current pulse I that simulates a return stroke signal by its rise and decay times, and by measuring the voltage response U over the grounding system. We used test current pulses with peak amplitudes of 10 ampere produced by our own current generator, although in the past we had an experience of using for this purpose a commercially available instrument. For the Morro do Cachimbo site in Brazil our measurements showed a grounding impedance of 28 ohm.

3. Results

In the course of our investigation we found that upward leaders from the towers which had measurable values of current were relatively rare. We estimated that only lightning flashes located less than 1 km away from the tower might induce upward leaders, because in order to start an upward leader from a 60-meter-tall tower, the required combined electric field from clouds and nearby downward leader needs to be greater than 40 kV m^{-1} (Aleksandrov *et al*. 2001).

A vertical tower that has capacitance C, effective height h_{eff}, and is in the ambient electric field E acts as a single receiving antenna if it is situated on a plane surface without any obstruction from nearby buildings or towers. For such a structure and for a lightning flash up to a few km away we applied the electrostatic assumption for the electric field to describe effects of electric field changes on induced currents (eq. 1), (Kasemir and Ruhnke 1958).

$$I = dE/dt * C * h_{eff}. \quad (1)$$

For the tower at Morro do Cachimbo with measured capacitance C of 1800 pF and an assumed effective height h_{eff} of 30 m, the relationship (1) is written as:

$$I(A) = 0.05 * dE/dt\,(V\,m^{-1}\mu s^{-1}). \quad (2)$$

It should be mentioned also that an isolated single receiving antenna would not have induced currents from magnetic field changes produced by nearby lightning.

The output of the fast antenna (dE/dt) can be integrated to yield the electrostatic field. For most cases the integrated dE/dt record, after correction of the record for the time constant of the slow antenna, produced a waveform identical to the output of the slow antenna (dE). We used this integration procedure also for verification of the integrity of the sensors. A field mill record was used to calibrate the slow and fast antennas.

When the structure is connected to ground by a single down conductor (as in the case of the Morro do Cachimbo tower), the induced current is consistent in its polarity and magnitude with those polarities and magnitudes obtained theoretically from the fast E-field changes (using eq. 1) produced by return strokes. We discovered, however, that in cases of nearby lightning flashes for three installations in the United States, the induced currents to the ground and also loop voltages exhibited quite different behaviours than that expected during upward leaders from the structure or direct lightning attachments to the structure. Figure 3 shows a case when polarities of the loop voltage and induced current are correct, while Figs. 4, and 5 show examples of records inconsistent with expectations.

We found that the loop voltage displayed a polarity dependence on the location of the return stroke attachment point relative to the direction of the coaxial cable that connects the independent ground point with the ground of the structure (Fig. 6). What this polarity dependence indicates is the existence of an induction loop consisting of the connecting coaxial cable and the ground, which is not a perfect conductor and is penetrated by electromagnetic waves (Fig. 7). With the induction loop present, we actually record the induced open circuit voltage from dH/dt of lightning magnetic field together with the voltage drop over the grounding impedance from the induced current on the tower. Thus, the loop voltage that we measured is, at best, a mixture of the induced voltage in this loop and the ground losses due to the current flowing to ground. The voltage in the loop (made of the coaxial cable and the ground) may be much higher than the voltage drop over the grounding resistance from the current in the mast. An additional contributor to the directional behaviour of the loop voltage might be the voltage drop on the ground due to currents from a lightning propagating into the soil and producing a potential distribution in the neighbourhood of the lightning impact point, i.e., the so-called “step voltage” (Lee 1977).

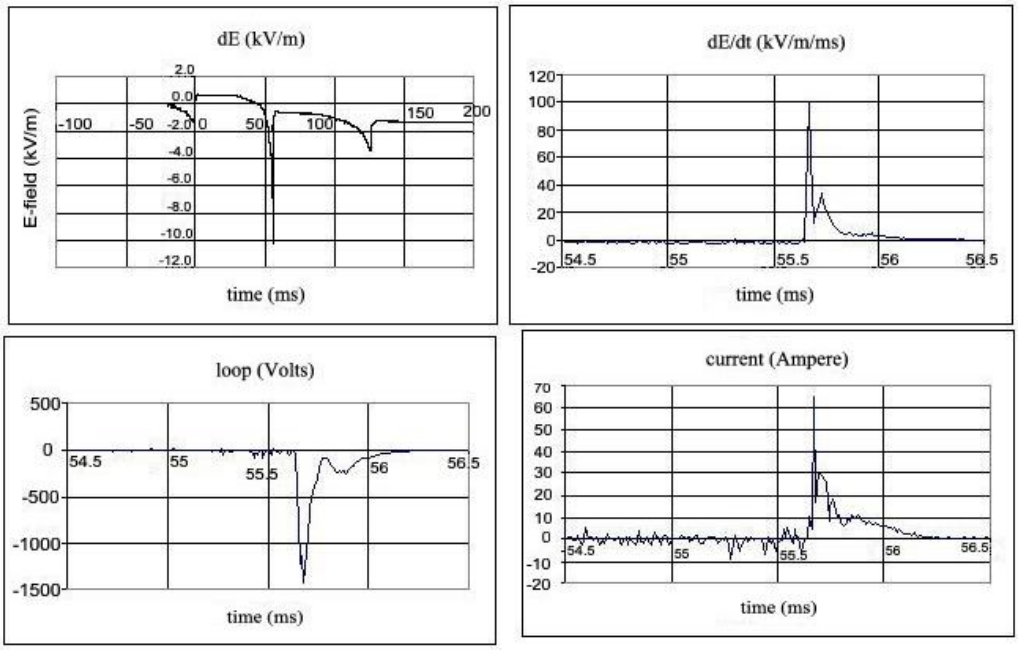

Fig. 3. The record from a nearby flash in Florida at the range of 0.6 km, Imax = −29.3 kA, with correct polarities of current and loop voltage.

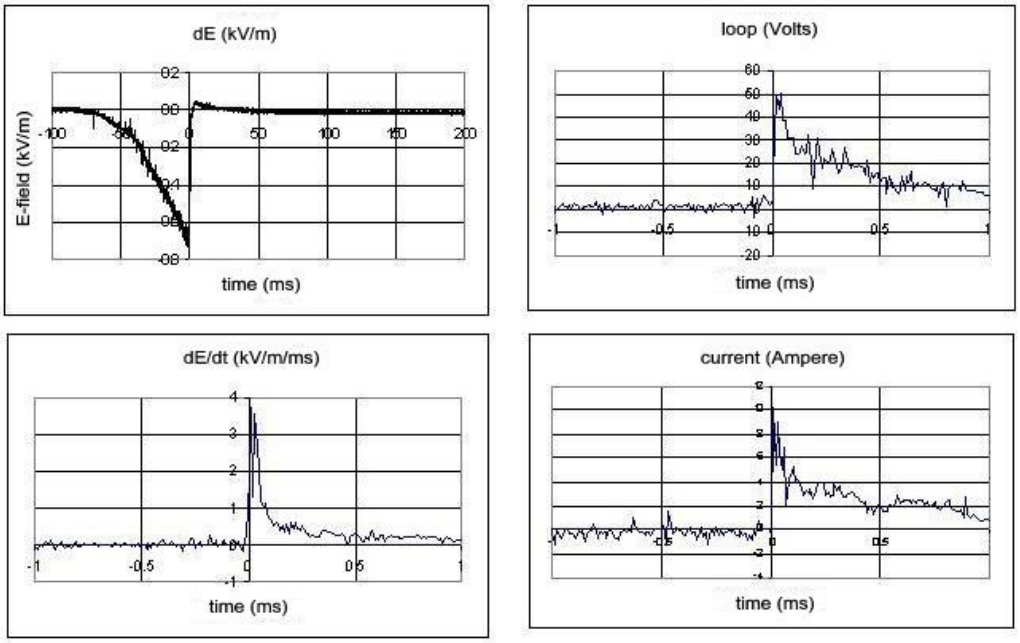

Fig. 4. The record from the nearby flash in Florida at the range of 2.6 km, Imax = 17.5 kA with right polarity of current and wrong polarity of loop voltage.

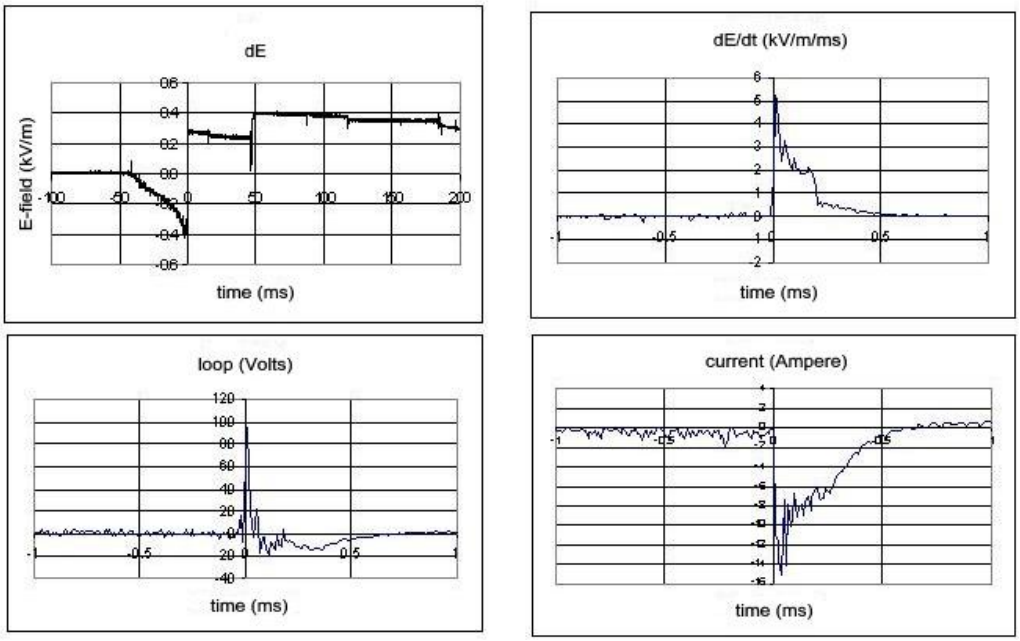

Fig. 5. A record from the nearby flash at range of 2.3 km and of Imax = 18.3 kA showing induced current and loop voltage of wrong polarities.

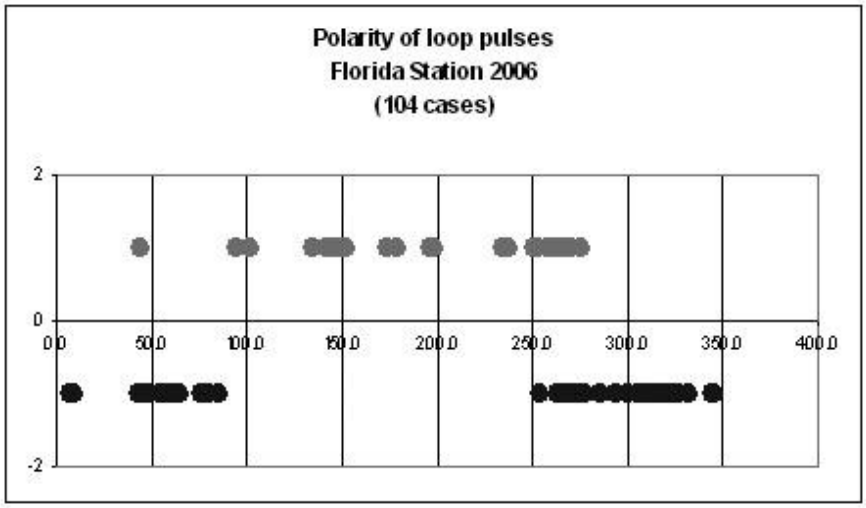

Fig. 6. Graph illustrating the polarity dependence of loop voltage pulses on the direction to the source of a dH/dt pulse (i.e., the direction to the return stroke of a cloud-to-ground flash), in cases of an induction loop made with a horizontally extended cable to a loop voltage probe at the Florida site. Positive and negative polarity values correspond to flashes in the sector of 90-270 degrees and that of 270-90 degrees relative to the orientation of the installation (North-South), respectively. Flashes from azimuth either 90 or 270 degrees do not produce any induced effect in the loop.

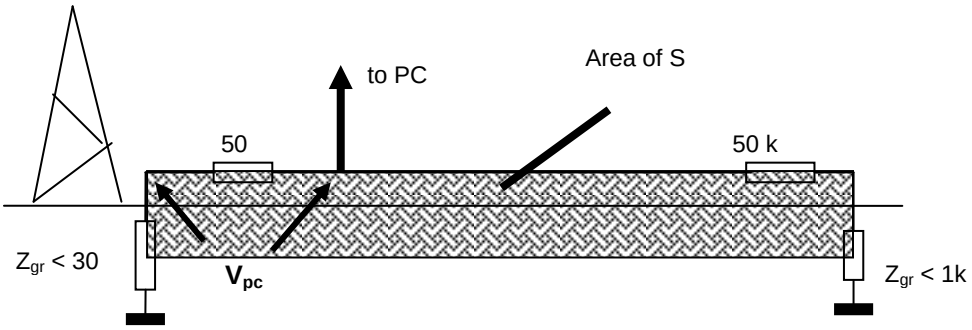

Fig. 7. An induced voltage circuit for dH/dt of nearby lightning flash made of loop of area S consisted of a central core of the coaxial cable and the ground. (Since the ground is not a perfect conductor, low frequency electromagnetic waves penetrate it.).

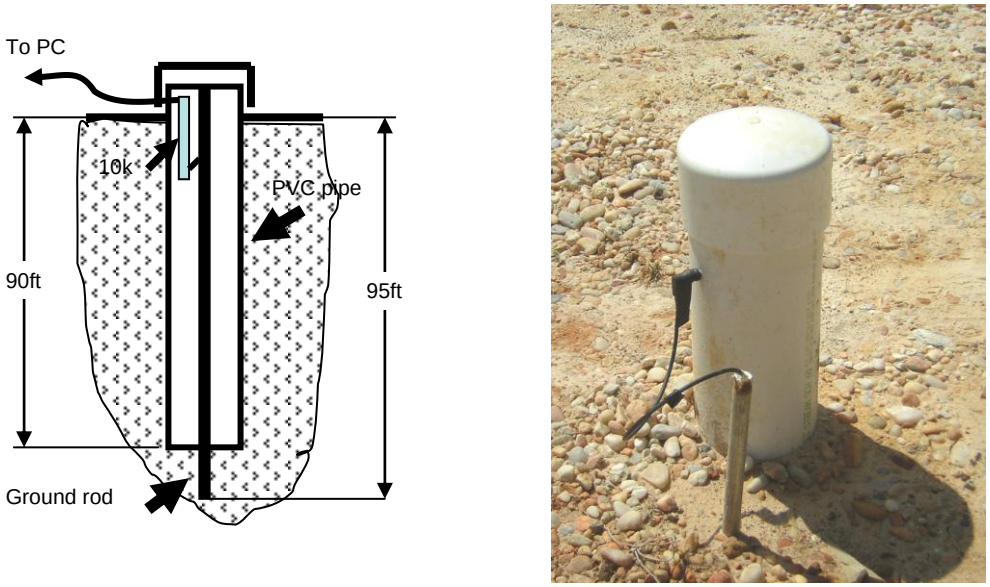

Fig. 8. A deep ground rod inside a PVC pipe that insulates the rod from the layer of ground above.

Thus, we discovered that using an independent ground point far away (horizontally) prevented us from obtaining the true value of the ground potential change due to the nearby lightning. The alternative is an independent ground point deep in the ground and practically inside the installation. Our attempts to find an independent ground point deep beneath the grounded mast in Texas did not succeed because we could not insert (manually) an insulated ground rod deep enough to achieve a desirable effect. Thus, so far we were not able to estimate correctly induced effects of a nearby lightning flash on the ground potential of the installation. Currently we are conducting measurements at a new site in Alabama utilizing an insulated ground rod installed at a depth of 30 meters as an independent ground point (see Fig. 8).

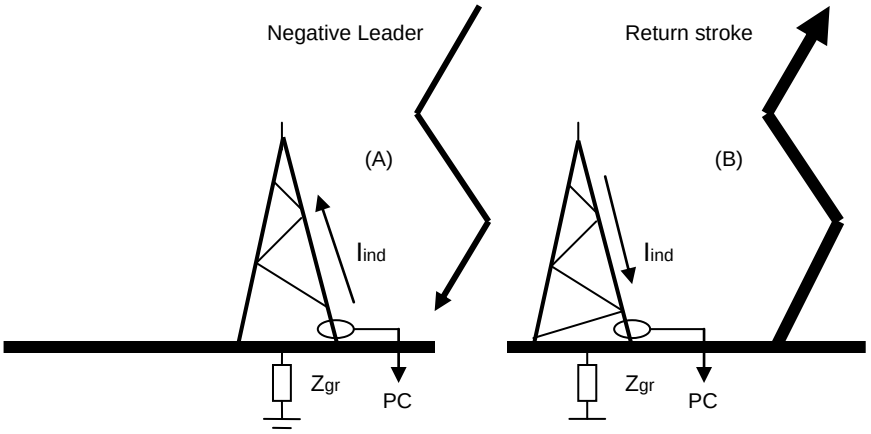

Fig. 9. Set-up for current measurements of induced current on a tower from a nearby cloud-to-ground flash. Notice change in direction of the induced current I_{ind} = dE/dt C h_{eff} for two stages of a cloud-to-ground flash. Negative leaders and return stroke have the same current polarity. Arrows show directions of propagation for negatively charged downward leader and positively charges return stroke, respectively.

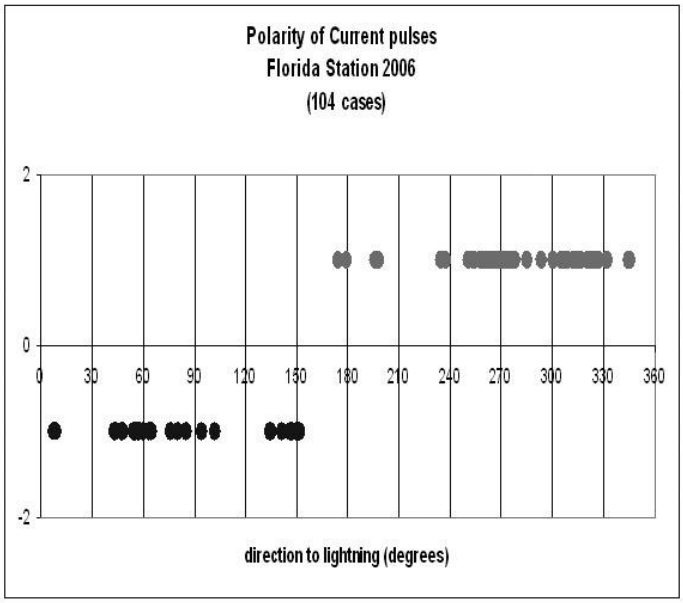

Fig. 10. Polarity dependence of current pulses to the source direction.

Currents flowing from the tall structure to ground were measured using current-to-voltage transducers clamped around a down conductor of a tower leg (Fig. 9). We determined that the induced current pulses associated with fast electric field changes during the return strokes of nearby cloud-to-ground flashes are of much greater amplitudes than those expected from the theoretical considerations (see eq. 1) for a given tower with a given ground impedance. The recorded current pulses were sensitive also

to directions to the current source (Fig. 10). This phenomenon characterized current measurements at all three installations in the United States, but not at the MCS tower in Brazil.

We found that there is a common feature in the configurations of the grounding systems in the U.S sites, namely, the extended ground grid connecting the down conductors (more than one) of the tower with the down conductors at other buildings in very close proximity to the tower (see Fig. 11). These are conductor loops subjected to induced currents from magnetic field changes of return stroke signals. On the other hand, the tower in Brazil that is resting on insulators had a single connection to the ground, and its grounding grid is of a small size and symmetric in relation to the tower.

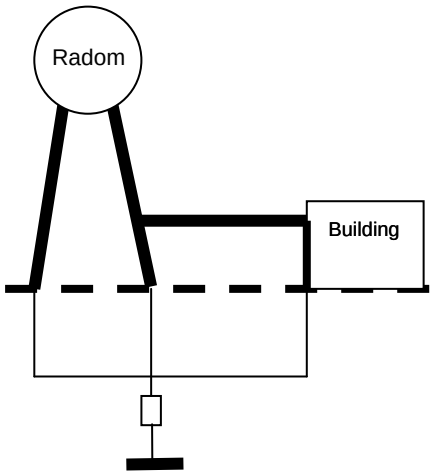

Fig. 11. Induction loops are formed by down conductors and other elements of the grounding system above and below the ground. Induced voltage at this Florida site is produced mainly by dH/dt penetrating the loop, which is in the plane (W to E) perpendicular to axis 350-170 deg AZ.

The directional dependence of induced current pulses in the U.S. sites brings into question the validity of using current measurement with magnetic link sensors at structures with multiple grounding conductors for estimating the current in lightning channels. In view of this discovery, it was interesting to compare our measurements with those obtained at structures with a single down conductor to ground. As expected, the data from the MCS tower in Brazil that has a single down conductor did not contain any directional effects in the records of induced currents. However, data from yet another mast with a single down conductor (a lightning protection mast at Indianhead, Maryland), did show, to our surprise, a directional dependence similar to those in tall structures with multiple grounding systems. Closer examination of the Indianhead site showed that this installation had a nearby building with its grounding system connected to the grounding grid of the mast. The presence of this building determined the directional dependence of induced currents. Figure 12 depicts the polarity dependence of return stroke signals sensed by a current probe on the Indianhead mast with a single down conductor but situated near a well grounded building.

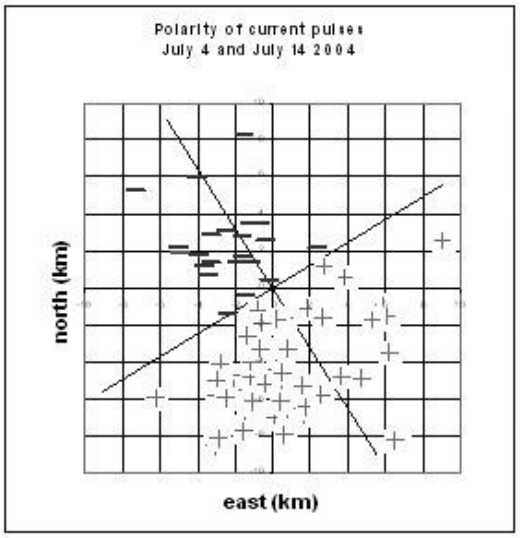

Fig. 12. Polarity dependence of current pulses at a mast with one down conductor in Indianhead, MD.

This finding proves that asymmetries in installations, e.g., some other structures in the close proximity to single masts, can have interacting effects if grounding resistance between mast and associated structure (building) is low enough. Such interactions are widely known in radio antennas, e.g., in Adcock antennas that rely on the interaction of two vertical antennas for producing a directional receiving pattern. As in Adcock antennas, the induced current flowing in an asymmetric installation has much grater amplitude than that in a single isolated mast, which is an analogy of a whip antenna. Our three installations in the United States have asymmetric structure, which explains why the induced current values we measured were so much higher than those expected under the electrostatic assumption (eq. 1).

Most of the above problems with measurements of induced currents and voltages do not exist in cases of direct strikes to structures or upward leaders from structures. However, direct strikes to the installations under study were rare and even upward leaders solely due to cloud electric fields did not occur during our studies. We anticipated that upward leaders from a tower would occur occasionally when either cloud electric fields of high magnitude were present and/or downward leaders preceding return strokes occurred within 1 km of our observation sites. In the latter case, upward leaders would be of short duration and would stop when the return stroke process starts. Figure 13A shows the current record of such upward leader from the Indianhead tower, with a cloud-to-ground flash reported by NLDN being 0.7 km away. Negative current pulses with a noticeable DC component rising with time appeared about 1 millisecond prior to the return stroke process that started at time zero, when the downward leader reached ground. A positive potential near the structure produced by positive charges on the return stroke channel killed the upward leader progression.

Figure 13B depicts a more frequent case of a similar nearby cloud-to-ground flash, but without an upward leader. The difference between these two cases is in the

presence of high ambient electric field in the case depicted in Fig. 13A, and the absence of such field in the case depicted in Fig. 13B, although the downward leader of a nearby cloud-to-ground flash was in evidence in both cases.

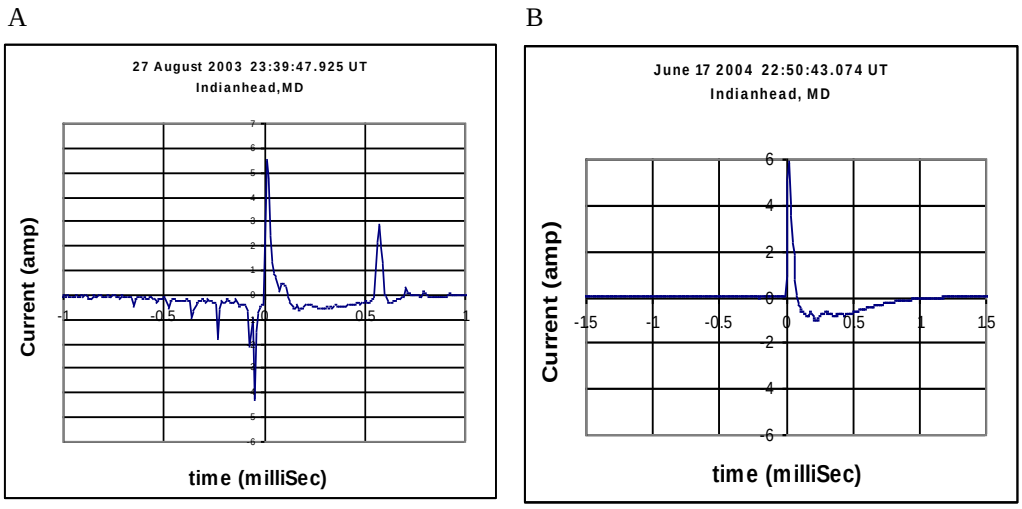

Fig. 13. Record of current at the base of a 40 m high mast showing in case (A) an upward leader followed by the return stroke, and in case (B)) a return stroke without a preceding upward leader.

4. Conclusions

The response of towers and other tall ground structures to nearby lightning flashes in form of induced current and voltages, although understood in principle, is poorly researched in regards to quantitative relationships between physical processes and structures involved. We found that induced currents in tall structures from nearby cloud-to-ground flashes may be strongly influenced by the design of the grounding system. The ways the elements of the grounding system are connected affect the magnitude and polarity of induced current pulses. We have found that the induced currents on towers or complex installations with asymmetric structure of the grounding system may be orders of magnitude higher than the induced currents produced by fast field variations (dE/dt) from nearby lightning flashes. Our interpretation of this finding is that the asymmetric installations connected through a grounding system with low impedance are acting like Adcock antennas. Then the induced current pulses of high amplitudes flow along the external elements of the structure, and may affect sensitive devices installed there.

Jones *et al*. (2004) who applied peak current magnetic cards (bandwidth of more than hundreds of MHz) to monitor currents on the external down conductors of lightning protection systems in the United Kingdom reported presumably induced current pulses from nearby lightning of up to 120 kA. Perhaps our explanation of the nature of very high values of induced current pulses in asymmetric installations can be applied to interpret the measurements in UK. This is under the realistic assumption that the lightning protection systems of munitions storage sites in UK, with its numer-

ous down conductors, resemble the asymmetric structures connected by a low impedance grounding grid.

The effects of nearby lightning on a ground potential of the installations of different configurations still remain to be determined, because our initially selected method of measuring this potential resulted in significant contaminations from several unrelated variations of lightning electric and magnetic fields. We intent to conduct measurements of the ground potential change using a point of independent ground deep down at the installation site, with a minimum horizontal exposure of a connecting coaxial cable.

Acknowledgments. This research was sponsored in part by the FAA under a cooperative agreement with the National Severe Storms Laboratory. We thank Vaisala, Inc. for complimentary NLDN data in support of this research. We appreciate the contribution of Christopher Karabin of the Indianhead Division of the Naval Surface Warfare Centre who provided Figures 12 and 13 from his data base. The invaluable help by Renato de Oliveira and Marcelo Felipe, graduate students of the Federal University of Minas Gerais, in maintaining the observation site at Morro do Cachimbo, Brazil, conducting data acquisition there, and assisting in data processing is deeply appreciated.

References

Aleksandrov, N.L., E.M. Bazelyan, R.B. Carpenter Jr., M.M. Drabkin, and Yu.P. Raizer (2001), The effect of coronae on leader initiation and development under thunderstorm conditions and in long air gaps, *J. Phys. D: Appl. Phys*. **34**, 3256-3266, DOI: 10.1088/0022-3727/34/22/309.

Diendorfer, G. (1990), Induced voltage on an overhead line due to nearby lightning, IEEE *Trans. Electromagn. Compat*. **32**, 292-299, DOI: 10.1109/15.59889.

Jones, M., D. Newton, and K. Kos (2004), Some recent studies into new lightning phenomena, hazards and response modeling. 18th International Lightning Detection Conference, Helsinki, Finland, June 2004.

Kasemir, H.W., and L.H. Ruhnke (1958), Antenna problems of measurement of the air-earth current. **In:** *Recent Advances in Atmospheric Electricity*, 137-147, New York: Pergamon Press.

Meinke, H., and F.W. Gundlach (1956), *Taschenbuch der Hochfrequenztechnik*, pp. 441, Springer Verlag, Berlin.

Lee, W.R. (1977), Lightning injuries and death. **In:** R.H. Golde (ed.), Lightning vol. 2, Lightning protection, 521-44, New York, Academic Press.

Miki, M., V.A. Rakov, T. Shindo, G. Diendorfer, M. Mair, F. Heidler, W. Zischank, M.A. Uman, R. Thottappillil, and D. Wang (2005), Initial stage in lightning initiated from tall objects and in rocket-triggered lightning, *J. Geophys. Res*. **110**, DO2109, DOI: 10.1029/2003JD004474.

Received April 17, 2009

PUBLS. INST. GEOPHYS. POL. ACAD. SC., D-73 (412), 2009

Modelling the Earth's Global Atmospheric Electric Circuit – Development, Challenges and Directions

Anna ODZIMEK, and Mark LESTER

Radio and Space Plasma Physics Group, Department of Physics and Astronomy, University of Leicester, University Road, Leicester LE1 7RH, United Kingdom

Abstract

In this paper we summarise modelling work to date concerning the Earth's global atmospheric electric circuit. We discuss the development of the models over last decades and some features that require improvements in future models. We consider various atmospheric and ionospheric data sets and models available which can support and improve the current and future modelling of the global electric circuit. We also highlight the new high-resolution model of the global atmospheric electric circuit, EGATEC, currently developed at the University of Leicester.

1. Overview of the global atmospheric electric circuit

The term Global Atmospheric Electric Circuit (GAEC or GEC) is referred to the flow of electric currents in the Earth's atmosphere. According to the "classical picture" of atmospheric electricity these currents are produced by electrically active cloud generators, thunderstorms and non-thunderstorm clouds, e.g., shower clouds, as suggested by Wilson (1920). Charge transfer in the atmosphere, associated with these cloud generators, is provided by conduction, point discharge currents, and currents carried through electrified precipitation, and tropospheric lightning discharges or upper atmosphere lightning discharges. These currents, except discharge current, can also be present in non-thunderstorm electrified clouds. Compendia by MacGorman and Rust (1998) and Rakov and Uman (2003) provide up-to-date information on the cloud electrical activity and associated phenomena. Some important topics in planetary atmospheric electricity, including global electric circuits, have been also reviewed recently in Leblanc *et al*. (2009).

According to Wilson, the electric currents are driven by the lower atmosphere cloud generators due to large voltages produced inside the clouds. These currents flow

upwards from the cloud tops to the ionosphere and between the ground and the bottom of the clouds. They also flow freely through the conducting ionosphere and are closed by downward currents in the less conducting fair-weather area of the atmosphere (as the so called air-Earth current) and currents in the well conducting ground. Due to continuous operation of the cloud generators over the globe, the potential of the ionosphere remains high (200-300 kV) with respect to the Earth at all times but exhibits diurnal, seasonal and irregular variations, as seen in atmospheric electrical measurements of the potential gradient or the air-Earth current density and the ionospheric potential (Kubicki *et al.* 2007, Markson 2007, Williams 2009, and references therein). The ionospheric potential and the total current flowing in the global circuit are the main GEC variables. Observationally, the density of the air-Earth current and the potential gradient (or the electric field) measured at the ground in various locations over the globe are the main indicators of the existence of the GEC.

Currents from the lower atmosphere are coupled to the magnetosphere-ionosphere current systems, as the ionosphere plays a significant role in both current systems, and the atmospheric circuit becomes part of the geospace global electric circuit GGEC (Michnowski 1998). The magnetospheric generators are due to the interaction of the Earth's magnetosphere with the solar wind and the interplanetary magnetic field. Electric fields produced by this interaction map along magnetic field lines at polar latitudes down to the ionosphere and result in dawn-to-dusk voltages across both polar caps (see e.g. Kelley 2009), and therefore the effect of this coupling is mainly seen at polar latitudes. In addition, there are the ionospheric and disturbance dynamo effects due to the neutral ionospheric winds produced by solar and auroral heating of the thermosphere. These processes and their effect on the potential of the ionosphere are discussed in Roble (1991), Rycroft *et al*. (2000) and Tinsley (2008). Markson (1978), Willett (1979) and Roble (1985) have discussed possible relationships between space weather and atmospheric electricity.

In recent years a number of effects correlated with GEC phenomena have been observed, for example, changes of atmospheric pressure, temperature or cloud cover on a regional or global scale (Tinsley 2008, and references therein). Tinsley divided them into five categories relating to five different GEC agents: global ionospheric potential, polar cap potential, relativistic electron flux, solar proton events, cosmic rays Forbush decreases.

Also, interest has risen in various cloud processes taking place in the troposphere and affected by the air-Earth current density (Tinsley 1996, Tinsley 2000, Harrison 2004, Harrison and Ambaum 2008). These results imply further connections of the Earth's GEC, space weather, atmospheric weather systems and even climate.

2. Global circuit models

A model of the global atmospheric circuit must include a model of the electrical properties of the atmospheric medium where electric current flow and a model of the sources that generate these currents, the lower atmosphere current generators (thunderstorms, shower clouds) in the first place. Atmospheric electrical conductivity is the important electrical parameter. In the lower atmosphere the conductivity is due to ions

produced by cosmic rays and natural radioactivity. The ions can be lost due to attachment to aerosols and cloud condensation nuclei. The production and loss of the ions and the ion mobilities can be modelled separately to create a complex lower atmosphere conductivity model. At higher altitudes (> 45-50 km) up to ionospheric altitudes electrons play main role and the Earth's magnetic field causes the anisotropy of the conductivity in the Earth's ionosphere. This must be taken into account in the models that consider the effect of magnetospheric-ionospheric generators.

Tinsley and Zhou (2006) have recently developed a sophisticated model of atmospheric resistivity which includes the effects of winter and summer tropospheric aerosols, stratospheric aerosols, and the effects of solar activity on ion production by cosmic rays and volcanic activity on stratospheric aerosols. This model can become an integral part of any modern GEC model, as demonstrated by Tinsley and Zhou (2006) and Odzimek *et al*. (2009).

There are a few analytical and numerical models of the Earth's global atmospheric electric circuit developed over the last few decades (Hays and Roble 1979, Roble and Hays 1979, Makino and Ogawa 1984, 1985, Sapkota and Varshneya 1990, Price *et al*. 1997, Kartalev *et al*. 2004b, Odzimek *et al*. 2009) which contain these two integral part of a GEC model – a model for the electrical properties of the atmospheric medium and a model for current generators. The first high resolution models of the atmospheric circuit were created by Roble and Hays (1979) and Hays and Roble (1979). They are mathematical models, providing a solution for the ionospheric potential as a series of spherical harmonics, at 5 degree resolution in latitude and longitude. Table 1 particularly compares high-resolution GEC models that are able to provide distributions of the main GEC variables over the globe and time variations.

A number of GEC-related thunderstorm generator models have also been developed which are concerned with the flow of the electric current from thunderstorms, playing the role of the sources driving the circuit, and the distribution of the electric potential in the vicinity of the thunderstorms, in the ionosphere above and the conjugate ionosphere, as well as in the cloud-free area of the circuit; for example, Park and Dejnakaritra (1973), Nisbet (1983), Tzur and Roble (1986), Stansbery *et al.* (1993), Kartalev *et al*. (2004a). Rycroft *et al*. (2007) modelled the current contribution from shower clouds for the first time.

Since the 1980s, various satellite measurements started to play role in the development of GEC models. Makino and Ogawa (1984) have used the Defense Meteorological Satellite Programme (DMSP) lightning flash densities in the development of their thunderstorm current generator model. More recently, the Optical Transient Detector (OTD) and Lightning Imaging Sensor (LIS) lightning flash rates have served similar purposes (Kartalev *et al*. 2004a, b, Odzimek *et al*. 2009). Price *et al.* (1997) were probably the first to use satellite observations of cloud properties and cloud cover from the International Satellite Cloud Climatology Project (ISCCP) data sets in their GEC cloud generator model, which was a significant step forward in the modelling of the GEC cloud generators.

As far as ionospheric and magnetospheric generators are considered, the ionospheric and magnetospheric dynamo effects have been incorporated in the model of Roble and Hays (1979). Kartalev *et al.* (2004b) considered the effect of the ionospheric

Table 1

Summary of high-resolution GEC models: HR79 (Hays and Roble 1979), RH79 (Roble and Hays 1979), MO84 (Makino and Ogawa 1984), SV90 (Sapkota and Varshneya 1990), EGATEC09 (Odzimek *et al*. 2009). Main features of the models are shown, in terms of the treatment of the atmosphere-ionosphere medium (upper table) and the electric generators considered in each model (bottom table)

Atmosphere-Ionosphere Medium											
Model	SI 1	CR 2	RA 3	AE 4	CCN 5	GMF 6	NEU 7	ION 8	Spatial Variations	Time Variations	Other Data and Models Used
Mathematical											
HR79	+	–	–	–	–	–	–	–	Geo(1)	I(1)	
RH79	+	–	–	–	–	–	–	–	Geo(1)	I(1)	
Engineering											
MO84	+	–	–	–	–	–	–	–	Lat(1)	I(2)	
MO85	–>	+	+	+	+	–	+	–	Geo(2-4,7)	I(2)	
SV90	–>	+	+	+	+	–	+	–	Geo(2-4)	I(2,4)	SA76(7)
EGATEC09	–>	+	+	+	+	+	+	–	Geo(2-7)	DD(5,7), S(4), SC(2)	TZ06(2-6) MSIS-E(7)

Model	THU 1	SHC 2	IDYN 3	ICONV 4	Spatial Variations	Time Variations	Other Data and Models Used
Mathematical							
HR79	+	–	–	–	Geo(1)	D(1)	
RH79	+	–	+	+	Geo(1,4)	D(1), I(3,4)	RC76(3), HE77(4)
Engineering							
MO84	+	–	–	–	Geo(1)	D(1)	DMSP(1)
MO85	+	–	–	–	Geo(1)	D(1)	MO84(1)
SV90	+	–	–	–	Geo(1)	D(1)	MO84(1)
EGATEC09	+	+	–	–	Geo(1-2)	DD, D, S(1)	ISCCP, OTD/LIS, TRMM(1-2)

Description: Sign "+" indicates the presence and "–" absence of an element in the model. The elements of the atmosphere-ionosphere medium include: SI – atmospheric ion conductivity, CR – ion production by cosmic rays, RA – ion production by natural radioactivity, AE – aerosols, CCN – cloud condensation nuclei, GMF – geomagnetic field, NEU – neutral atmosphere, ION – ionospheric conductivities. SI or more advanced model of conductivity derived from CR, RA, AE and CCN could be used – such case is indicated by "–>". The electric generators include: THU – thunderstorms, SHC – shower clouds or non-thunderstorm clouds, IDYN – ionospheric dynamo, ICONV – ionospheric convection. Last two columns inform about spatial and time variation which can be obtained with each model, as well as the model elements which cause these variations, in brackets. "Lat" indicates variations depending on geographical latitude, and "Geo" – variations both in latitude and longitude; the spatial resolution is usually 5 degrees in both longitude and latitude. Time variations are: DD – day-to-day, D – diurnal average, S – seasonal, SC – solar cycle, I – irregular (e.g., due to solar events or cosmic rays Forbush decrease type of events). Other necessary datasets and models used in each of the GEC model are listed in the last column, including the GEC element they refer to, in brackets; these are: DMSP – Defense Meteorological Satellite Programme lightning flash rates (Turner and Edgar 1982), OTD/LIS – Optical Transient Detec-

tor/Lightning Imaging Sensor lightning flash rates (Christian *et al*. 1999, 2003), ISCCP – International Satellite Cloud Climatology Project cloud data (Rossow and Schifer 1991), TRMM – Tropical Rainfall Measuring Mission precipitation data (Kummerow *et al*. 1998), MSIS – Mass Spectrometer Incoherent Scatter neutral atmosphere model (Hedin 1991), TZ06 – Tinsley and Zhou (2006) atmospheric conductivity model, RC76 – Richmond (1976) empirical ionospheric dynamo field model, HE77 – Heppner (1977) empirical ionospheric convection model.

convection and Makino and Takeda (1984) and Kartalev *et al*. (2004a) considered the effect of non-equipotential and magnetised ionosphere.

The effects resulting from changes of conductivity during events such as major solar flares or Forbush decreases on natural profiles of the atmospheric conductivity and the global circuit have also been investigated in some of the GEC models mentioned above (e.g., Hays and Roble 1979, Roble and Hays 1979, Makino and Ogawa 1984, 1985, Sapkota and Varshneya 1990).

2.1 High-resolution engineering models

Representation of the GEC in the form of a simple electrical circuit has been used many times ever since the modelling work on GEC started, either as a quantitative illustration of the current flow in the GEC and relationships between the GEC components and agents (Markson 1978, Willett 1979, Ogawa 1985, Tinsley 1996, Rycroft *et al*. 2000) or as the background environment of a single cloud current source which was analysed in more detail (Nisbet 1983, 1985a, 1985b, Rycroft *et al*. 2007, Rycroft and Odzimek 2009a, b).

In some high-resolution models this "engineering" approach has also been exploited. This draws from the possibility of modelling the global atmospheric electric circuit as a network of electrical elements, resistances and current sources, using input from data sets and models, and, if numerical solution is not straightforward simulating the circuit using electrical engineering software.

The model of Makino and Ogawa (1984) is a 5-degree resolution model of GEC with thunderstorm current sources and atmospheric resistance distributed over the globe and represented as a network of branches consisting of 72×36 resistances. The circuit elements were connected in parallel between two circuit nodes representing the ideally conducting ground and the ionosphere. This enabled to solve the circuit analytically relatively straightforward.

Makino and Ogawa (1985) and Sapkota and Varshneya (1990) used the same method and current source distribution but introduced significant improvements in the atmospheric conductivity model, which is an integral part of any GEC model. EGATEC is a new high resolution electrical engineering model which we describe in more detail in Section 4.

3. Some outstanding issues related to GEC and GEC models

Williams (2009) has recently reviewed current state of knowledge about the Earth's global atmospheric circuit. Even though this topic has been present in research for almost one hundred years, some fundamental questions remain unanswered. These

questions concern, for example, variations in the GEC on different time scales. In the first place, the dominance of the American tropospheric electric activity centre over that in the African and Asian sectors which is observed in the Carnegie Curve, or diurnal variation, is not well explained, and two very different explanations have been suggested (Williams and Sátori 2004, Kartalev *et al*. 2004a). Also, different trends in the last decades' variation of the GEC have been reported from observations. Williams (2009) discusses this latter problem in detail. Long-term variations of the GEC, on time-scales longer than a decade remain also unknown.

Standard values of the main GEC parameters cited in GEC-related publications broadly agree with various observations but these estimates may be far from accurate on particular days and in particular regions. Realistic modelling of the GEC can provide answers to some of the questions and test various hypotheses, but this requires progress in the modelling of various GEC components, mainly the lower atmosphere as well as magnetosphere and ionosphere current generators. Tinsley and Zhou (2006) describe the situation as follows: "An accurate value for the total upward current supplied to the ionosphere has not been determined; instead, it is estimated at 700-2000 A on the basis of estimates of ionospheric potential (150-600 kV) from tropospheric potential measurements extrapolated through the stratosphere, and estimates of the column resistance of the global ionosphere-Earth return path (200-300 Ω) from conductivity measurements and their extrapolations. These values roughly agree with similarly uncertain estimates of the upward current per thunderstorm and the total number of thunderstorms occurring at any one time. Thus the uncertainties are compatible with additional sources of current from nonthunderstorm shower clouds, and additional sources of column resistance in the stratosphere and troposphere due to aerosol layers, water vapor and clouds, which have not been considered previously". Below we summarise some specific problems that require further consideration and studies in order to improve successful GEC modelling. Many of them are related to the issues mentioned by Williams (2009), which concern the knowledge of the Earth's GEC in general.

3.1 Contribution of particular cloud systems

The charge structure of various thunderstorm systems has been studied recently by Stolzenburg and Marshall and colleagues (Stolzenburg and Marshall 2008, and references therein). These studies have revealed multi-layer charge structures (i.e., more charge layers in addition to the main structure) and that the structure differs in different storms (e.g. small isolated storms, supercells or mesoscale systems), and also varies in different areas of the storm (e.g. convective part, cloud anvil, precipitation region). It was also discovered that the large stratiform areas of Mesoscale Convective Systems (MCSs) may have a discharging effect on the global circuit; early modelling results by Davydenko (2004) have indicated 20 A downward conduction current driven by these systems. Later estimates also give positive values of the same order depending on the charge structure of these stratiform areas. Thus, the total contribution of some thunderstorm system to the GEC may vary from storm to storm.

Mach *et al*. (2009) have recently published a summary of the results of measurements of the conduction currents above thunderstorm systems in the southeastern US, western Atlantic Ocean, the Gulf of Mexico, central America, central Brazil and the

South Pacific north of Australia. These results confirm that in the majority of cases electric currents flow upwards and charge the ionosphere positively. But there are about 7% cases of storms where the current flows downwards, thus discharging the ionosphere. They also note that it was unclear whether this was due to an inverted main charge structure in these storms or perhaps the effect of the charge of the screening layer at the top of the cloud. It is perhaps worth noting that a similar percentage (7-10%) of inverted charge structures have been observed in non-thunderstorm clouds (Imyanitov and Shifrin 1962). It is not clear why some clouds may have those inverted charge structures. What has been usually observed is that the charge and electric field structure depends greatly on the microphysics of the clouds (see, for example, Chalmers 1958, Imyanitov *et al*. 1974, MacGorman and Rust 1998). Our conclusion is that future models of cloud generators should take into account regional characteristics of electrified cloud systems and also incorporate some microphysical cloud parameters.

3.2 Role of electric discharges

It is generally accepted that tropospheric cloud-to-ground (CG) lightning discharges contribute to the dc global atmospheric circuit by transferring the electric charge from the cloud to the ground: negative – negative charge to the ground (i.e., charge the ionosphere positively with respect to the ground), positive – positive charge to the ground (i.e., discharge). Contribution from intra-cloud discharges have not been usually considered with respect to the GEC.

Even though the contribution of lightning current in the total GEC current seems to be less than previously considered (Williams Heckman 1993, Williams and Sátori 2004, Rycroft *et al*. 2007, Maggio *et al*. 2009) the magnitude of this current is still not known very well. Global rates of the lightning discharges are known more accurately, mainly from satellite observations (Turman and Edgar 1982, Christian *et al*. 2003). It is the electric charge transferred by an average lightning discharge (in the sense of the lightning's current amplitude and polarity) that is not very well known, or, alternatively, the charge transferred by negative, positive and intra-cloud discharges separately. This issue is discussed in Odzimek *et al*. (2009).

The discovery of the upper atmosphere lightning discharges (or Transient Luminous Events, TLEs) have brought in the last two decades more attention to the electric activity of particulary active thunderstorm systems, like the MCSs, and positive cloud-to-ground lightning discharges, which are usually associated with sprites, the most commonly observed TLEs (Füllekrug *et al*. 2006). Although the positive CGs discharges are rarer than negative (10-15% of all CGs), and usually have single return stroke, their charge transfer is large due to the long-lasting and strong continuing currents which they often exhibit; these continuing currents seem to play a role particularly in the creation of carrot sprites (Rycroft and Odzimek 2009a, b). Model results by both Price *et al*. (1997) and Rycroft *et al*. (2007) show that globally the net effect of the more frequent negative CGs is larger than the opposite effect of positive CGs, although the magnitude of the total lightning current differs in these two models by factor of ten, mainly due to different value of charge transferred by an average lightning discharge, used in their models. Füllekrug and Rycroft (2006) and Rycroft *et al*. (2007) showed that the effects of a sprite on the circuit was to discharge it but

the effect was relatively very small. Cummer *et al*. (2009) have calculated that the charge transfer in some cases of gigantic jets recently observed in the US were of the order of charge transferred by strong CGs but, in the case of these TLEs, the rates of occurrences are rather poorly known (the occurrences rate of sprites has been estimated so far, on the basis of available measurements, Ignaccolo *et al*. 2006), and neither the total contribution can be determined very well. Some recently developed techniques of the analysis of observations of magnetic field generated by lightning discharges, in the extremely low frequency range (Kułak *et al*. 2006, 2009), can be helpful in accurate determination of the current contribution of cloud-to-ground lightning discharges in future.

With regard to intra-cloud lightning discharges, a simulation by Rycroft and Odzimek (2009a) showed that a 10 kA intra-cloud discharge between bottom negative layer and upper positive layer in their model thundercloud discharged the ionosphere by 2 C, indicating that intra-cloud discharges do have some effect and it is to discharge the circuit if the discharge reduces the voltage created by the separation of charges inside a cloud (which normally causes charging of the ionosphere positively). Recent observations also acknowledge the effect of intra-cloud flashes (see e.g. Maggio *et al*. 2009). Taking into account that intra-cloud discharges are the major fraction (~85%) of all lightning discharges this result complicates our understanding of the role of lightning discharges in the circuit.

More importantly, not only the lightning current seems to be an issue. In fact, the relative contribution of conduction, precipitation current and corona (point discharge) current are poorly determined. Measurements provide a wide range of current density values for each of these processes which often are of opposite sign and of the order or comparable to the total current density which can be associated to a cloud system (Imyanitov and Shifrin 1962, MacGorman and Rust 1998). Williams and Heckman (1993) show examples of the diurnal variation of point discharge and precipitation current from single sites concluding that next to conduction currents, they contribute the most to maintaining the high potential of the ionosphere. However, Imyanitov and Shifrin (1962) pointed out that the current budget may be different at different locations. This issues require serious modelling efforts combined with observation campaigns of various cloud systems in different regions of the globe and different time of season, similar to the work of Nisbet (1985b), Michnowski *et al*. (1987), Nisbet *et al*. (1990a, b). Such models are practically nonexistent for non-thunderstorm clouds, except perhaps the model by Chalmers (1958) of the altitude profile of the electric potential in snow and rain Nimbostratus clouds, created on the basis of electric current density and potential gradient measurements under these clouds in the UK.

3.3 Thunderstorm current and non-thunderstorm current

Even though shower clouds have been considered to generate electric current in the GEC, their contribution has not been determined so far. The electric activity of non-thunderstorm clouds has been studied more extensively in the former USSR – see e.g. Imyanitov and Shifrin (1962), Imyanitov *et al*. (1974) and MacGorman and Rust (1998, Chapter 2). The interpretation of these results indicates that the mid-layer clouds such as Nimbostratus may charge the ionosphere positively. Measurements of

current density under Nimbostratus in the UK by Harrison and Nicoll (2008) are in broad agreement with the modelled current contribution of shower clouds in Rycroft *et al*. (2007), who estimated the non-thunderstorm current as 40% of the total GEC current. The effect of non-thunderstorm clouds has been also modelled recently with EGATEC model (Odzimek *et al*. 2009, Section 4). Preliminary results from this model are that the thunderstorm contribution is ~80% *versus* ~20% from non-thunderstorm clouds. This requires further investigation. In addition, the uncertainties mentioned in the previous subsection, in relation to the role of MCSs, the role of precipitation, corona and lightning current, further complicate this issue.

3.4 Cloud conductivity

The electric conductivity is critical parameter in any electrical circuit, including GEC. While significant progress has been made to model air conductivity including the effect of aerosols (Sapkota and Varshneya 1990, Tinsley and Zhou 2006) there are less advances in GEC models in the electric conductivity of cloudy air, especially in various types of clouds. Considering that clouds cover ~50% of the Earth and that cloud conductivity can be a few times less than that of free air (Imyanitov and Shifrin 1962, MacGorman and Rust 1998), there must be a significant contribution of clouds to the total atmospheric resistance. This includes the resistance of clouds-current generators (which has been considered in some models, e.g., Makino and Ogawa (1984, 1985), Sapkota and Varshneya (1990), Rycroft *et al.* (2007) and also clouds which are rather passive. The conductivity of thunderclouds is an interesting issue on its own, as discussed in MacGorman and Rust (1998, Chapter 7).

It should also be noted here that the model results mentioned in the previous paragraphs by Davydenko *et al*. (2004) or Rycroft *et al*. (2007), related to the contribution of cloud current to the GEC, are very sensitive to the cloud conductivity which was used in those models. Therefore, it is important to use realistic models of the conductivity.

3.5 Coupling to the magnetosphere-ionosphere current system

The GEC is linked directly with space weather effects of the electrodynamics of the interaction between the solar wind and the Earth's magnetic field. This effect has always been evident particularly at high latitudes where the ionospheric convection affects the electric field at the ground the most (Burns *et al*. 1995, Tinsley 1998, Frank-Kamenetsky *et al*. 1999, Corney *et al*. 2003, Michnowski *et al*. 2007, and references to earlier papers therein) but can also be significant at middle latitudes (Nikiforowa *et al*. 2005, Kleimenowa *et al*. 2008). In the analysis of observations of the potential gradient in Antarctic these effects have been usually subtracted from the effect of lower atmosphere generators using various empirical models of the potential difference caused by the magnetospheric generators, for example, model by Heppner (1977) or more recent Weimer (1996) and IZMEM model by Papitashvili *et al*. (1994). These models calculate the potential difference over a specific location from a statistical potential pattern parametrised by the components of the interplanetary magnetic field; the latter could be obtained from satellite observations. But as far as high-resolution GEC models are concerned, since the model by Roble and Hays (1979) and recent

work by Kartalev *et al*. (2004b) there seems to be no significant update on the modelling of the combination of the lower atmosphere and the ionosphere-magnetosphere current systems, although modelling of the latter components has improved over the years (Roble 1991). This can now be improved using new observations of the plasma flow at ionospheric heights with high frequency radar technique. This was established as continuous monitoring in the 1990's, by the radar network SuperDARN, currently run by an international consortium of nine countries. SuperDARN (Chisham *et al*. 2007) currently consists of twenty operational radars in the northern and southern hemispheres which are able to monitor the high latitude electric field on a continuous basis. There are plans to expand the network equatorwards to form StormDARN, which will enable the electric field during highly disturbed intervals, geomagnetic storms, to be measured.

The SuperDARN observations available at present give an opportunity to revise this particular model component using the ionospheric electric potential patterns calculated from the SuperDARN observations (Ruohoniemi and Greenwald 1996). These SuperDARN polar cap potential data, necessary for the evaluation of higher latitude current generators (Chisham *et al*. 2007), are available from 1995 onwards with the best coverage in both hemispheres from 2000 onwards. The developing StormDARN should provide more material for the modelling of such effects at middle latitudes in near future.

As far as the impact of the ionospheric dynamo on the GEC is considered, it is expected that wind models, such as the Horizontal Wind Model (HWM, Hedin 1996) or the Thermosphere-Ionosphere Electrodynamics General Circulation Model (TIE-GCM) (Richmond *et al.* 1992) can provide the necessary input.

4. EGATEC

The Engineering model of the Global Atmospheric Electric Circuit (EGATEC) was proposed to start the development of a novel engineering quasi-3D model of the Earth's DC global atmospheric electric circuit at the University of Leicester. EGATEC is a high-resolution electrical engineering model.

In the current version of EGATEC, the lower atmosphere current generators are modelled with current sources. The coverage of the generators is determined on the basis of the satellite measurement of surface area covered by various types of clouds, available from the ISCCP cloud data (Rossow and Schiffer 1991), and TRMM (Tropical Rainfall Measuring Mission, Kummerow *et al*. 1998) precipitation. Model current densities produced by the cloud generators are used, derived from available observations of the electric activity of such clouds, in particular the satellite OTD/LIS lightning flash rates. The area of the globe where the electric current is generated as well as current source-free area can be estimated with the spatial resolution of 5 degrees in latitude and longitude and 3 hour time resolution, which is mainly limited by the ISCCP D1 data resolution. The resistance load of the atmosphere is calculated using the atmospheric conductivity model by Tinsley and Zhou (2006) which is also spatially dependent and has the same spatial resolution. The current sources and resistance of the cloud generators and resistance of the cloud-free area associated with a latitude and longitude in a model grid create one circuit branch. These branches can be

connected in a network and create an electric circuit representing the GEC which can be solved either numerically according to the standard circuit theory or using a circuit simulation software PSpice. A result of such calculation or simulation is the global distribution and diurnal variation of the main GEC variables.

Nisbet (1983) was the first to introduce the idea of using circuit analysis software for simulations of a network representing a thunderstorm and its electrical environment (i.e., GEC) and used the Electrical Circuit Analysis Program (ACAP). Many of these programs are available on different system platforms for today's computers. For example, SPICE, developed at the University of Berkeley, is a general-purpose circuit simulation program for DC, AC and transient analyses (Kielkowski 1995, Dobrowolski 2004). SPICE is currently available in some software packages (as PSpice) and the capability of this simulator is sufficient to create a high-resolution model of the DC global atmospheric electric circuit, with parameters distributed with latitude, longitude and altitude, and including simultaneously the effect of various processes operating in the circuit more realistically.

In EGATEC the air-Earth electric current density due to lower atmosphere current generators and vertical electric field can be calculated with the spatial and time resolution used for the input data. The total GEC current can also be calculated. The circuit can be constructed assuming the ionosphere as equipotential or non-equipotential surface while the ground is always assumed to be an ideally conducting surface. The main advantages of this model are:

- Input to the model is based on currently available satellite observations of clouds and cloud properties and activity, and the model includes a model of atmospheric conductivity. The model treats clouds more realistically by taking into account the role of the cloud conductivity in the global resistance and by assessing of the contribution of clouds as current generators;
- The main GEC parameter can be obtained at 3-hour time resolution and global distributions of the air-Earth current density and electric field at spatial resolution of 5 degrees in geographic coordinates;
- The model can be used for investigations of diurnal and seasonal variations of the GEC;
- The model is a high-resolution representation of the global atmospheric electric circuit created using an equivalent electric network. Standard algorithms and software can used for calculating and solving the model circuit.

The next version of EGATEC is under development and the developments include:

- Modelling of the coupling to the ionosphere-magnetosphere current system;
- Increasing spatial resolution of the model;
- Input from observed aerosol concentrations;
- Improving cloud generator model and cloud conductivity model.

5. Conclusions

The GEC is a global phenomenon and represents all natural static electric forces affecting the environment on both regional and global scales. However, there remain

many unresolved questions about the GEC and many GEC-related phenomena and processes are not fully understood or determined. It is necessary to not only continue monitoring the circuit by observations but also to improve our understanding through modelling and simulations of the GEC and its effects.

Developments of new techniques for measuring different electrical parameters and new findings in the area of atmospheric electricity require newer models and re-examination of previous results. Thus, the necessity of the development of such a model that treats realistically the overall processes contributing to the phenomenon. New facilities, measurements and projects that have been established worldwide can support GEC-related research and enable the electrical effects of the global electric circuit in the atmosphere to be established. Such facilities provide various useful data-sets which together with new modelling tools will lead to major improvements in modelling the global atmospheric circuit.

Acknowledgments. We would like to thank the Editors for the invitation to contribute to this special publication. A. Odzimek acknowledges support from the European Commission through the Marie Curie European Reintegration Grant No. PERG-GA-2007-203298 within the 7th European Community Framework Programme (FP7).

References

Burns, G.B., M.H. Hesse, S.K. Parcell, S. Malachowski, and K.D. Cole (1995), The geoelectric field at Davis station, Antarctica, *J. Atmos. Terr. Phys*. **57**, 14, 1783-1797, DOI: 10.1016/0021-9169(95)00098-M.

Chalmers, J.A. (1959), The electricity of Nimbo-Stratus clouds. **In:** L.G. Smith (ed.), "Recent Advanaces in Atmospheric Electricity", Pergamon Press, London, pp. 309-315.

Chisham, G., M. Lester, S.E. Milan, M.P. Freeman, W.A. Bristow, A.Grocott, K.A. McWilliams, J.M. Ruohoniemi, T.K. Yeoman, P.L. Dyson, R.A. Greenwald, T. Kikuchi, M. Pinnock, J.P.S. Rash, N. Sato, G.J. Sofko, J.-P. Villain, and A.D.M. Walker (2007), A decade of the Super Dual Auroral Radar Network (SuperDARN): scientific achievements, new techniques and future directions, *Surv. Geophys.* **28**, 1, 33-109, DOI: 10.1007/s10712-007-9017-8.

Christian, H.J., R.J. Blakeslee, D.J. Boccippio, W.L. Boeck, D.E. Buechler, K.T. Driscoll, S.J. Goodman, J.M. Hall, W.J. Koshak, D.M. Mach, and M .F. Stewart (2003), Global frequency and distribution of lightning as observed from space by the Optical Transient Detector, *J. Geophys. Res*. **108**, D1, 4005, DOI: 10.1029/2002LD002347.

Christian, H.J., R.J. Blakeslee, S.J. Goodman, D.A. Mach, M.F. Stewart, D.E. Buechler, W.J. Koshak, J.M. Hall, W.L. Boeck, K.T. Driscoll, and D.J. Boccippio (1999), The Lightning Imaging Sensor. **In:** "Proceedings of the 11th International Conference on Atmospheric Electricity", Guntersville**,** Alabama**,** June 7-11**,** pp. 746-749.

Corney, R.C., G.B. Burns, K. Michael, A.V. Frank-Kamenetsky, O.A. Troshichev, E.A. Bering, V.O. Papitashvili, A.M. Breed, and M.L. Duldig (2003), The influence of polar-cap convection on the geoelectric field at Vostok, Antarctica, *J. Atmos. Sol.-Terr. Phys*. **65**, 3, 345-354, DOI: 10.1016/S1364-6826(02)00225-0.

Cummer, S.A., J. Li, F. Han, G. Lu, N. Jaugey, W.A. Lyons, and T.E. Nelson (2009), Quantification of the troposphere-to-ionosphere charge transfer in a gigantic jet, *Nature Geoscience* **2**, 617-620, DOI: 10.1038/ngeo607.

Davydenko, S.S., E.A. Mareev, T.C. Marshall, and M. Stolzenburg (2004), On the calculation of electric fields and currents of mesoscale convective systems, *J. Geophys. Res*. **109**, D11103, DOI: 10.1029/2003JD003832.

Dobrowolski, A. (2004), *Under the mask of SPICE*, 232 pp., BTC Publishing, Warszawa (in Polish).

Frank-Kamenetsky, A.V., G.B. Burns, O.A. Troshichev, V.O. Papitashvili, E.A. Bering, and W.J.R. French (1999), The geoelectric field at Vostok, Antarctica: its relation to the interplanetary magnetic field and the cross polar cap potential difference, *J. Atmos. Sol.-Terr. Phys.* **61**, 18, 1347-1356, DOI: 10.1016/S1364-6826(99)00089-9.

Füllekrug, M., and M.J. Rycroft (2006), The contribution of sprites to the global atmospheric electric circuit, *Earth Planets Space* **58**, 9, 1193-1196.

Füllekrug, M., E.A. Mareev, and M.J. Rycroft (eds.) (2006), *Sprites, Elves and Intense Lightning Discharges*, NATO Science Series. Series II: Mathematics, Physics and Chemistry **225**, Springer, Dordrecht., 398 pp.

Harrison, R.G. (2004), The global atmospheric electrical circuit and climate, *Surv. Geophys.* **25**, 5-6, 441-484, DOI: 10.1007/s10712-004-5439-8.

Harrison, R.G., and M.H.P. Ambaum (2008), Enhancement of cloud formation by droplet charging, *Proc. R. Soc. A* **464**, 2098, 2561-2573, DOI: 10.1098/rspa.2008.0009.

Harrison, R.G., and K.A. Nicoll (2008), Air-earth current density measurements at Lerwick; implications for seasonality in the global electric circuit, *Atmospheric Research* **89**, 1-2, 181-193, DOI: 10.1016/j.atmosres.2008.01.008.

Hays, P.B., and R.G. Roble (1979), A quasi-static model of global atmospheric electricity. 1 – The lower atmosphere, *J. Geophys. Res*. **84**, A7, 3291-3305, DOI: 10.1029/JA084iA07p03291.

Hedin, A.E. (1991), Extension of the MSIS thermosphere model into the middle and lower atmosphere, *J. Geophys. Res*. **96**, A2, 1159-1172, DOI: 10.1029/90JA02125.

Hedin, A.E., E.L. Fleming, A.H. Manson, F.J. Schmidlin, S.K. Avery, R.R. Clark, S.J. Franke, G.J. Fraser, T. Tsuda, F. Vial, and R.A. Vincent (1996), Empirical wind model for the upper, middle and lower atmosphere, *J. Atmos. Terr. Phys.* **58**, 13, 1421-1447, DOI: 10.1016/0021-9169(95)00122-0.

Heppner, J.P. (1977), Empirical models of high-latitude electric fields, *J. Geophys. Res*. **82**, 7, 1115-1125, DOI: 10.1029/JA082i007p01115.

Ignaccolo, M., T. Farges, A. Mika, T.H. Allin, O. Chanrion, E. Blanc, T. Neubert, A.C. Fraser-Smith, and M. Füllekrug (2006), The planetary rate of sprite events, *Geophys. Res. Lett*. **33**, L11808, DOI: 10.1029/2005GL025502.

Imyanitov, I.M., and K.S. Shifrin (1962), Present state of research on atmospheric electricity, *Sov. Phys. Usp.* **5**, 2, 292-322, DOI: 10.1070/PU1962v005n02ABEH003413.

Imyanitov, I.M., E.V. Chubarina, and J.W. Szwarc (1974), *Cloud Electricity*, 139 pp., Państwowe Wydawnictwo Naukowe, Warszawa (in Polish).

Kartalev, M.D., M.J. Rycroft, M. Fuellekrug, V.O. Papitashvili, and V.I. Keremidarska (2006), A possible explanation for the dominant effect of South American thunderstorms on the Carnegie curve, *J. Atmos. Sol.-Terr. Phys*. **68**, 3-5, 457-468, DOI: 10.1016/j.jastp.2005.05.012.

Kartalev, M.D., M.J. Rycroft, and V.O. Papitashvili (2004), A quantitative model of the effect of global thunderstorms on the global distribution of ionospheric electrostatic potential, *J. Atmos. Sol.-Terr. Phys.* **66**, 13-14, 1233-1240, DOI: 10.1016/j.jastp.2004.05.012.

Kelley, M.C. (2009), *The Earth's ionosphere*, International Geophysics Series, 556 pp., Academic Press, second edition.

Kielkowski, R.M. (1995), *Inside SPICE*, 258 pp., McGraw-Hill.

Kleimenova, N.G., O.V. Kozyreva, S. Michnowski, and M. Kubicki (2008), Effect of magnetic storms in variations in the atmospheric electric field at midlatitudes, *Geomagnetism and Aeronomy* **48**, 5, 622-630, DOI: 10.1134/S0016793208050071.

Kubicki, M., Michnowski, S., Mysłek-Laurikainen, B. (2007), Seasonal and daily variations of atmospheric electricity parameters registered at the Geophysical Observatory at Świder (Poland) during 1965-2000**. In:** Proceedings of the 13 Conference on Atmospheric Electricity, Beijing, China, I, p. 50-54.

Kułak, A., Z. Nieckarz, and S. Zięba (2009), Observations of ELF transients produced by intense atmospheric events 1. Analytical description of intense lightning discharges, *J. Geophys. Res*., submitted.

Kułak, A., J. Młynarczyk, S. Zięba, S. Micek, and Z. Nieckarz (2006), Studies of ELF propagation in the spherical shell cavity using a field decomposition method based on asymmetry of Schumann resonance curves, *J. Geophys. Res*. **111**, A10304, DOI: 10.1029/2005JA011429.

Kummerow, C., W. Barnes, T. Kozu, J. Shiue, and J. Simpson (1998), The Tropical Rainfall Measuring Mission (TRMM) sensor package, *J. Atmos. Oceanic Technol.* **15**, 3, 809-817.

Leblanc, F., K.L. Aplin, Y. Yair, R.G. Harrison, J.P. Lebreton, and M. Blanc (eds.), (2009), *Planetary Atmospheric Electricity*, Space Science Series of ISSI, 532 pp., Springer.

MacGorman, D., and W.D. Rust (1998), *The electrical nature of storms*, 422 pp., Oxford University Press, New York.

Mach, D.M., R.J. Blakeslee, M.G. Bateman, and J.C. Bailey (2009), Electric fields, conductivity, and estimated currents from aircraft overflights of electrified clouds, *J. Geophys. Res.* **114**, D10,204, DOI: 10.1029/2008JD011495.

Maggio, C.R., T.C. Marshall, and M. Stolzenburg (2009), Transient currents in the global electric circuit due to cloud-to-ground and intracloud lightning, *Atmospheric Research* **91**, 2-4, 178-183, 13th International Conference on Atmospheric Electricity – ICAE 2007, DOI: 10.1016/j.atmosres.2008.07.008.

Makino, M., and T. Ogawa (1984), Responses of atmospheric electric field and air-earth current to variations of conductivity profiles, *J. Atmos. Terr. Phys*. **46**, 431-445.

Makino, M., and T. Ogawa (1985), Quantitative estimation of global circuit, *J. Geophys. Res*. **90**, D4, 5961-5966, DOI: 10.1029/JD090iD04p05961.

Makino, M., and M. Takeda (1984), Three-dimensional ionospheric currents and fields generated by the atmospheric global circuit current, *J. Atmos. Terr. Phys*. **46**, 3, 199-206.

Markson, R. (2007), The global circuit intesity: its measurement and variation over the last 50 years, *Bull. Amer. Meteorol. Soc*. **88**, 2, 223-241.

Markson, R. (1978), Solar modulation of atmospheric electrification and possible implications of the sun-weather relationship, *Nature* **273**, 103-109, DOI: 10.1038/273103a0.

Michnowski, S., M. Kubicki, N. Kleimenova, N. Nikoforova, O. Kozyreva, S. Israelsson (2007), The polar ground-level electric field and current variations in relation to solar wind changes. **In:** Proceedings of the 13th International Conference on Atmospheric Electricity, Beijing, China, I, p. 9-12.

Michnowski, S. (1998), Solar wind influences on atmospheric electricity variables in polar regions, *J. Geophys. Res*. **103**, D12, 13,939-13,948.

Michnowski, S., S. Israelsson, J. Parfiniewicz, M.A. Enaytollah, and E. Pisler (1987), A case of thunderstorm system development inferred from lightning distribution, *Publs. Inst. Geophys. Pol. Acad. Sc*. D-26, 198 pp.

Nikiforova, N.N., N.G. Kleimenova, O.V. Kozyreva, M. Kubicki, and S. Michnowski (2005), Unusual variations in the atmospheric electric field during the main phase of the strong magnetic storm of October 30, 2003, at Świder Polish midlatitude observatory, *Geomagnetism and Aeronomy* **45**, 1, 140-144.

Nisbet, J.S., T.A. Barnard, G.S. Forbes, E.P. Krider, R. Lhermitte, and C.L. Lennon (1990), A case study of the thunderstorm research international project storm of July 11, 1978 1. Analysis of the data base, *J. Geophys. Res.* **95**, D5, 5417-5433.

Nisbet, J.S., J.R. Kasha, and G.S. Forbes (1990), A case study of the thunderstorm research international project storm of July 11, 1978 2. Interrelations among the observable parameters controlling electrification, *J. Geophys. Res.* **95**, D5, 5435-5445.

Nisbet, J.S. (1983), A dynamic model of thundercloud electric fields, *J. Atmos. Sci*. **40**, 2855-2873, DOI: 10.1175/1520-0469(1983)040.

Nisbet, J.S. (1985a), Thundercloud current determination from measurements at the Earth's surface, *J. Geophys. Res*. **90**, D3, 5840-5856.

Nisbet, J.S. (1985b), Currents to the ionosphere from thunderstorm generators: a model study, *J. Geophys. Res*. **90**, D3, 9831-9844.

Odzimek, A., M. Lester, and M. Kubicki (2009), EGATEC – the Engineering model of Global Atmospheric Electric Circuit. 1. Lower atmosphere, *J. Geophys. Res*. (in preparation).

Ogawa, T. (1985), Fair-weather electricity, *J. Geophys. Res*. **90**, D4, 5951-5960.

Papitashvili, V.O., B.A. Belov, D.S. Faermark, Ya.I. Feldstein, S.A. Golyshev, L.I. Gromova, and A.E. Levitin (1994), Electric potential patterns in the northern and southern polar regions parameterized by the interplanetary magnetic field, *J. Geophys. Res*. **99**, A7, 13,251-13,262.

Park, C.G., and M. Dejnakarintra (1973), Penetration of thundercloud electric fields into the ionosphere and magnetosphere, 1. Middle and Subauroral Latitudes, *J. Geophys. Res.* **78**, 28, 6623-6633, DOI: 10.1029/JA078i028p06623.

Price, C., J. Penner, and M. Prather (1997), NO_x from lightning 2. Constraints from the global atmospheric electric circuit, *J. Geophys. Res.* **102**, D5, 5943-5951.

Rakov, V.A., and M.A. Uman (2003), *Lightning. Physics and Effects*, 687 pp., Cambridge University Press.

Richmond, A. (1976), Electric field in the ionosphere and plasmasphere on quiet days, *J. Geophys. Res*. **81**, 7, 1447-1450, DOI: 10.1029/JA081i007p01447.

Richmond, A., E. Ridley, and R. Roble (1992), A termosphere-ionosphere general circulation model with coupled electrodynamics, *Geophys. Res. Lett*. **19**, 6, 601-604.

Roble, R.G. (1985), On solar-terrestrial relationships in atmospheric electricity, *J. Geophys. Res.* **90**, D4, 6000-6012, DOI: 10.1029/JD090iD04p06000.

Roble, R.G. (1991), On modelling component processes in the Earth's global electric circuit, *J. Atmos. Sol.-Terr. Phys*. **53**, 9, 831-847.

Roble, R.G., and P.B. Hays (1979), A quasi-static model of global atmospheric electricity. II – Electrical coupling between the upper and lower atmosphere, *J. Geophys. Res.* **84**, A12, 7247-7256, DOI: 10.1029/JA084iA12p07247.

Rossow, W.B., and R.A. Schiffer (1991), ISCCP cloud data products, *Bull. Amer. Meteorol. Soc.* **71**, 2-20.

Ruohoniemi, J.M., and R.A. Greenwald (1996), Statistical patterns of high-latitude convection obtained from Goose Bay HF radar observations, *J. Geophys. Res*. **101**, A10, 21,743-21,763.

Rycroft, M.J., and A. Odzimek (2009a), Quantifying the effects of lightning and sprites on the ionospheric potential, using an analog model of the global electric circuit, and threshold effects on sprite initiation, *J. Geophys. Res*., submitted.

Rycroft, M.J., and A. Odzimek (2009b), The impact of lightning flashes and sprites on the Earth's global electric circuit: An overview of recent modeling results, *AIP Conference Proceedings* 1118, 124-135.

Rycroft, M.J., S. Israelsson, and C. Price (2000), The global atmospheric electric circuit, solar activity and climate change, *J. Atmos. Sol.-Terr. Phys*. **62**, 17-18, 1563-1576 DOI: 10.1016/S1364-6826(00)00112-7.

Rycroft, M.J., A. Odzimek, N.F. Arnold, M. Füllekrug, A. Kułak, and T. Neubert (2007), New model simulations of the global atmospheric electric circuit driven by thunderstorms and electrified shower clouds: The roles of lightning and sprites, *J. Atmos. Sol.-Terr. Phys*. **69**, 17-18, 2485-2509, DOI: 10.1016/j.jastp.2007.09.004.

Sapkota, B.K., and N.C. Varshneya (1990), On the global atmospheric electrical circuit, *J. Atmos. Terr. Phys.* **52**, 1, 1-20.

Stansbery, E.K., A.A. Few, and P.B. Geis (1993), A global model of thunderstorm electricity, *J. Geophys. Res*. **98**, D9, 16,591-16,603, DOI: 10.1029/93JD01356.

Stolzenburg, M., and T.C. Marshall (2008), Charge structure and dynamics in thunderstorms, *Space Science Reviews* **137**, 1-4, 355-372, DOI: 10.1007/s11214-008-9338-z.

Tinsley, B.A. (2008), The global atmospheric electric circuit and its effects on cloud microphysics, *Rep. Prog. Phys.* **71**, 066801, 31 pp., DOI: 10.1088/0034-4885/71/6/066801.

Tinsley, B.A. (2000), Influence of solar wind on the global electric circuit, and inferred effects on cloud microphysics, temperature, and dynamics in the troposphere, *Space Science Reviews* **94**, 1-2, 231-258, DOI: 10.1023/A:1026775408875.

Tinsley, B.A., W. Liu, R.P. Rohrbaugh, and M.W. Kirkland (1998), South Pole electric field responses to overhead ionospheric convection, *J. Geophys. Res*. **103**, D20, 26,137-26,146.

Tinsley, B.A. (1996), Correlations of atmospheric dynamics with solar wind-induced changes of air-earth current density into cloud tops, *J. Geophys. Res*. **101**, D23, 29,701-29,714.

Tinsley, B.A., and L. Zhou (2006), Initial results of a global circuit model with variable stratospheric and tropospheric aerosols, *J. Geophys. Res*. **111**, D16205, DOI: 10.1029/2005JD006988.

Turman, B., and B. Edgar (1982), Global lightning distribution at dawn and dusk, *J. Geophys. Res*. **87**, C2, 1191-1206.

Tzur, I., and R.G. Roble (1986), The interaction of a dipole thunderstorm with its global electrical environment, *J. Geophys. Res*. **90**, D4, 5989-5999.

Weimer, D.R. (1996), A flexible, IMF dependent model of high-latitude electric potentials having "space weather" applications, *Geophys. Res. Lett*. **23**, 18, 2549-2552.

Willett, J.C. (1979), Solar modulation of the supply current for atmospheric electricity?, *J. Geophys. Res*. **84**, C8, 4999-5002, DOI: 10.1029/JC084iC08p04999.

Williams, E.R. (2009), The global electrical circuit: A review, *Atmospheric Research* **91**, 2-4, 140-152.

Williams, E.R., and S.J. Heckman (1993), The local diurnal variation of cloud electrification and the global diurnal variation of negative charge on the Earth, *J. Geophys. Res*. **98**, D3, 5221-5234.

Williams, E.R., and G. Sátori (2004), Lightning, thermodynamic and hydrological comparison of the two tropical continental chimneys, *J. Atmos. Sol.-Terr. Phys*. **66**, 13-14, 1213-1231, DOI: 10.1016/j.jastp.2004.05.015.

Wilson, C.T.R. (1920), Investigation on lightning discharges and on the electric field of thunderstorms, *Phil. Trans. Roy. Soc. London, Ser. A* **211**, 73-115.

Received September 21, 2009
Accepted October 6, 2009

PUBLS. INST. GEOPHYS. POL. ACAD. SC., D-73 (412), 2009

Variations of the Mid-Latitude Atmospheric Electric Field (*Ez*) Associated with Geomagnetic Disturbances and Forbush Decreases of Cosmic Rays

Natalia KLEIMENOVA[1], Olga KOZYREVA[1], Marek KUBICKI[2], and Stanisław MICHNOWSKI[2]

[1] Institute of the Earth, Physics Russian Academy of Sciences
Bolshaya Gruzinskaya st., 10, 123995, Moscow, Russia

[2] Institute of Geophysics, Polish Academy of Sciences
Księcia Janusza 64, 01-452, Warszawa, Poland

Abstract

Observations of the atmospheric vertical electric field component (*Ez*) at the mid-latitude Polish station Świder have been analyzed during 14 strong and moderate magnetic storms. Only data recorded under the so-called "fair weather" periods have been used for this analysis. The daily *Ez* variations under quiet geomagnetic conditions were established. The seasonal *Ez* level variations have demonstrated the winter maximum and summer minimum. The effect of the main phase of magnetic storm was discovered in the daytime mid-latitude *Ez* variations during any local magnetic activity. Short-time strong negative *Ez* excursion relative to the magnetically quiet daily level has been observed in the daytime simultaneously with magnetosphere substorm onset at the night sector. The long-duration depletion of the *Ez* amplitudes was found in association with Forbush decreases of galactic cosmic rays.

The results obtained can be interpreted as a significant influence of the changes in the solar wind-magnetosphere-ionosphere system on the global electric circuit state.

1. Introduction

Variability of the atmospheric vertical electric field component (*Ez*) near the Earth surface has been investigated in many studies. It has been commonly accepted that the integrated worldwide thunderstorm activity is considered as a main source of the atmospheric electricity variations. However, different solar wind effects manifested in

geomagnetic phenomena can provide some influence on *Ez* behavior due to ionosphere electric field disturbances which may significantly control the global electric circuit state (e.g., Sao 1967, Olson 1971, Apsen *et al*. 1888, Michnowski 1998, Tinsley 2000, Rycroft *et al*. 2000). Strong manifestations of the solar wind interactions with the magnetosphere and ionosphere processes, evident especially at the auroral and polar zones, were observed in high latitude *Ez* variations (e.g., Olson 1971, Nikiforova *et al*. 2003, Kleimenova *et al*. 1995, Michnowski 1998). The physical base of the solar wind influence on the high-latitude atmospheric electricity has been pointed out by Michnowski (1998).

Recently, the effects of magnetic storms in *Ez* ground-based measurements were found also at middle latitudes (Kleimenova *et al*. 2008, Kubicki 2008). In the present paper we continue the investigations of these newly discovered effects. In addition, we extend our study on a possible influence of the cosmic rays Forbush decreases associated with magnetic storms. Effects of transmission of the ionospheric and interplanetary electric fields to the lower atmosphere are to be distinguished.

There is still a serious difficulty in separating various local meteorological effects, existing in *Ez* variations even under the "fair weather" conditions, from the changes caused by solar wind, magnetosphere and ionosphere disturbances. Here we try to explain some of these problems by including in our analysis a study of the seasonal variability of *Ez* daily distributions observed under the geomagnetically quiet periods.

2. Observations

This study is based on regular registrations of the vertical component of atmospheric electric field (*Ez*) at mid-latitude Polish geophysical observatory at Świder (geographical coordinates are $\varphi = 52^{\circ}07'$N, $\lambda = 21^{\circ}15'$E, and the geomagnetic ones are $\Phi = 47.8^{\circ}$, $\Lambda = 96.8^{\circ}$). Magnetic local noon is at ~10 UT. The instruments and their location are described by Kubicki (2001). We used the 1-hour data as well as the 1-min sampling data averaged at 5 min intervals, rejecting the short period fluctuations.

Only the data obtained during the so-called "fair weather" periods lasting through all 24 hours during the given day have been used for our analysis. The "fair weather" conditions request the absence of rain, drizzle, snow, hail, fog, lower cloudiness, local and distant thunderstorms, wind velocity exceeding 6 m/s, negative *Ez* values. Such demands in long-lasting intervals are usually seldom satisfied, so we could find not more than ~40-60 "fair weather" days in the year (i.e., ~12-15% of the total observations).

3. *Ez* diurnal variations

Historically, the diurnal global variations of the atmosphere electric field were studed during the cruises of the research vessel Carnegie in the early decades of the 20-th century. An average ground-level electric field diurnal curve (known as "Carnegie curve") with a minimum near 03-05 UT and a main maximum near 18-21 UT was obtained due to longitudinal distribution of the global centers of the thunderstorm

activity. The "Carnegie curve" is still generally accepted as a reference standard global synchronous signature of the "fair-weather" atmospheric electric field behavior. This curve was obtained in the sea regions. At middle-latitude land stations, the diurnal *Ez* variations are strongly affected by local convective turbulent currents, which are attenuated in the night and significantly enhanced with sunrise that leads to *Ez* values increasing in that time (e.g., Apsen *et al*. 1988).

To find out the possible effects of the solar wind–magnetosphere disturbances on the atmospheric electricity it is very important to establish the mid-latitude *Ez* diurnal variations under quiet geomagnetic conditions. For this analysis we used the 1-hour averaged *Ez* registrations at Świder observatory and selected about 30 days of the "fair weather" under Kp ~ 0-2 in the years 1996-2005. The daily *Ez* variations in all selected days are shown in Fig. 1.

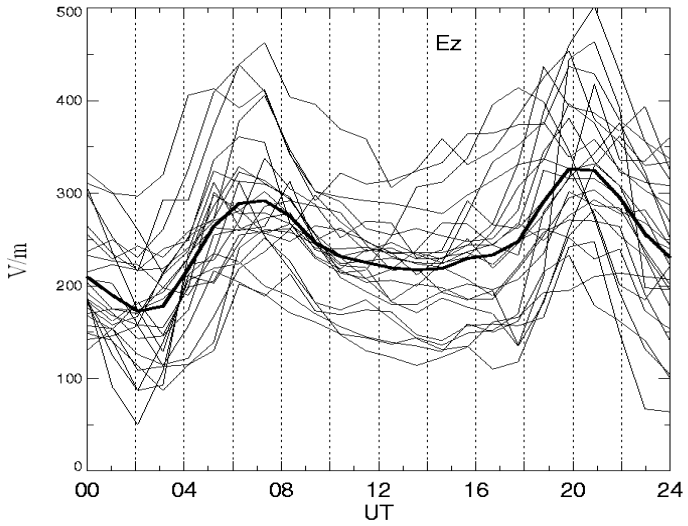

Fig. 1. The *Ez* diurnal variations at Świder under magnetically quiet periods (Kp ≤ 2); solid line – averaged quiet day data.

Despite a very strong dispersion of *Ez* amplitudes, a common tendency is seen. There were two enhancements that roughly matched the "Carnegie curve": before local noon (at ~06-10 UT, which corresponds to 08-12 MLT) and in the local evening (at ~14-18 UT, which corresponds to 16-20 MLT). These maxima correspond to the American and African thunderstorm activity centers.

In many cases, a comparison of the *Ez* measurements in two consecutive magnetically quiet days has not demonstrated any significant *Ez* amplitude differences (Fig. 2). It is possible to expect that the observed *Ez* values scattering is at least a result of the seasonal changes in the global electric circuit state, partly due to seasonal variations of the worldwide thunderstorm activity. In fact, Fig. 2 demonstrates that the *Ez* amplitude level in summer (the bottom panel) was significantly smaller (particularly the evening maximum) than that in spring (the middle panel) and in autumn (the upper panel).

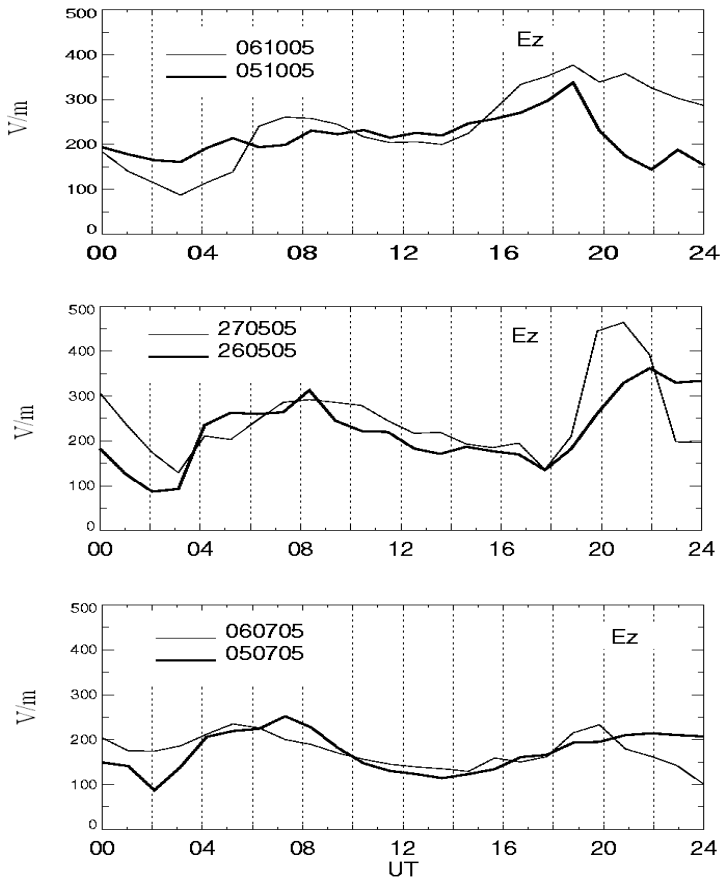

Fig. 2. Examples of the *Ez* diurnal variations in two consecutive magnetically quiet days.

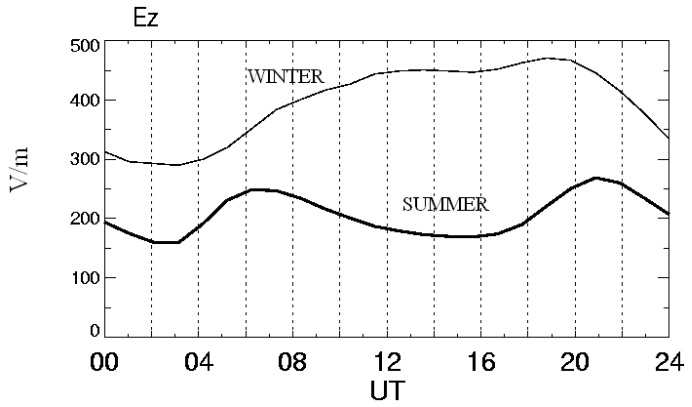

Fig. 3. The averaged diurnal *Ez* variations in winter and summer.

The statistical study of more than 30 year data (without the separation of the magnetically quiet and disturbed periods) (Kubicki *et al.* 2007) supported this assump-

tion. The daily variations of the averaged *Ez* values at Świder in the summer and winter seasons are shown in Fig. 3. The winter *Ez* values are much higher than the summer ones.

Similar seasonal *Ez* variations were reported by Adlerman and Williams (1996) with the local summer (May–September) minimum, observed at 9 mid-latitude stations at the northern hemisphere. Earlier, the same result was reported by Paramonov (1950) and Israel (1973).

In our analysis we compared the observed *Ez* amplitudes in each studied event with the *Ez* records in the previous magnetically quiet days because the application of the year-averaged fair-weather data is not correct. This is demonstrated in Fig. 4, where the 5-min sampled *Ez* variations in three consecutive magnetically quiet days are presented in comparison with the year averaged *Ez* variations (solid curve).

4. Effect of the magnetic storm main phase on the *Ez* variations

We analyzed 14 magnetic storms in 2000-2004 observed under "fair weather" periods. We use the Dst-index, the 1-min sampled solar wind and interplanetary magnetic field (IMF) parameters data collected from the OMNI base (ftp://nssdcftp.gsfc.nasa.gov/spacecraft_data/omni/high_res_omni/monthly_1min/) as well as the calculated interplanetary electric field variations. Two-day data of the May 23-24, 2000, and March 30-31, 2001, magnetic storms are presented in Fig. 5 and compared with the *Ez* observations at Świder. The previous day was the "fair weather" magnetically quiet day.

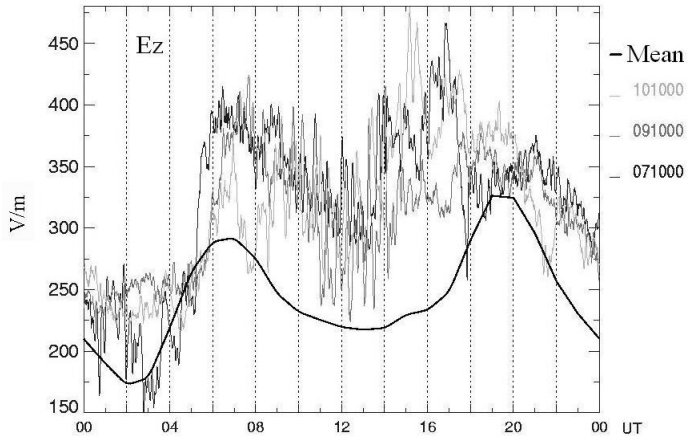

Fig. 4. The examples of the *Ez* diurnal variations in three magnetically quiet days by comparison with year averaged data (solid line in Fig. 1).

As a rule, a magnetic storm main phase development is accompanied by night side magnetosphere substorms and energetic electron precipitations in the high latitude ionosphere. The magnetograms from two auroral stations: College (CMO, $\Phi = 64.7^{\circ}$, $\Lambda = 263^{\circ}$) and Sodankyla (SOD, $\Phi = 63.8^{\circ}$, $\Lambda = 108^{\circ}$) and the mid-latitude station Belsk (BEL, $\Phi = 47.3^{\circ}$, $\Lambda = 96^{\circ}$) are shown in the lower part of Fig. 5. CMO is located at the opposite side of the Earth than Świder, thus the magnetic local noon at Świder

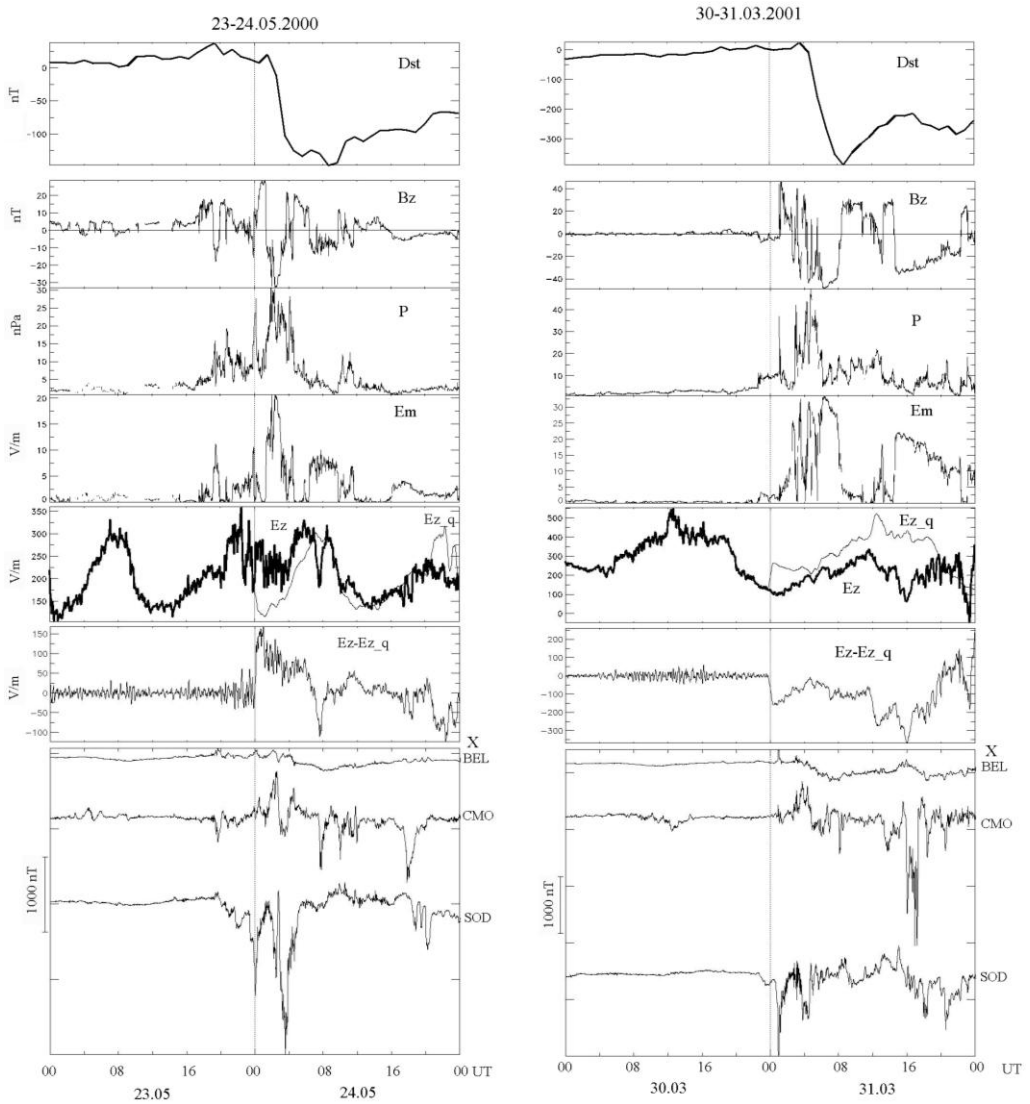

Fig. 5. Two examples of magnetic storms; from the top down: Dst-index, the interplanetary magnetic field (IMF) Bz component, solar wind dynamic pressure (P), interplanetary electric field (Em), the *Ez* observations (solid line), the difference between the observed and quiet *Ez* values, and the magnetograms at BEL, CMO, and SOD.

(~10 UT) approximately corresponded to the magnetic local midnight at CMO (~11 UT). The strong magnetic substorms were observed during the main phase of considered magnetic storms; the simultaneous negative daytime *Ez* deviations relative to the magnetically quiet *Ez* level were observed at Świder (at ~08 UT on 24.05.2000, and at 12-16 UT on 31.03.2001).

The auroral observatory SOD is located in the same longitudinal sector as Świder, and in that time there were no significant magnetic disturbances either there or at mid-latitude observatory Belsk (BEL), located not far from Świder. A similar day-

time *Ez* decrease associated with night-side substorms was typical for all analyzed magnetic storms.

5. *Ez* changes associated with Forbush decreases of cosmic rays

It is well known that one of the important effects of the solar coronal mass ejection (CME) caused magnetic storms (e.g., Cane 2000) is a Forbush decrease of the galactic cosmic rays. The Forbush decrease starts with an interplanetary shock arrival and storm sudden commencement (SSC) onset.

We have analyzed several cases of Forbush decrease observed in the course of magnetic storm. Two such examples (August 16-19, 2001, and September 10-12, 2005) are shown in Fig. 6. The AE-index represents the global night side substorm activity. One can see the strong *Ez* depletion in the days of Forbush effect development. Besides, the evening *Ez* maximum, typical for quiet daily variations, was sometimes completely ceased, as it is seen on 17.08.2001 and 11.09.2005.

Earlier, the decrease of the atmospheric electric field at times of Forbush decrease events was reported, e.g., by Apsen *et al*. (1988) and Märcz (1997), but without a comparison with the geomagnetic conditions.

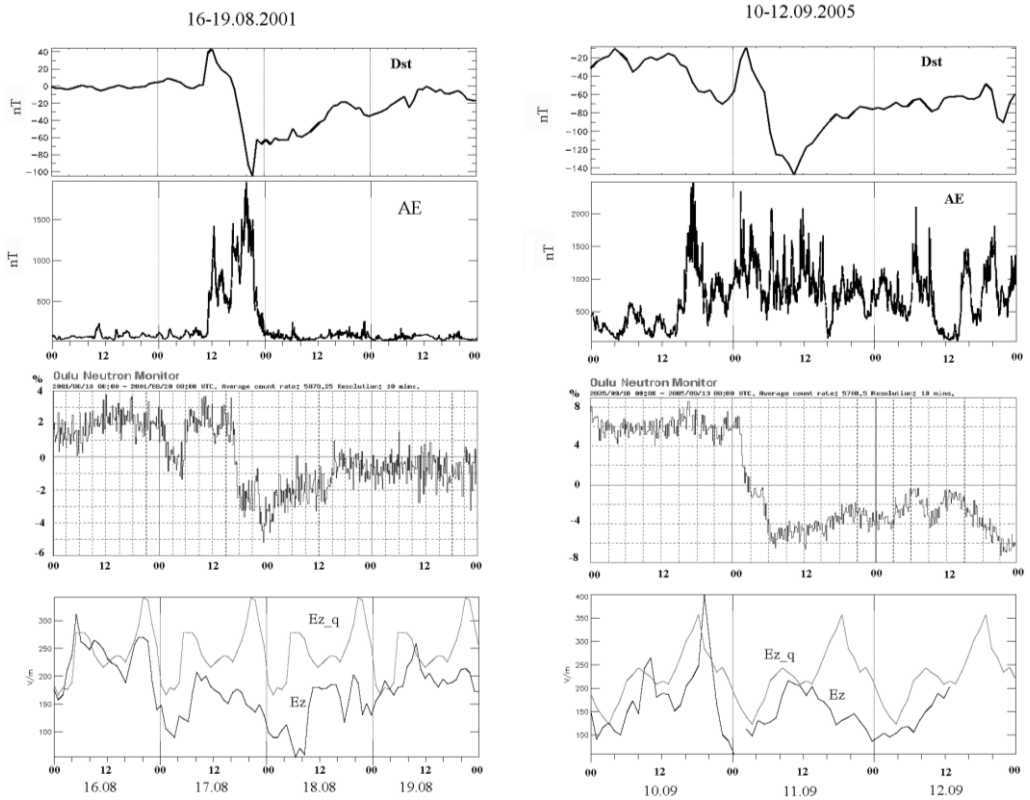

Fig. 6. Two examples of the Forbush decrease influence on the *Ez* changes; from the top down: Dst-index, auroral AE index, the data of neutral monitor in Oulu, and the *Ez* observations (solid line) in reference to the averaged magnetically quiet *Ez* variations in the correspondent season (thin line).

6. Discussion

Typically, the magnetic storm main phase is accompanied by magnetosphere substorms and corresponding strong impulsive auroral AE index magnification, associated with particle precipitation at auroral latitudes, which strongly enhances the ionosphere conductivity. The cosmic ray Forbush decreases are observed also in the main phase of magnetic storms under strong ring current enhancement due to the injection of particles from the magnetosphere tail, which later precipitate into the high-latitude ionosphere. As a result, the total resistance of the ionosphere part of the global electric circuit may decrease.

According to previous authors (e.g., Olson 1971, Apsen *et al*. 1988, Nikiforova *et al*. 2003, 2005), magnetosphere substorms and visible auroras at high latitudes are accompanied by negative night-side *Ez* anomalies. But in the presented study similar *Ez* changes were for the first time revealed at mid-latitude station Świder in the daytime. The considered effect of the storm main phase in atmospheric electricity could be a result of large-scale changes in the ionosphere part of the global electric circuit and the energetic particle precipitation into the lower ionosphere. There is one more agent that could affect the mid-latitude *Ez* variations. That is the penetration of the interplanetary electric field (Em) to the low-latitude ionosphere, as discussed by Huang *et al*. (2005). However, there is no linear dependence between the observed *Ez* effects and Em intensity (Fig. 5).

The seasonal variations of *Ez* level in the northern hemisphere demonstrate the summer minimum. It is important to mention that according to Adlerman and Williams (1996), the minimum in the *Ez* seasonal variations at the southern hemisphere stations (e.g., Buenos Aires and Johannesburg) was observed also in local summer (from October to April). It means, there is the opposite phase between the hemispheres. This fact strongly points to the dominance of a local influence over a global one. According to Lutz (1939) and Israel (1973), the seasonal variations of the atmospheric conductivity demonstrate the summer maximum, i.e., opposite to *Ez* seasonal change. The *Ez* seasonal variations appear to be the result of several seasonal factors, including the variations of the boundary layer aerosol concentration. The air conductivity increase leads to the atmospheric electric field (*Ez*) decrease.

7. Summary

1. For the first time there was found the effect of the main phase of a magnetic storm in the daytime *Ez* changes at mid-latitude as short time negative *Ez* anomalies associated with night-side magnetospheric substorm development under any local magnetic activity.

2. During the days of cosmic ray Forbush decrease development, the mid-latitude *Ez* depletion was found in comparison with magnetically quiet-time *Ez* data.

3. The season dependence of the *Ez* diurnal variations at mid-latitudes were established, demonstrating the local summer minimum and local winter maximum.

References

Adlerman, E.J., and E.R. Williams (1996), Seasonal variation of the global electric circuit, *J. Geophys. Res*. **101**, D-23, 29,679-29,688.

Apsen, A.G., Kh.D. Kanonidi, S.P. Chernishova, D.N. Chetaev, and V.M. Shefte'l (1988), *Magnetospheric Effects in Atmospheric Electricity*, Nauka, Moscow, 150 pp.

Cane, H.V. (2000), Coronal mass ejections and Forbush decreases, *Space Sci. Rev*. **93**, 1-2, 55-77, DOI: 10.1023/A:1026532125747.

Huang, C.-S., J.C. Foster, and M.C. Kelley (2005), Long-duration penetration of the interplanetary electric field to the low-latitude ionosphere during the main phase of magnetic storms, *J. Geophys. Res*. 110, A11309, DOI: 10.1029/2005JA011202.

Israel, H. (1973), *Atmospheric Electricity*. Vol. II, Fields, Charges, Currents. Published for the National Science Foundation by the Israel Program for Scientific Translation, Jerusalem, 796 pp.

Kleimenova, N.G., S. Michnowski, N.N. Nikiforova, and O.V. Kozyreva (1996), Long-period geomagnetic pulsations and fluctuations of the atmospheric electric field intensity at the polar cusp latitudes, *Geomagn. Aeron*. **35**, 4, 469-477.

Kleimenova, N.G., O.V. Kozyreva, S. Michnowski, and M. Kubicki (2008), Effect of magnetic storms in variations in the atmospheric electric field at midlatitudes, *Geomagn. Aeron*. **48**, 5, 622-630, DOI: 10.1134/S0016793208050071.

Kubicki, M. (2001), Results of atmospheric electricity and meteorological observations S. Kalinowski geophysical observatory at Świder, *Publs. Inst. Geophys. Pol. Acad. Sci*. **D-56**, 333, 3-7.

Kubicki, M., S. Michnowski, and B. Mysłek-Laurikainen (2007), Seasonal and daily variations of atmospheric electricity parameters registered at the Geophysical Observatory at Świder (Poland) during 1965-2000. **In**: Proc. 13th Inter. Conf. Atmospheric Electricity, ICAE 2007, Beijing, China, 50-54.

Kubicki, M. (2008), Atmospheric electricity research at the Institute of Geophysics in the years 2006-2007, *Publs. Inst. Geophys. Pol. Acad. Sci*. **D-72**, 403, 105-109.

Lutz, C.W. (1939), Die wichtigen luftelectrischen Gruben für München, *Gerl. Beitr. Geopys*. **54**, 337-347.

Märcz, F. (1997), Short-term changes in atmospheric electricity associated with Forbush decreases, *J. Atmos Sol.-Terr. Phys*. **59**, 9, 975-982, DOI: 10.1016/S1364-6826(96)00076-4.

Michnowski, S. (1998), Solar wind influences on atmospheric electricity variables in polar regions, *J. Geophys. Res*. **103**, D12, 13939-13948.

Nikiforova, N.N., N.G. Kleimenova, O.V. Kozyreva, M. Kubicki, and S. Michnowski (2003), Influence of auroral-latitude precipitations of energetic electrons on variations in the atmospheric electric field at polar latitudes (Spitsbergen Archipelago), *Geomagn. Aeron*. **43**, 4, 29-35.

Nikiforova, N.N., N.G. Kleimenova, O.V. Kozyreva, M. Kubicki, and S. Michnowski (2005), Unusual atmosphere electric field variations during the main phase of the huge magnetic storm of October 30, 2003 at the Polish mid-latitude station Świder, *Geomagn. Aeron*. **45**, 1, 148-152.

Olson, D.E. (1971), The evidence for auroral effects on atmospheric electricity, *Pure Appl. Geophys*. **84**, 1, 118-138, DOI: 10.1007/BF00875461.

Paramonov, N.A. (1950), On the annual variations of the atmospheric electrical potential gradient, *Dokladi, Akademya Nauk USSR* **71**, 39-40 (in Russian).

Rycroft, M.J., S. Israelsson, and C. Price (2000), The global atmospheric electric circuit, solar activity and climate change, *J. Atmos. Sol.-Terr. Phys*. **62**, 17-18, 1563-1576. DOI: 10.1016/S1364-6826(00)00112-7.

Sao, K. (1967), Correlation between solar activity and the atmospheric potential gradient at the Earth's surface in the polar regions, *J. Atmos. Sol.-Terr. Phys*. **29**, 2, 213-215, DOI: 10.1016/0021-9169(67)90135-3.

Tinsley, B.A. (2000), Influence of solar wind on the global electric circuit, and inferred effects on cloud microphysics, temperature, and dynamics in the troposphere, *Space Sci. Rev*. **94**, 1-2, 231-258, DOI: 10.1023/A:1026775408875.

Received September 1, 2009

PUBLS. INST. GEOPHYS. POL. ACAD. SC., D-73 (412), 2009

Preliminary Analysis of Dynamic Evolution and Lightning Activity Associated with Supercell Event: Case Story of the Severe Storm with Tornado and Two Heavy Hail Gushes in Poland on 20 July 2007

Jan PARFINIEWICZ[1], Piotr BARAŃSKI[2], and Wojciech GAJDA[1]

[1] Institute of Meteorology and Water Management,
01-673 Warszawa, ul. Podleśna 61, Poland

[2] Institute of Geophysics, Polish Academy of Sciences,
01-452 Warszawa, ul. Księcia Janusza 64, Poland

Abstract

A violent explosion of deep convection struck many countries in Europe on 20 July 2007. In that day, severe thunderstorms were accompanied by floods and harmful winds, and even by one 8-minute incident of tornado in Poland. In this paper we have presented the detail analysis of supercell dynamic development connected with tornado incident and the time and space behavior of its lightning activity detected by the SAFIR/PERUN network system. For this purpose, we have used reflectivity data from four Doppler radars, i.e., in Ramża, Pastewnik, Brzuchania and Legionowo, to obtain as realistic as possible history of the 3-dimensional dynamic evolution of convective complex which started to develop over south Poland. We were able to distinguish 5 stages of such a convective evolution, i.e., for the time interval 00–04 UT – the nocturnal dissipation of previous convective structures; between 04 and 10 UT – the further development and dissipation of few new convective cells; between 10 and 14 UT – the development of one large convective cluster and a new convective single cell – a precursor of the next aggregation and supercell; between 14 and 16 UT – the further growth/enlargement of the supercell; and finally between 16 and 18 UT – the mature stage of supercell with tornado near Częstochowa associated with a growth of a new convective complex developing over the Tatra mountains and Slovakia. To perform relevant interpretation of the composite radar pictures we prepared, we used two computer simulations with different grid resolutions; the first one concerned the region over Europe, with 14 km grid step and divided into 35 levels, and the other one, nested over Poland (the COSMOLM model, see Steppeler *et al*. 2003), with grid step squeezed up to 2.8 km and vertical resolu-

tion of 50 levels. Moreover, we have taken into account two additional important sources of data: the cloud coverage from satellite observations and the accompanying lightning activity from the SAFIR/PERUN detection system. The numerical forecast model applied predicted many characteristic singularities of the observed real weather situation and gave us also a possibility to get a much deeper insight into some fine mechanisms which could be considered as steering for the studied case, e.g., the occurrence of right- and left-mover wind patterns during convective development of the tornado system. We have also included to our analysis the examination of the observed lightning rate changes of particular convective complexes before and after the supercell aggregation. On the other hand, locations of positive and negative return strokes of cloud-to-ground flashes (RS_+ and RS_-), and intra cloud discharges (IC) given by the SAFIR/PERUN system in the supercell area revealed their specific clustering co-located with precipitation/hail shafts and previous widespread IC lightning activity followed by grouped $CG_\pm$ flash strokes.

Key words: supercell storm, tornado, hail gush, lightning activity, lightning detection.

1. Introduction

On July 20, 2007, about 16:05 UTC, the Rędziny, Kłomnice i Mostów regions of the Częstochowa district were struck by tornado, which destroyed dwelling houses, farm buildings, transmission lines and poles, falling down tens of hectares of forest, and displacing automobiles (Bebłot *et al*. 2007). The Katowice branch of the Institute of Meteorology and Water Management made an inspection of the site, aerial photographs, interviewed the eyewitnesses (a videotape is available), and estimated the losses. Strong hailstorms were observed an hour before, during, and after the tornado. According to the eyewitness reports, the hailstones were initially of pea size, then large and irregular ice pieces, some 5 cm or more in diameter. The ground was covered by a thick ice layer reaching to the knees. During the tornado and right afterwards, horizontally moving hailstones of a tennis-ball size were observed. The tornado trail length was about 14 km, and the width of the destruction track was up to 500 m. The mean speed of displacement was some 45 km/h. On the basis of the type of damage, the tornado was classified as between F1 and F2 in Fujita-Pearson scale (Fujita 1981), or T4 in the 11-step TORRO scale. The wind speed in the vortex could reach 60 m/s (Bebłot *et al*. 2007).

2. Measuring equipment and main sources of data

Our database prepared for examination of the considered supercell incident in Poland is based on four Doppler radar observations carried out routinely within 10 minute interval for 250 km range. These radars of METEOR 500C type and GEMATRONIK production are placed at Ramża, Pastewnik, Brzuchania and Legionowo site and are a part of the national Polish radar net named POLRAD. More information about the POLRAD net organization is available on the web site: www.pogodynka.pl.

On the other hand, all data about IC and CG lightning flashes activity detected over Poland territory and connected with the analyzed supercell and tornado occurrence were obtained from the Polish SAFIR/PERUN lightning location and detection network system. This network consists of nine VHF/LF detection stations of the type SAFIR 3000 (Vaisala 2003, Chap. 2 pp. 7-87) covering the whole Poland country and giving the lightning flash location accuracy below 1 km for 90% of that area. Additional technical data and information about basic principles of its operational and discrimination rules can be found in some manual reference books supplied by the present producer of that system (e.g., SAFIR 2001: Chap. 3, pp. 9-11, Chap. 5, pp. 16-20 and SAFIR 2003: Chap. 2, pp. 18-45).

The changes in cloud coverage over Europe in the visible light range during the analyzed severe weather condition period were taken from the satellite observations done by the EUMETSAT which were received and processed by the IMWM Department in Cracow.

3. Synoptic background

Going back to July 12, 2007, in the 300 hPa temperature field over the Atlantic the drop of cold Arctic air started moving from Greenland towards the British Isles, eventually modifying the formation of the Atlantic branch of the polar jet stream. Figure 1 presents the 300 hPa temperature field at 00 UTC on July 20, 2007, i.e., after 8 days of the cold air movement over North Atlantic. In Fig. 2 we see the isotachs which indicate the location of the polar jet stream. These two objects determined the synoptic situation which led to the explosion of convection over Europe on this day, including the tornado over Poland. The Atlantic branch of the jet stream extended northeasterly and was pumping the hot and moist tropical air masses over Europe, as shown in the 850 hPa temperature field (see Fig. 3).

In Fig. 4 we present the 315 K isentrope (potential temperature surface) with a characteristic swelling over England which represents the above-mentioned cold drop, and a jets stream embedded into it. The isobars at the 8 km level make it possible to evaluate their mutual vertical configuration. After 16 hours, the jet stream over Europe was torn away by an abrupt explosion of convection (Fig. 5), still retaining its two weakening branches: the one directed towards the British Isles and the other directed easterly, over Germany and Poland.

The synoptic situation was difficult to analyze because of the fact that the dominant driving process for the abrupt convection over Europe was an inflow in the upper troposphere of a cold arctic air over a warm and humid tropical air; such a mechanism has been well recognized in meteorology (Browning 1985). Differences in the msl synoptic analysis made by English, German, Dutch, and Polish services point to a difficulty in working out a concept how to analyze the development of upper fronts.

While the large-scale traits of synoptic process, expressed through the pressure field, horizontal wind, and even the humidity, were satisfactorily reproduced by the model, the cloud water of the convective clouds was underestimated; see Fig 6 and compare it with the satellite photo (Fig. 7).

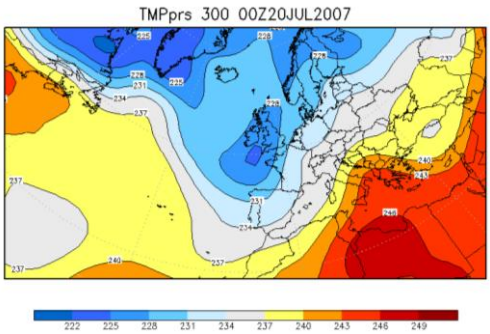

Fig. 1. July 20, 2007, 00 UTC, temperature at the 300 hPa level.

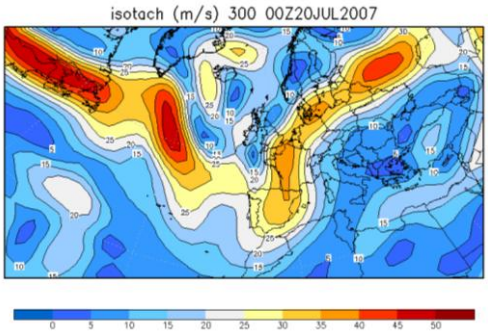

Fig. 2. July 20, 2007, 00 UTC, jet at the 300 hPa level.

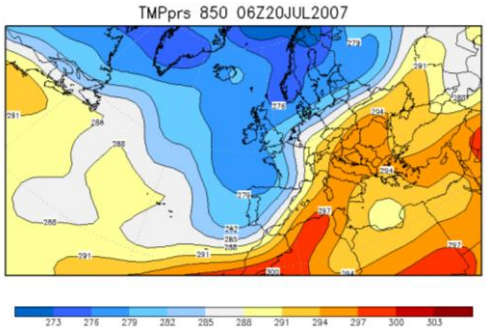

Fig. 3 July 20, 00 UTC, temperature at the 850 hPa level.

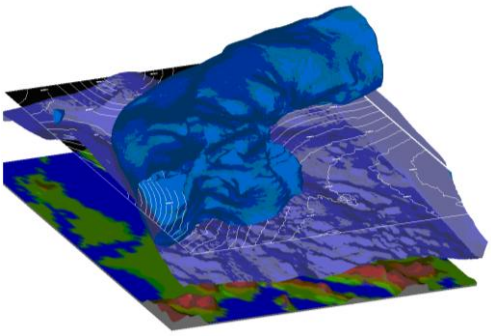

Fig. 4. The 315 K isentrope with the jet stream.

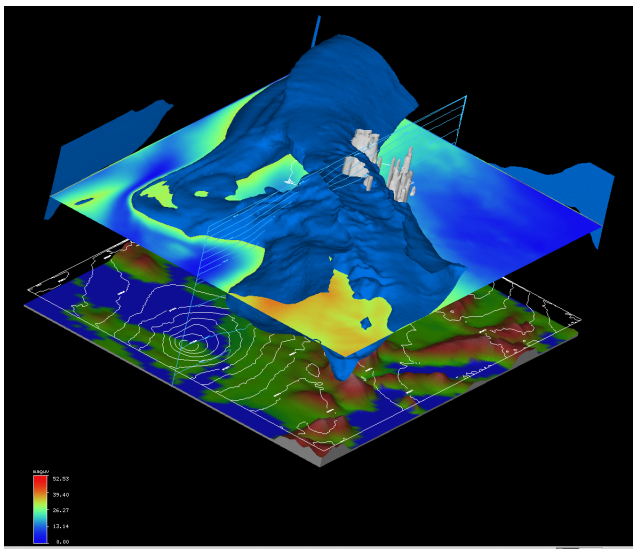

Fig. 5. 16 UTC: Jet at 30 m/s surface and wind speed on 10.2 km level. Pressure on 1.5 km altitude and radar reflectivity over southern Poland. Vertical cross-section of potential temperature, where squeezing temperature isopleths represent passage to the stratosphere.

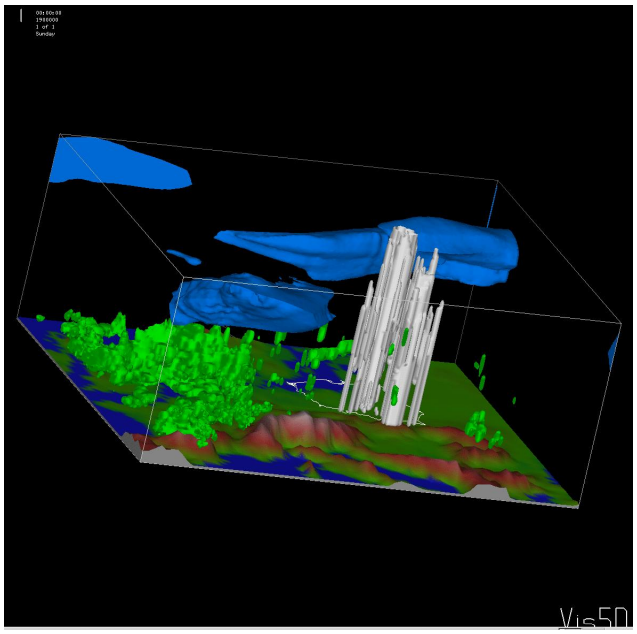

Fig. 6. Cloud water from the model for 16 UTC and radar reflectivity against the background of jet stream.

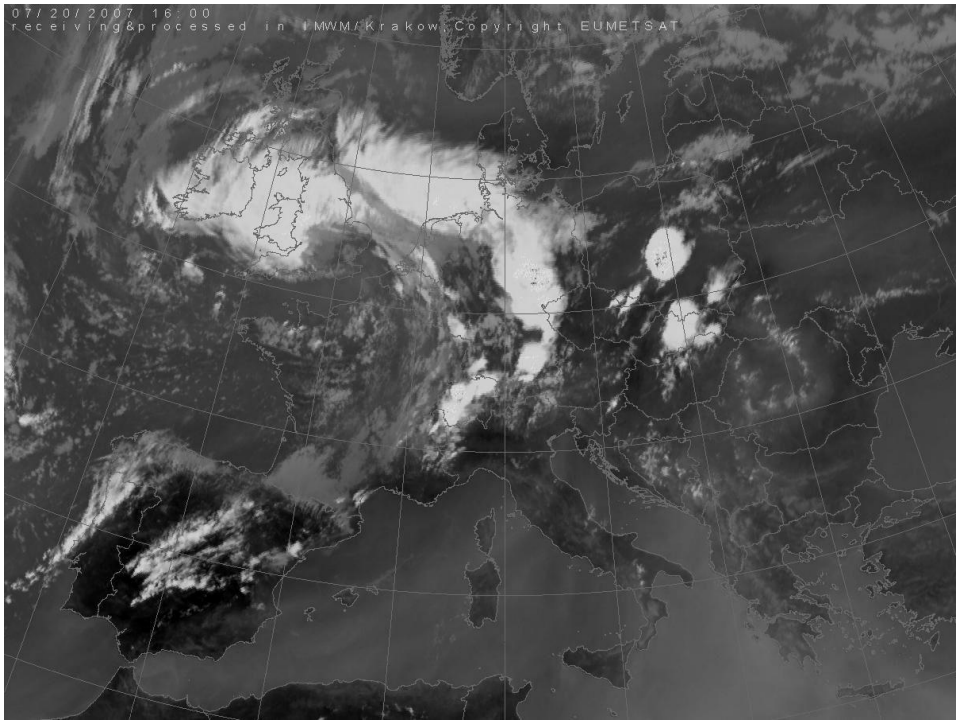

Fig.7. Infrared satellite photo at 16 UTC which displays the supercell in the Częstochowa region and the convective complexes over the Tatra mountains and Slovakia.

On the three-dimensional image in Fig. 6, at 16 UTC, we see a jet stream (in blue) disrupted by convection and the cloud cover (cloud water): (a) the image (light green) generated in 4-hour forecast (tumbled structures not much elevated above the orography surface), (b) the real cloudiness reconstructed from the radar reflectivity; the bright two objects are the convective complexes, the one in the region around Częstochowa and the other around the Tatra mountains. The convective complex around Częstochowa was identified as a thunderstorm supercell (Browning and Ludlam 1962), underneath which the tornado had formed. The object is 30 km wide and 18 km high.

4. History of the convective system development over south Poland: synthesis and stages

An analysis of the whole material makes it possible to distinguish the following main synoptic processes that led to the formation of tornado: (a) the inflow of cold and dry arctic air mass in the upper troposphere over warm and humid tropical air prevailing underneath, (b) cyclone-genesis in the shade of mountains (the so-called lee cyclongenesis) north of the Moravian Gate, (c) extremely high maximum temperature values, reaching 40^{o}C, (d) local vorticity transport, with distinct positive (cyclonal, anticlockwise) and negative (anticyclonal, clockwise) directions. The following periods of the convective situation development were distinguished:

(A) Nocturnal disintegration of the preceding convective complex; 00-04 UTC,

(B) Development and disintegration of individual convective cells; 04-10 UTC,

(C) Formation of a convective cluster, i.e., a slowly moving clockwise convective object of the right-mover type, and an initiating cell for a further supercell formation, i.e., a very strongly moving and abruptly upwelling huge cumulonimbus cloud with a supposed anticlockwise rotation of the left-mover type; 10-14 UTC,

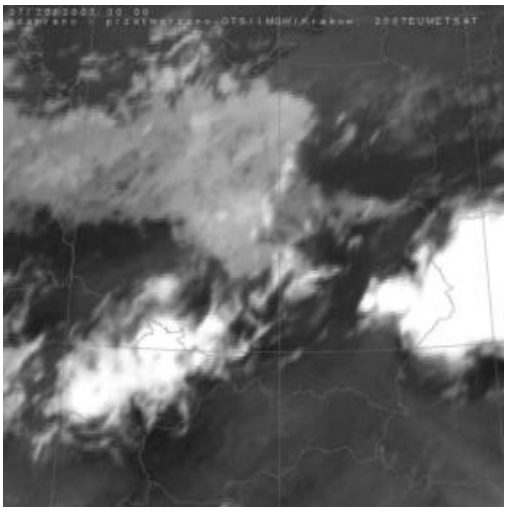

Fig. 8. Satellite photo at 8:00 UTC.

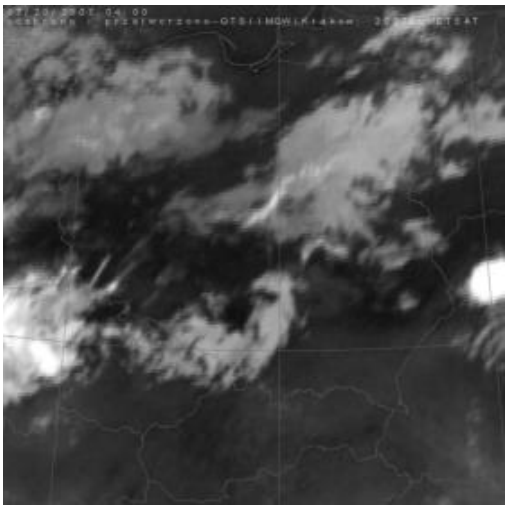

Fig. 9. Satellite photo at 04 UTC.

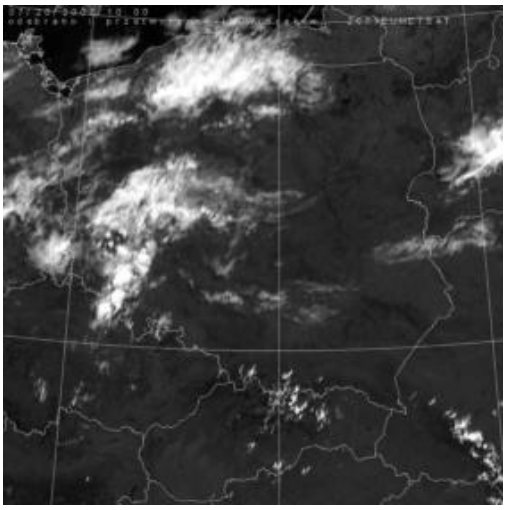

Fig. 10. Satellite photo at 10 UTC.

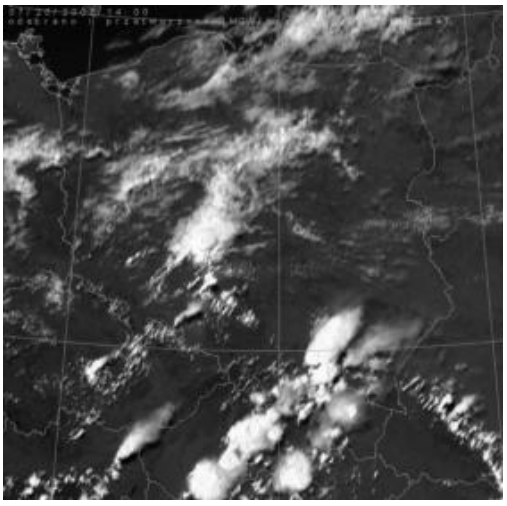

Fig. 11. Satellite photo at 14 UTC.

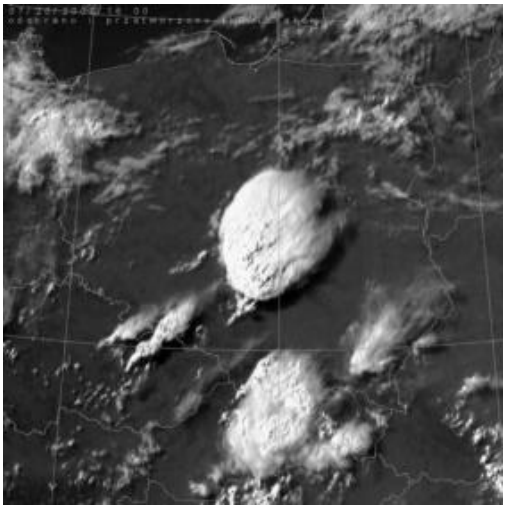

Fig. 12. Satellite photo at 16 UTC.

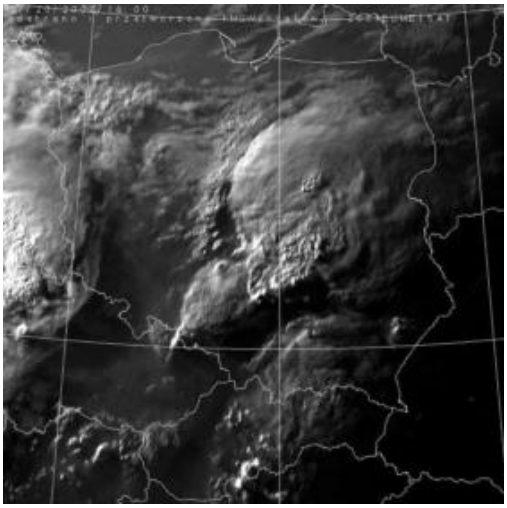

Fig. 13. Satellite photo at 18 UTC.

(D) Formation of a supercell from the merging of slowly-moving clockwise convective complex with a huge cumulonimbus cloud abruptly upwelling, being embedded in the positive vorticity region; 14-16 UTC,

(E) Mature supercell stage, with a tornado in the Częstochowa region (16:05 – 16:15 UTC) and a convective complex originated over the Tatra mountains and Slovakia; 16-18 UTC.

The variability of convective situation is illustrated by the satellite photographs in visible light.

The lee cyclone-genesis effect (equivalent to the increase of vorticity in the lower layer), as shown in Figs. 14A and 14B, and the effect of surface temperature growth

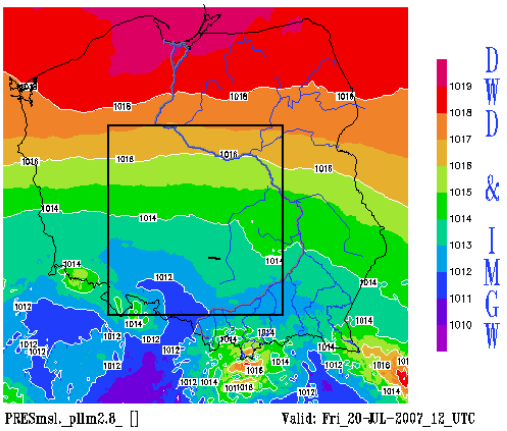

Fig. 14A. Pressure on msl at 12 UTC.

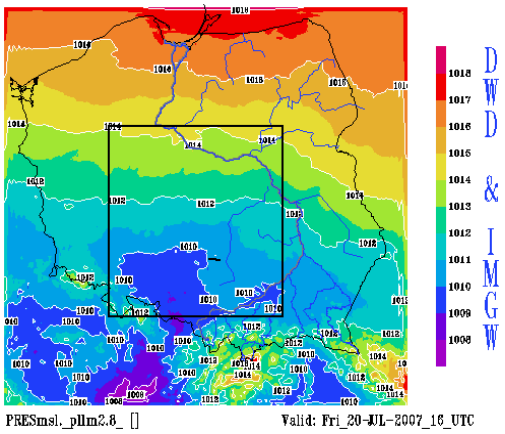

Fig. 14B. Pressure on msl at 16 UTC.

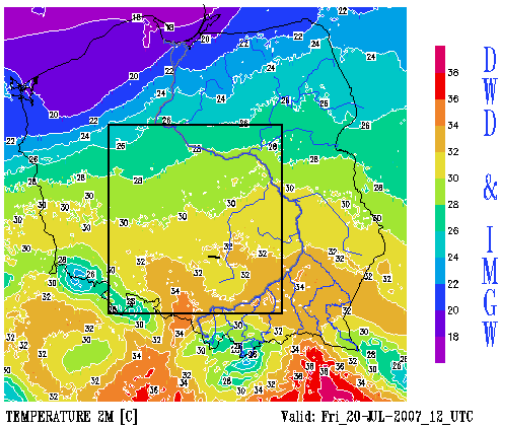

Fig. 15A. Temperature on 2 m level at 12 UTC.

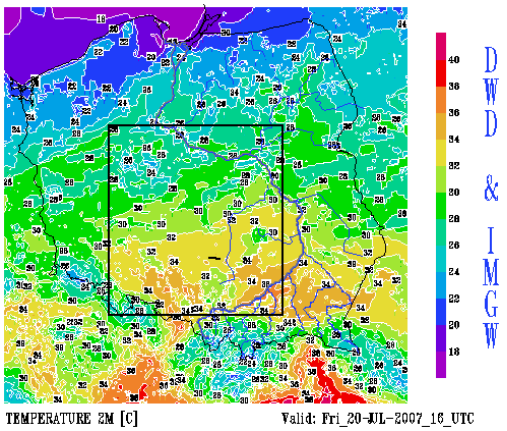

Fig. 15B. Temperature on 2m level at 16UTC.

(equivalent to the CAPE instability growth), as shown in Figs. 15A and 15B, can be best demonstrated by animation (time loop). Here we will restrict ourselves to documenting the period between 12 and 16 UTC, although the pressure-decrease process in the Carpathian-Sudetes Foreland had started earlier, already at 00 UTC, and was not steady.

5. Comparing computer simulations on different grid nets and examples of 3D analyses at a dense grid

5.1 Comparing computer simulations on different grid nets (downscaling): PL14/35 vs. PL2.8/50 for 16:00 UTC

The following computer simulations by COSMO-Lm model have been performed: (a) for domain over Europe: grid 14 km/35 levels, simulation range 00-18 h; grid 07 km/35 levels, range 12-18 h; grid 07 km/50 levels, range 12-18 h; (b) for domain over

Poland: grid 2.8km/50 levels, range 12-18 h. The initial and boundary data has been provided on the operational routine basis according to mutual agreement between DWD and IMGW. The detail comparison between all the simulations would be time consuming and deserves separate work; here we investigate the most distinguished runs and limit the area of search to Poland: PL14/35, PL2.8/50 and concentrating on 16 UTC, the term close to tornadogenesis. By their nature, tornados (especially the weak ones) „omit" the standard surface observation network. For this case, out of the neighboring Częstochowa SYNOP reports, only in Częstochowa SYNOP (only 5 km from the place and 5 min past the term the tornado has gone) we found some significant wind turn and wind gust between 15 and 17 UTC. According to code DD FF FF_911: (060, 04, –1000) => (330, 10, 19) => (320, 8, 17), with pressure practically the same. The most credible testimony of the tornado event remains eye-witnessing and analysis *in situ* (Bebłot *et al*. 2007). The tornado impact is seen also on radars reflectivity (in dBZ) and radial wind from Doppler radars (however, within the distance limited to 100 km), and on infrared and visible satellite pictures. Having knowledge on the tornado event we may look for signs of confirmation in the products of computer simulation. The following meteorological elements were chosen as sensitive to the case: msl pressure, vertical motions, cloud water, wind direction and velocity over the surface with its maximal velocity for 6 h, temperature at 2 m, tops of convective clouds, vorticity. Not always, the higher resolution forecast PL2.8/50 was better enlightening the event. And so:

(a) For the msl pressure, PL2.8/50 better than PL14/35 reflects the lee cyclone-genesis in the East Sudetes mountain range,

(b) For vertical motions, simulations with PL2.8/50 generated chaotic pattern and difficulties with interpretation comparing to PL14/35,

(c) The cloud water content is strongly correlated with the heights of cloud tops (i.e., atmospheric instability). Both model versions faulty forecasted cloud water. PL14/35 creates a fictive band of cloudiness over Wielkopolska Lowland, PL2.8/50 dried this band and creates singular clouds cells south of Poland border, which is possibly better,

(d) For the direction and wind velocity 2 m over the surface, both simulations give in general the same flow pattern. However, PL2.8/50 provides far more details and occasionally strengthens the wind velocity,

(e) For the maximal wind velocity over 6 hours we found significant enforcing and particularisation by PL2.8/50: it shows the zone of the very strong winds on the tornado domain. Despite the fact that the zone of strong winds is moved north, it must be unequivocally associated with supercell. PL2.8/50 is significantly better than PL14/35 (see Figs. 16A and 16B),

(f) For the temperature 2 m near the surface, the general view of the field is preserved by both model versions; PL2.8/50 gives some new values of T-2 m > 36 deg near the tornado track,

(g) vorticity (hcurl according to the program GrADS) is calculated as a mean value in the lower atmosphere, and the streamlines of direct and relative wind are taken for this particular mean level. Vorticity (hcurl) and the streamlines of direct and relative wind are presented in Fig. 17A and 17B.

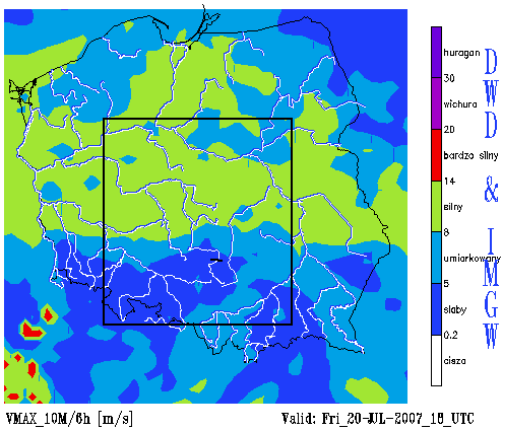

Fig. 16A. VMAX according to PL14/35, where VMAX denotes maximal wind.

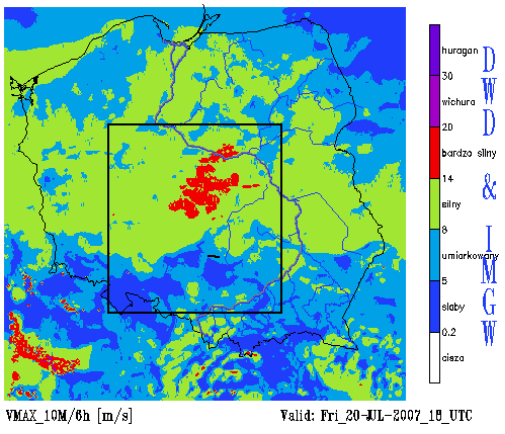

Fig. 16B. VMAX according to PL2.8/50 velocity over 6 hours.

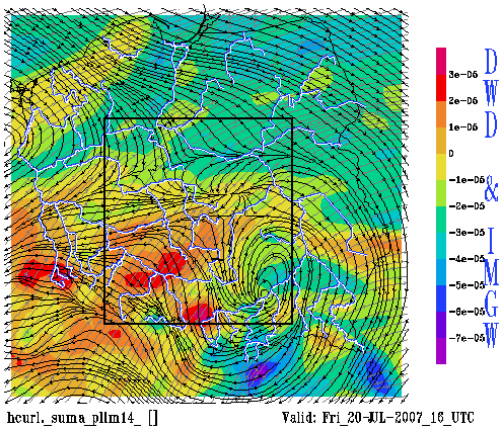

Fig. 17A. Vorticity hcurl and streamlines: PL14/35.

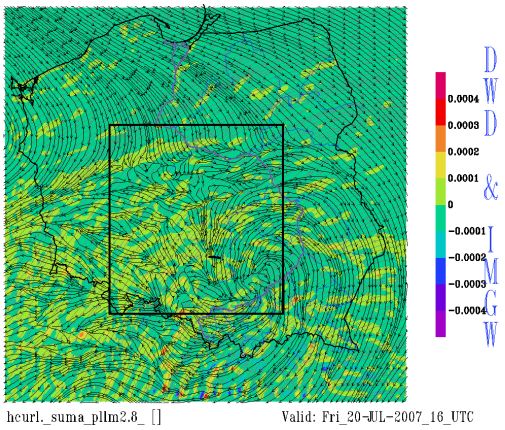

Fig. 17B. Vorticity hcurl and streamlines: PL2.8/50.

The PL2.8/50 view is significant particularisation, but rising ambiguity (loss of transparency). In general, the relative motion pattern remains preserved. Despite the track near the tornado, we got new rotational nuclei. Thus, PL14/35 stands for clarity, especially distinctly separates area of positive and negative vorticity (see Fig. 17A).

Concerning 3D analysis we concentrate on PL2.8/50 simulations trying to interpret compound 3D composites in favour of the model ability to reproduce, as expected, "real" tornado. Many synoptic futures were correctly reproduced by the model and helped to understand the mechanisms of the case and deduce even such subtle processes like right and left moving wind patterns of tornado convective system. Nevertheless, the QC (cloud water) convective structures as simulated by the model remain underestimated. One of the reasons of the fault is that the proper radar assimilation scheme was not adopted, but the second suspicion is that the ageostrophic flow just under the jet stream was not adequately represented.

5.2 Clockwise movement of a supercell – the right-mover type

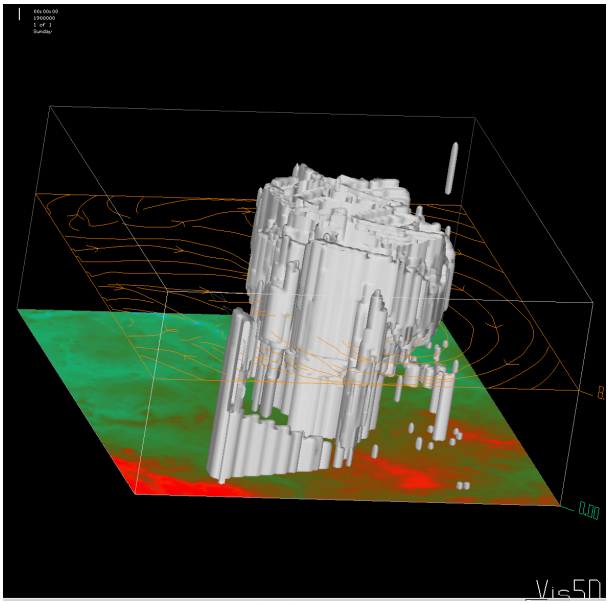

Fig. 18. The 3D structure of a right-mover type supercell reconstructed from radar reflectivity, with the current lines in relative movement obtained by subtraction of the selected horizontal velocity vector profile over the tornado site from the horizontal wind profile in the whole domain. The selected fixed wind profile represents the supercell movement as one compact object; once the wind field is subtracted, there remains the relative air movement in the cell itself, and the reduction of horizontal velocity makes the effect of vertical velocity more pronounced. The array of horizontal current lines depends on the altitude. The vertical extent: 15 km.

5.3 Vertical cross-section of the supercell: wind jump and the vortex pipe

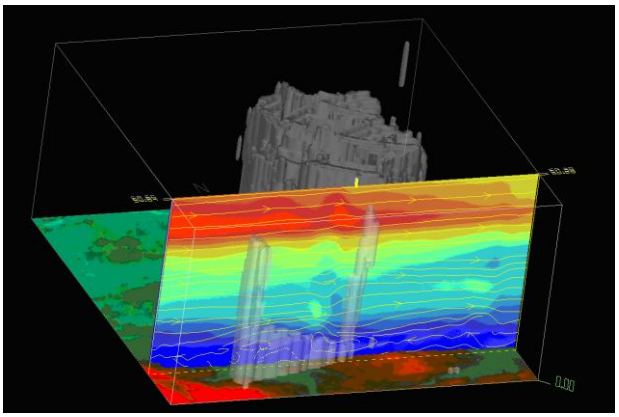

Fig. 19. The vertical cross-section of the supercell with wind field streamlines in the velocity field. A characteristic wind jump in the lower troposphere, with a trace of vortex pipe in the velocity field above the jump is seen. The radar reflectivity in the background. The vertical extent: 15 km.

5.4 Vertical cross-section of the supercell: wind field in the relative motion

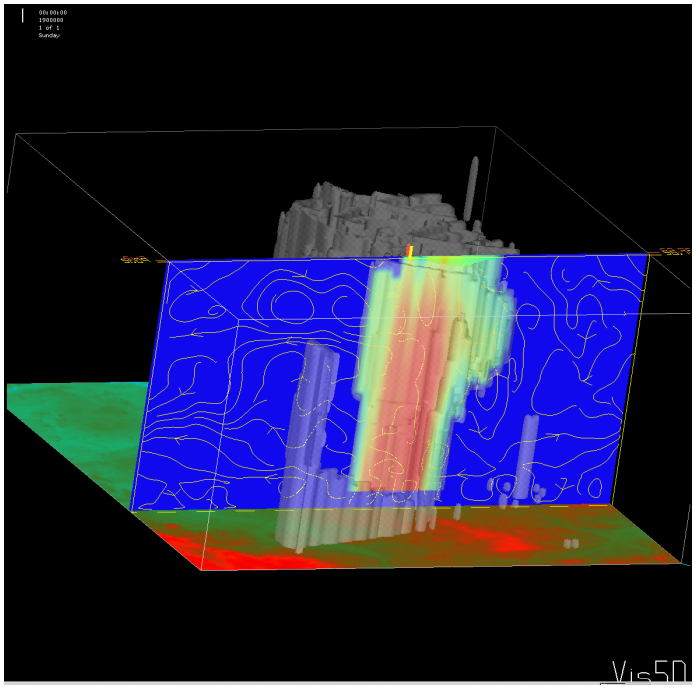

Fig. 20. The vertical cross-section in the rear part of the supercell, with wind field streamlines in the relative motion: the effect of the vertical velocity is enlarged. The vertical extent: 15 km.

5.5 Vertical cross-section of the supercell: exaggerated relative motion

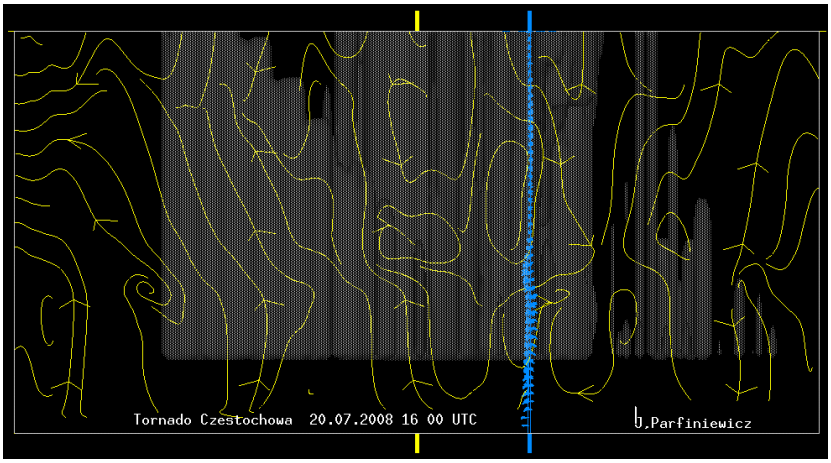

Fig. 21. Vertical cross-section of a supercell with the wind field streamlines in the relative motion. The view from the south. The vertical extent: 5 km. The wind vector profile is on the axis of supposed mesocyclone. Characteristic "chimney" alignment of the upgoing and down-going currents next to each other is a certain approximation of how the real movement field is organized.

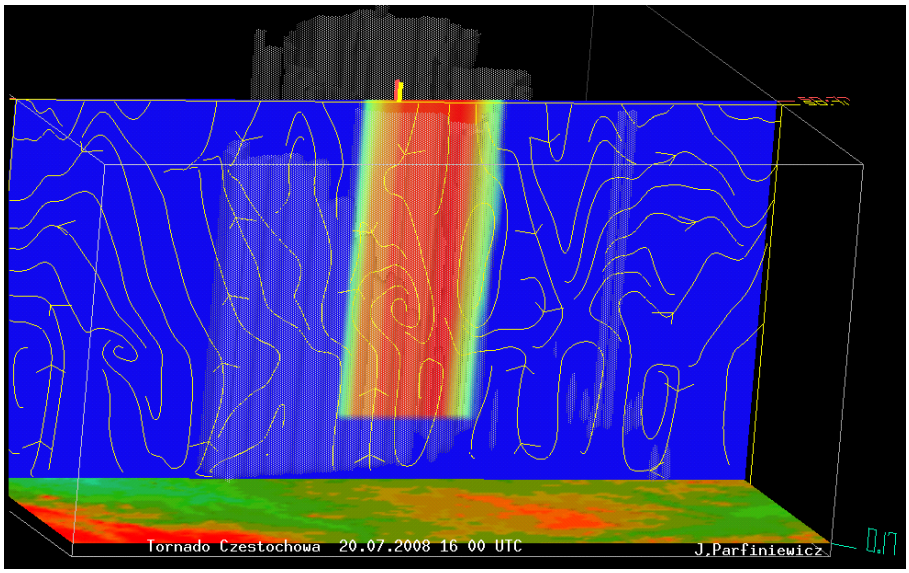

Fig. 22. Vertical cross-section of the supercell with the wind field streamlines in the relative motion, as in Fig. 21, but in the SW perspective. The vertical extent: 5 km.

6. An analysis of thunderstorm lightning activity during the supercell and tornado formation process

From our collected database of the considered tornado formation, we have presented in Figs. 23 and 24 the overlapping of reflectivity radar maps obtained from the Legionowo radar and lightning discharge locations, both for cloud-to-ground and intracloud ones, that were detected by the SAFIR/PERUN system at the moment just before the merging of the convective complex with the abruptly rising cumulonimbus cloud, which

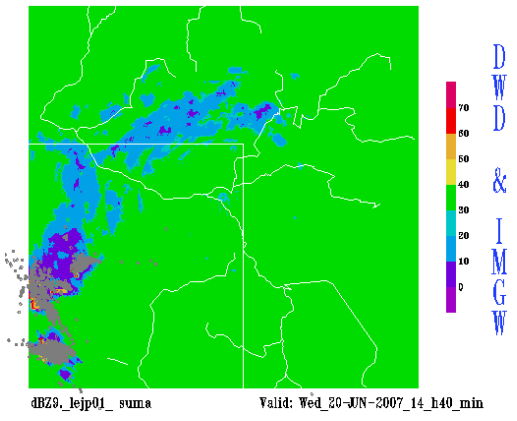

Fig. 23. The Leginowo radar reflectivity map, at 14:40 UTC, in dBz, indicated by colored scale and lighting strokes locations denoted by small grey squares during the time interval 14:40–50 UTC.

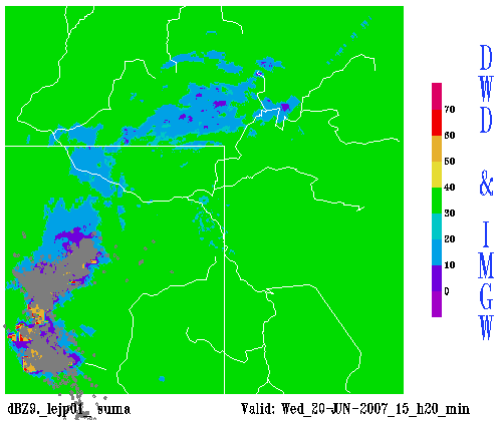

Fig. 24. The Leginowo radar reflectivity map, at 15:20 UTC, in dBz, indicated by colored scale and lighting strokes locations denoted by small grey squares during the time interval 15:20–30 UTC.

was fast moving northward from the Moravian Gate region. Two instants of time were selected for the presentation, i.e., 14:40 and 15:20 UTC, to indicate the appearance of a possible interaction mechanism between the particular thunderstorm lightning activity pattern and dynamic convection evolution directed toward a supercell formation. However, this problem should be explained in greater detail, with an attempt of determining the electric space charge structure of merging active thunderstorm cells. Thus, further field investigations are needed to be performed, e.g., by using in situ balloon electric field soundings of aggregating thunderclouds and at least 3D lightning locations mapper giving more information about the height distribution of cloud/electric space charge region involved in initiation of IC and CG lightning strokes.

6.1 The course of lightning activity recorded during the development of supercell convective complex

6. 1.1 Changes of lightning rate

Taking into account the particular stages of dynamic evolution of the considered supercell convective complex and using the space domain that was especially chosen for this purpose, we also examined the time variation of frequency of different types of lightning discharges detected by the SAFIR/PERUN network system, i.e., positive and negative return strokes (RS_+ and RS_-) of cloud-to-ground flashes (CG), intra cloud discharges (IC), and other, not fully recognized discharges, and named isolated points (IP), in order to obtain and display some characteristic features of special kind pattern of lightning activity accompanying the studied severe weather phenomena. Namely, we have found (see Fig. 25) that the first peak of lightning frequency histogram, with a total of 1422 lightning strokes per 10 minute interval and for 4 stroke types detected by the SAFIR/PERUN system, preceded by 25 minutes the onset of first heavy hail gush, by 1 hour and 10 minutes the moment of visible tornado onset, and by 1 and half hour the second episode with heavy hail gush. On the other hand, the next, much more distinct peak of such lightning frequency, with a total of 5065 lightning strokes per 10 minute interval, followed by 65 minutes the onset of first heavy hail gush and by 20 minutes the moment of visible tornado and overlapped with the onset of the second episode with heavy hail gush. Thus, it seems reasonable to expect that such information about the rapid and great changes of lightning rate, operationally supplied by the SAFIR/PERUN detection network system, could be used as a significant predictor for nowcasting and preparing warnings of approaching dangerous storm hazards.

Some details of peculiar changes of lightning activity connected with the biggest increase of lightning rate that occurred between 15:50 and 16:10 (see Fig. 27) are given more distinctly by Table 1. Thus, we can see that the tornado incident was preceded by meaningful jump of IP and IC counts per 10 minute interval, whereas counts of RS_- were decreased slightly, with nearly the same small number of RS_+. In result we obtained increasing and a great value of ratio IC/RS_-+RS_+, which was finally about 6 times grater than that one observed during ordinary thunderstorms in Poland (Barański *et al*. 2002).

Many lightning characteristics gathered during supercell event observations reviewed and reported recently by Tessendorf (2009) have indicated that the IC/CG ratio

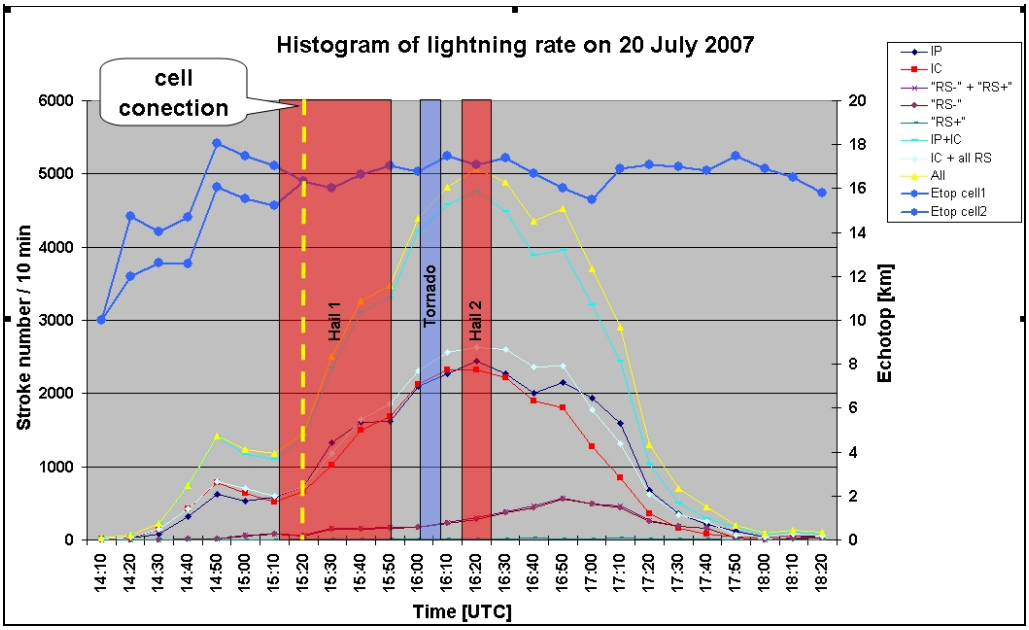

Fig. 25. Histogram of lightning frequency for different types of discharges detected by the SAFIR/PERUN network system in the chosen area containing two separated convective cells (see Fig. 26A) and the considered supercell complex after cell aggregation (see Fig. 26B), i.e., positive and negative return strokes of cloud-to-ground flashes (RS_+ and RS_-), intracloud discharges (IC), and not fully recognized discharges named isolated points (IP). Additionally the time changes of radar echo top of those cells and supercell are overlapped with the same time interval.

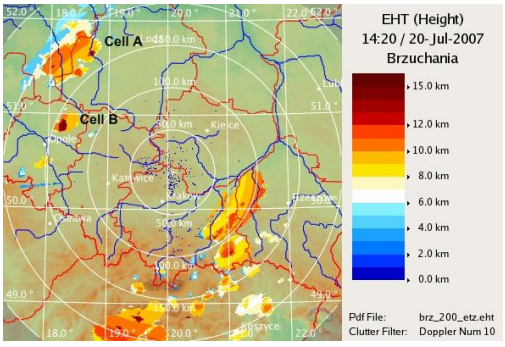

Fig. 26A. Brzuchania radar echo top map at the 14:20 UTC showing two separated convective cells A (bigger but lower) and B (smaller but higher).

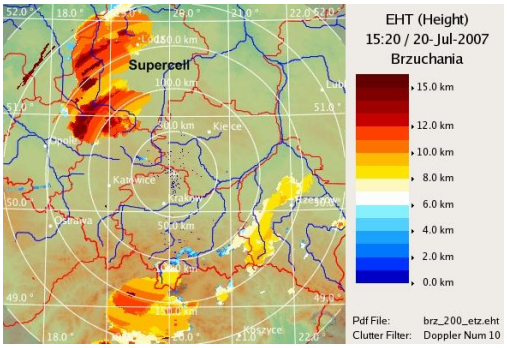

Fig. 26B. Brzuchania radar echo top map moment 15:20 UTC showing the supercell complex just after connection of A and B cells.

tends to increase with increasing storm severity and its electrical activity. Thus, it could also be used as an indicator of enhanced severe weather potential. Moreover, Goodman *et al*. (1999), basing on his experience with severe and tornadic storms in

Central Florida (USA), has noticed that sudden increases in the lightning rate, which he referred to as lightning "jumps", have preceded the occurrence of severe weather phenomena by 10 or more minutes. These jumps were typically 30–60 flashes/min^2, and were easily identified as anomalously large derivatives in the flash rate. For our case of supercell event (see Fig. 25), the maximum value of total lightning rate was of the order 10 strokes/min^2 and occurred about 5 minutes before the tornado visible appearance.

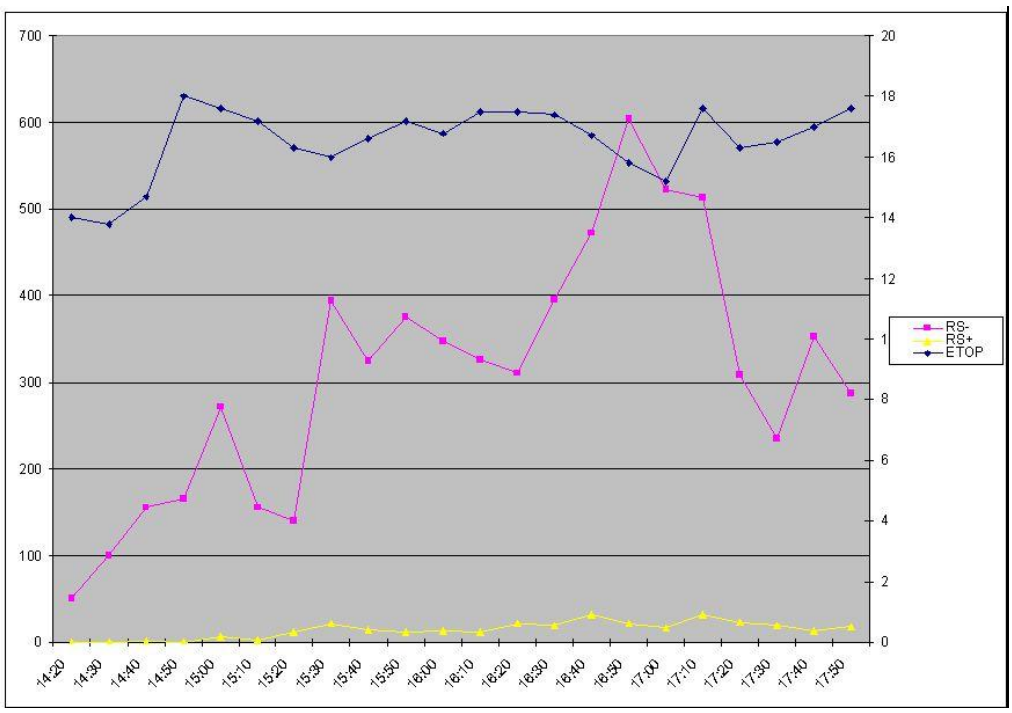

Fig. 27. Number of RS_+ (yellow curve) and RS_- (violet curve) strokes per 10 minute interval compared with radar echo top of the considered two aggregating convective cells (A and B) and the resulting supercell complex.

Table 1

Counts of different lightning types, i.e., IP, IC and $RS_\pm$ and ratio IC/RS_-+RS_+, indicated by the SAFIR/PERUN detections during rapid, increasing phase of lightning rate and for three selected time moments (see Fig. 25)

Time [UTC]	IP	IC	RS_-	RS_+	IC/RS_-+RS_+
15:50	2625	2559	375	11	6.63
16:00	2987	2902	348	13	8.04
16:10	3014	2919	326	12	8.64

6.1.2 Clustering of CG lightning discharges during the observed supercell event

To show how clustering of CG flashes detected by the SAFIR/PERUN system in time of supercell evolution was progressing, we have distinguished, basing on Fig. 25, five characteristic time episodes of its development as follows:

- at 14:50, i.e., the first peak of lightning frequency rate with a total of 1422 lightning strokes detected per 10 min interval and before the supercell onset with two separated convective complexes,
- at 15:20, i.e., the beginning of the first hail event connected with the local minimum of lightning frequency rate and with a total of about 1100 lightning strokes detected per 10 min interval,
- at 16:00, i.e., the beginning of tornado incident with its visible appearance and with a total of about 4200 lightning strokes detected per 10 min interval,
- at 16:10, i.e., the end of tornado incident with a total of about 4600 lightning strokes detected per 10 min interval,
- at 16:20, i.e., the second hail event with the maximum value of lightning frequency rate reaching a total of 5065 lightning strokes detected per 10 min interval.

All the stages mentioned above are depicted in Figs. 28–32, respectively. On the other hand, the existence of a mature stage of the supercell formation is indicated by finding of the so-called bounded weak echo region (BWER), first described by Chisholm and Renick(1972), and is shown in Fig. 33. According to Browning hypothesis (Browning and Ludlam 1960) the BWER is a result of very rapid air rising by very strong updrafts so that insufficient time is available for the formation of precipitation particles, which may be detected by radar scan.

Time evolution of the considered supercell formation together with time and space changes of the accompanying $CG_{\pm}$ activity shown by the sequence of five episodes in Figs. 28–32 have revealed that the majority of $CG_{\pm}$ flashes detected by the SAFIR/PERUN system was negative and they were located very close to the main precipitation shafts indicated by simultaneous radar scans. Hence, these observations may point out that, likewise for a typical thundercloud, also for our case of supercell event the precipitation phenomena are a driving factor for the initiation of the CG lightning strokes and their amount. However, it is worth to note that in the case of supercell it has covered not only one, but several large regions with high-altitude intense precipitation/hail shafts. It was also an amazing and unexpected observation result that this supercell precipitation shaft connected with tornado event has generated only one single and strong CG_{-} stroke. The possible reason of such weak lightning activity behavior in tornado area may be a fast removal of small lower positive charge centers (LPCC's) from that part of supercell by an appearing tornado wind field pattern.

Taking into account simultaneous time changes of lightning rate for different types of lightning flash activity and radar echo top parameter recorded during supercell storm event in Poland (see Fig. 25 and Fig. 27) we can note that the local minimum value of supercell echo top has coincided with the maximum value of total lightning rate, while the maximum value of lightning rate for RS_{-} strokes has preceded the maximum value of supercell echo top by 20 minutes (see scale zoom given in Fig. 27).

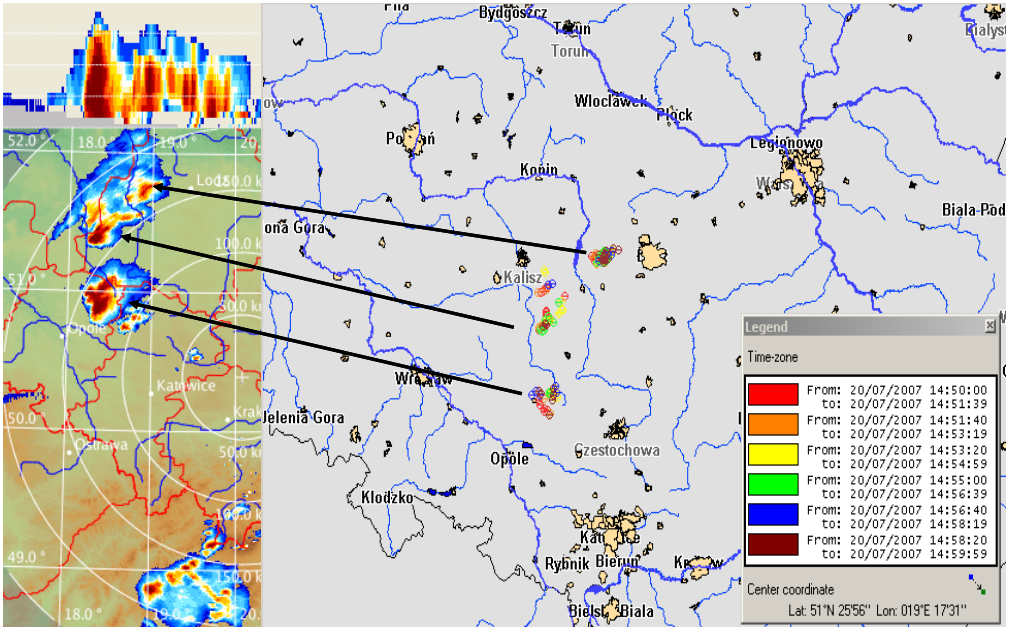

Fig. 28. Brzuchania radar data and lightning detections before the supercell onset; description of radar reflectivity and altitude of radar echo scale is given in Fig. 31. Space collocations between particular CG clusters and radar reflectivity/precipitation cores are indicated by arrows.

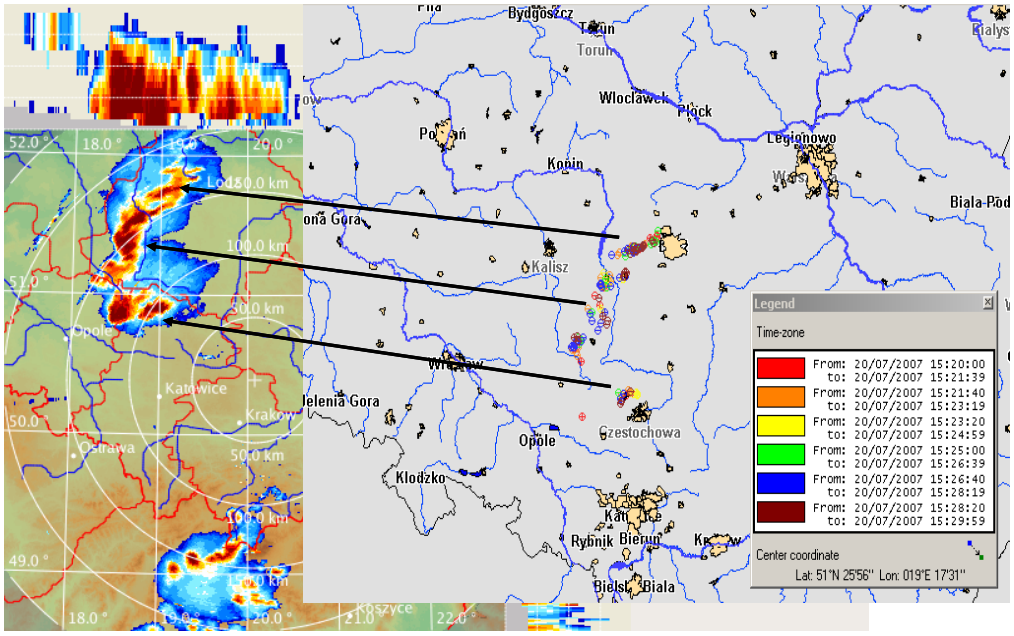

Fig. 29. Brzuchania radar data and lightning detections at the beginning of first hail event; description of radar reflectivity and altitude of radar echo scale is given in Fig. 31. Space collocations between particular CG clusters and radar reflectivity/precipitation cores are indicated by arrows.

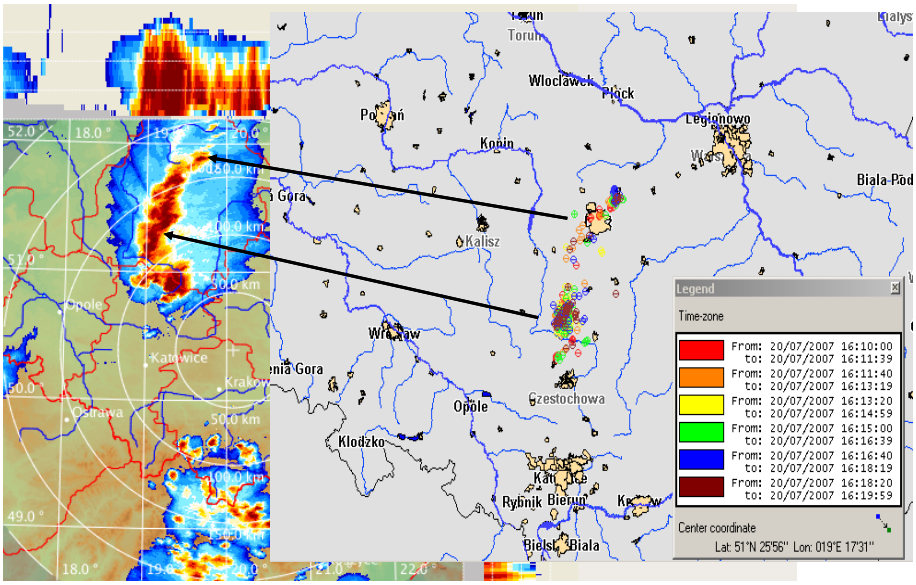

Fig. 30. Brzuchania radar data and lightning detections after tornado incident; description of radar reflectivity and altitude of radar echo scale is given in Fig. 31. Space collocations between particular CG clusters and radar reflectivity/precipitation cores are indicated by arrows.

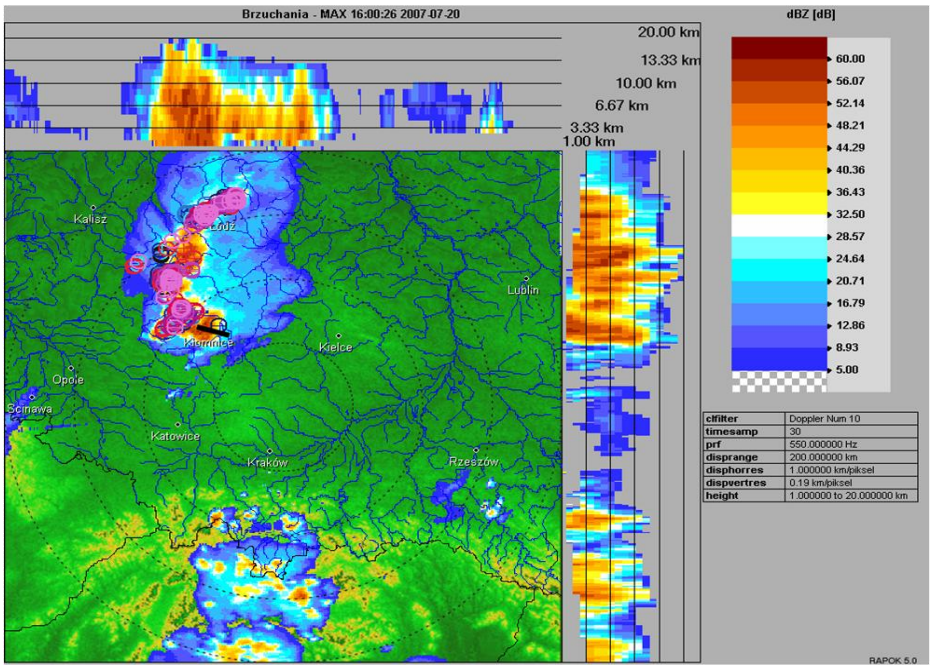

Fig. 31. Brzuchania radar data with overlapping lightning CG detections during 10 minute interval covering the tornado incident; single negative CG lightning flash detected by the SAFIR/PERUN system that was located very close to the tornado trace (shown as a black bar) is indicated as small black open circle; its estimated return stroke lightning current was equal to –47.1 kA.

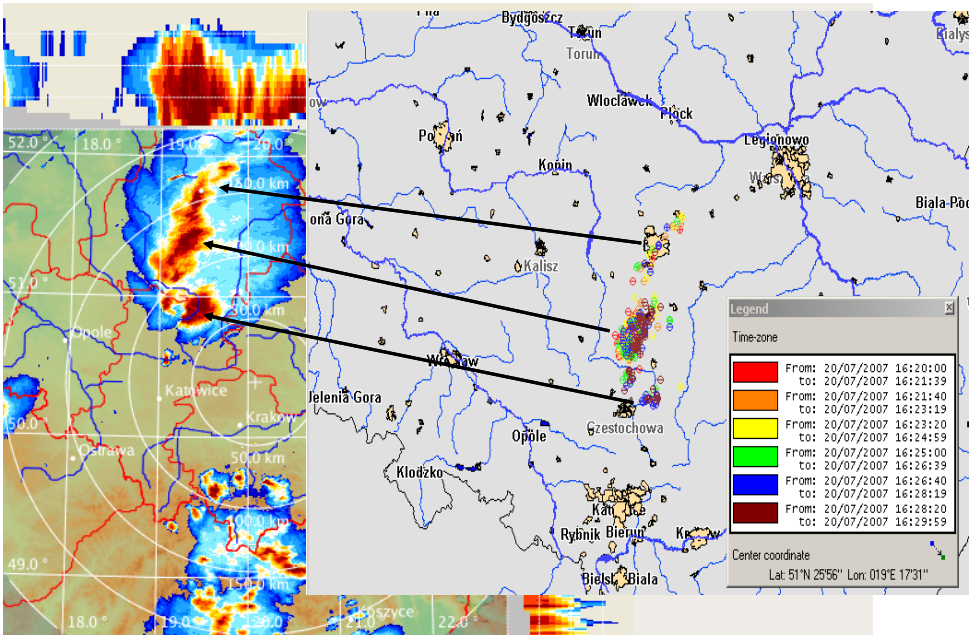

Fig. 32. Brzuchania radar data and lightning detections at the beginning of the second hail event; description of radar reflectivity and altitude of radar echo scale is given in Fig. 31. Space collocations between particular CG clusters and radar reflectivity/precipitation cores are indicated by arrows.

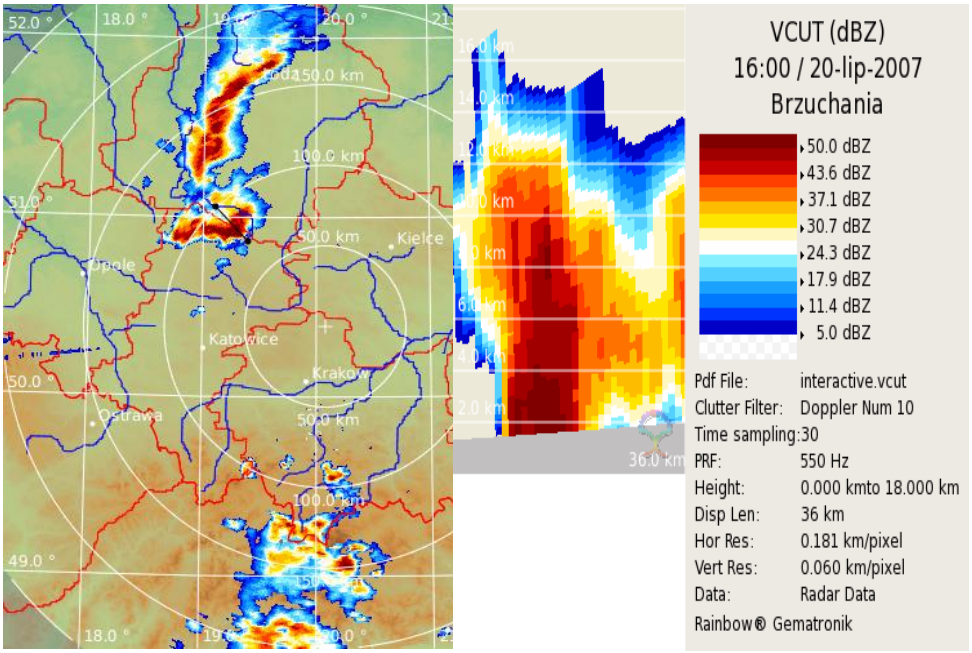

Fig. 33. The example of PPI and VCUT radar scans taken from Brzuchania site which displaying the supercell region with hook echo; black bar on the left side picture denotes the direction of performed VCUT which is presented on the right panel.

The first time relationship may be caused by the occurrence in that time of some downdrafts which were increasing the supercell IC strokes activity during the second hail episode. On the other hand, the second time relation can agree with a scenario presented by Rust *et al*. (1981) and showing typical location of to-ground channels for different polarity of CG flashes relative to supercell storm dynamic structure driven by strong updraft associated with mesocyclone wind field pattern and when total CG flash activity is not dominated by RS_+ strokes. Also MacGorman and Nielsen (1991) reported the case when RS_- flash rates were larger than RS_+ ones throughout a storm that produced a strong tornado and was classified as a supercell for an hour.

6.1.3 Lightning current distribution of CG flashes during the observed supercell event

Discrimination of $CG_\pm$ flashes that are allowed and processed by algorithm procedures of the SAFIR/PERUN system implemented in the Polish network enables us to obtain their estimated lightning current distribution as such shown in Fig. 34 and with discarding all return strokes having lightning current less than 3 kA. Hence, we can note that during the whole life time of the considered supercell, its CG flashes activity was dominated by weak negative return strokes having the bin peak lightning current of –10 kA for 6200 strokes. On the other hand, positive return strokes were considerably less numerous than negative ones, and had the bin peak lightning current of 10 kA for 400 strokes.

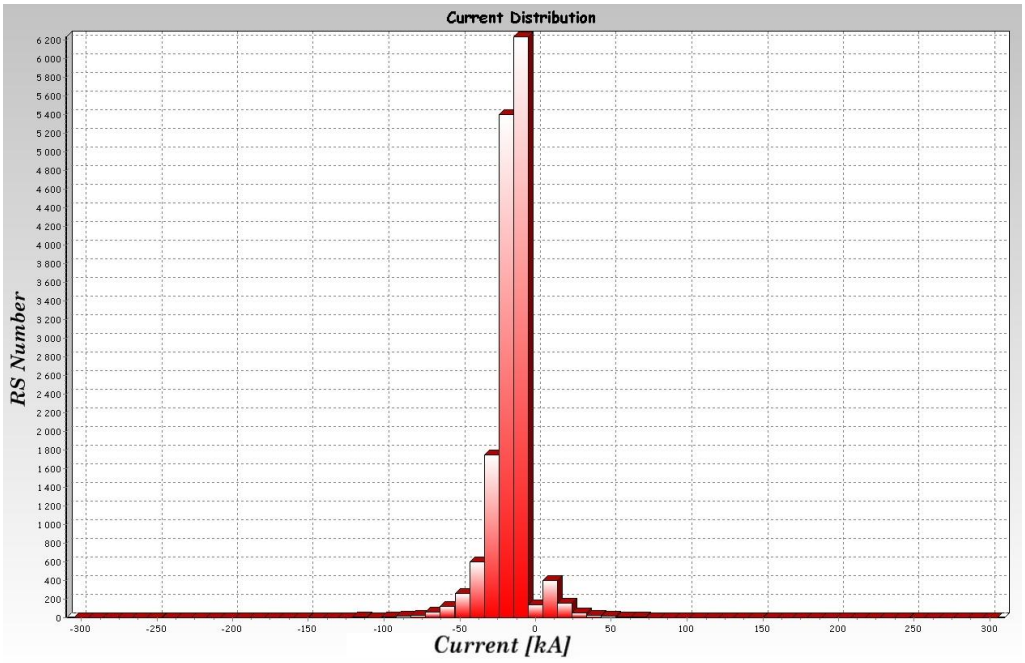

Fig. 34. Histogram of the estimated peak value of positive and negative return strokes of CG flashes detected by SAFIR/PERUN system during supercell event in Poland on 20 July 2007.

7. Conclusions and summarizing remarks

The development of convective situation over south Poland on July 20, 2007, was conditioned in the synoptic scale by a degradation of the Polar Front and dissipation of the combined polar and tropical jet streams, with a characteristic inflow of cold polar mass (an active upper cold front) over warm and humid tropical air masses. A process of this type generates the so-called conditional potential instability and releases a strong convection. The macro synoptic situation favorable for the development of a strong convection over south Poland was realized through the lee cyclogenesis in the shade of the Moravian Gate (hence an increase of vorticity in the lower layer) and a strong increase of temperature enhancing the instability and accumulation of the available potential energy (CAPE), which initiated the convection. The convective system was analyzed and stages of development and mature were determined. The time moment was defined in which the huge right convective complex collided with a gigantic cumulonimbus cloud with positive vorticity spin. Once the two cells merge, a supercell is formed with right-moving (most probably dominant at the moment, but with tendency to vanish) macro circulations and the inner mesocyclone rotating to the left. The mesocyclone can be noticed in the mature development phase of the supercell development on the visible light satellite photo. The relatively weak tornado thus formed was short-lived, and the supercell circulation, already deprived of the characteristic near-ground whirl, was entirely left moving. The behavior of thunderstorm activity was analyzed and characteristic traits of the discharges accompanying the tornado onset were determined, with a supposed eventful influence of thunderstorm electricity on the fusion of thunderstorm cells making up the supercell and tornado.

The increasing number of huge disasters over the world caused by severe weather phenomena, such as tropic storms and tornados, which are sometimes connected with violent floods has focused the efforts of atmospheric research community on more scrutinized post-time examination of such incidents taking into account a possible mutual interaction mechanism between their dynamic development and associated lightning activity. And so, for example, the last issue of Atmospheric Research journal published in July 2009 (No. 1-3) is almost completely devoted to presentation of recent reports and considerations on that subject. Here, the most important thing is to answer the basic question to what extent the observed lightning activity accompanying severe hail/supercell or MCS (Mesoscale Convective System) complexes may be used as a good proxy of their dynamic development. As for now, we do not see any straight way which will be directed to achieve full and wide understanding of that hot problem. Nevertheless, further experimental and theoretical studies are strongly needed to get deeper knowledge about the relationship between lightning behavior and evolution of severe weather conditions that would help us to enhance the warning decision tree and improve short term forecasting of approaching dangerous storm hazards. Moreover, such studies are also crucial for gaining the greatest benefit from the modern advanced lightning detection and location technologies, i.e., 3D lightning mapping ground-based networks which should be more widespread and satellites which should have the capability to measuring total lightning flash rates and bringing that data online. Due to such research action more information on lightning discharges in severe supercell thunderstorms will be collected and analyzed.

Acknowledgments. This work was partially supported by grant No. COST/204/2006 from Polish Ministry of Science and High Education. The authors would like to express their gratitude to Stanisław Michnowski for giving his inspiration to do this examination of supercell case in Poland and to include into it some important and specific features of lightning activity accompanying this event.

References

Barański, P., P. Bodzak, and A. Maciążek (2002), Some results of the SAFIR, radar and field mill observations for selected thunderstorms near Warsaw, *Abstracts of the 2002'SAFIR Workshop, Budapest.*

Bebłot, G., I. Hołda, and K. Rorbek (2007), The tornado in the Częstochowa region on 20 July 2007, IMGW, Oddział Kraków, Górnośląskie Centrum Hydro-Meteorologiczne w Katowicach, p.18 (in Polish).

Browning, K.A., and F.H. Ludlam (1960), Radar analysis of a hailstorm, *Tech. Note* **5**, Dept. of Met., Imperial College, London.

Browning, K.A., and F.H. Ludlam (1962), Airflow in convective storms, *Quart. J. Roy. Met. Soc.* **88**, 376, 117-135, DOI: 10.1002/qj.49708837602.

Browning**,** K.A. **(**1985), Conceptual models of precipitation systems, *Meteor***.** *Mag*. **114**, 293-319.

Browning, K.A., P. Panagi, and E.M. Dicks (2002), Multi-sensor synthesis of the mesoscale structure of a cold-air comma cloud system, *Meteorol. Appl.* **9**, 2, 155-175, DOI: 10.1017/S1350482702002025.

Chisholm, A.J., and J.H. Renick (1972), The kinematics of multicell and supercell Alberta hailstorms, Alberta Hail Studies, *Res. Conc. Alberta Hail Stud. Rep*. No. 72-2, 24-31.

Fujita, T.T. (1981), Tornadoes and downbursts in the context of generalized planetary scales, *J. Atmos. Sci.* **38**, 8, 1511-1534, DOI: 10.1175/1520-0469(1981)038<1511:TADITC>2.0.CO;2.

Goodman S.J., D. Buechler, S. Hodanish, D. Sharp, E.R. Williams, R.A. Boldi, A.M. Matlin, and M.E. Weber (1999), Total lightning activity associated with tornadic storms. **In:** *Proceedings of the 11th Int. Conference on Atmospheric Electricity, Gunthersville*, Alabama, USA, June 7-11, 1999, pp. 515-518.

MacGorman, D.R., and K.E. Nielsen (1991), Cloud-to-ground lightning in a tornadic storm on 8 May 1986, *Monthly Weath. Rev*. **119**, 7, 1557-1574, DOI: 10.1175/1520-0493(1991)119<1557:CTGLIA>2.0.CO;2.

Michnowski, S., S. Israelsson, J. Parfiniewicz, M.A. Enaytollah, and E. Pišler (1987), A case of thunderstorm system development inferred from lightning distribution, *Publs. Inst. Geophys. Pol. Acad. Sc.* **D-26**, 198, 3-57.

Rust, W.D., W.L. Taylor, D.R. MacGorman, and R.T. Arnold (1981), Research on electrical properties of severe thunderstorms in the Great Plains, *Bull. Am. Meteor. Soc*. **62**, 9, 1286-1293, DOI: 10.1175/1520-0477(1981)062<1286:ROEPOS>2.0.CO;2.

Steppeler, J., G. Doms, U. Schättler, H.W. Bitzer, A. Gassmann, U. Damrath, and G. Gregoric (2003), Meso-gamma scale forecasts using the nonhydrostatic model LM, *Meteor. Atm. Phys.* **82**, 1-4, 75-96, DOI: 10.1007/s00703-001-0592-9.

SAFIR (2001), 3000 SCM, User Manual (SAFIR/SOFT/SCM/UM/01), Vaisala SA, Europarc de la Sainte Victoire, 13590 Meyreuil, France, July 2001.

SAFIR (2003), 3000 Software User Manual (Data Analysis Module, DAMen-2.1), Vaisala SA, Europarc de la Sainte Victoire, 13590 Meyreuil, France, July 2003.

Tessendorf, S.A. (2008), Characteristics of lightning in supercells, Chap. 4, pp. 83-114. **In:** H.D. Betz, U. Schumann, and P. Laroche (eds.), *Lightning: Principles, Instruments and Applications*, Springer Netherlands, DOI: 10.1007/978-1-4020-9079-0_4.

Vaisala (2003), SAFIR 3000–3, User Manual, DS Settings and Control Manual, Release 2.3, Helsinki, Finland, July 2003.

Received September 7, 2009
Accepted October 29, 2009

PUBLS. INST. GEOPHYS. POL. ACAD. SC., D-73 (412), 2009

Dynamics of Lightning Channel Corona Sheath Predicted by Return-Stroke Models with Specified Longitudinal Current Distribution

Grzegorz MASLOWSKI [1], and Vladimir A. RAKOV [2]

[1] Department of Electrical and Computer Engineering
Rzeszow University of Technology, Rzeszów, Poland
e-mail: maslowski@prz.edu.pl

[2] Department of Electrical and Computer Engineering
University of Florida, Gainesville, Florida, USA
e-mail: rakov@ece.ufl.edu

Abstract

We consider dynamics of the lightning-channel corona sheath that is implicitly specified by lumped-current-source (LCS) type (transmission-line-type) and distributed-current-source (DCS) type (traveling-currents-source type) lightning return-stroke models. A relaxation model of charge motion in the corona sheath is used to investigate the rate of its expansion and shrinking. This model can be viewed as a generalization of the model proposed by Maslowski and Rakov (2006) and can be applied to both LCS and DCS return-stroke models with specified longitudinal current distribution.

1. Introduction

When leader charge is deposited on a thin lightning channel core (away from the leader tip), the deposited charge will create a radial electric field which exceeds the breakdown value and pushes the charge away from the core. As a result, the leader channel consists of a thin core surrounded by a radially formed corona sheath. The corona sheath expands outward from the channel core until the radial electric field is less than the breakdown value, assumed to be about 2 MV/m by Baum and Baker (1990) and 1 MV/m by Kodali *et al*. (2005). It is generally thought (e.g., Baum and Baker 1990, Rakov 1998) that the bulk of the leader charge is stored in the corona sheath whose radius is of the order of meters, while the highly conductive channel core (probably

less than 0.5 cm in radius) carries essentially all the longitudinal current. The return-stroke current wave traverses the leader-channel core and serves to bring it to ground potential. As a result, the leader charge stored in the corona sheath collapses into the channel core and is transferred to ground. More information on the role of corona envelopes in various lightning processes is found in Heckman and Williams (1989).

Maslowski and Rakov (2006), based on their consideration of the lightning corona sheath dynamics, inferred the existence of two zones around the lightning channel core during the return stroke stage. The inner zone (Zone 1) has net positive charge, and the outer zone (Zone 2) contains negative charge, with the net charge inside the entire corona sheath being equal to zero. It was assumed that the final neutralization of corona charge occurs after the return stroke stage. Similar electrical structure of the return-stroke corona sheath has been considered by Gorin (1985), who studied corona processes during the return stroke stage of long laboratory sparks. Recently, two improved models for prediction of charge motion in the corona sheath are proposed and the radial expansion of Zone 1 and its shrinking was examined (Maslowski *et al*. 2009). Both models include the motion of negative leader charge from the outer to the inner zone, towards the core and can be viewed as generalizations of the model proposed by Maslowski and Rakov (2006). In this paper, we consider detailed dynamics of the corona sheath predicted by lumped-current-source (LCS) type and distributed-current-source (DCS) type return-stroke models with specified longitudinal current distribution (Maslowski and Rakov 2007).

2. Dynamics of the Corona Sheath

A lightning return-stroke model with specified longitudinal current distribution (an engineering return-stroke model) is usually defined as an equation relating the longitudinal channel current $i(z',t)$ at any height z' and any time t to the current $i(0,t)$ at the channel origin, $z'=0$ (e.g., Rakov and Uman, 2003), that is

$$i(z',t) = u(t - z'/v_f)\, P(z')\, i(0, t - z'/v), \tag{1}$$

where u is the Heaviside function equal to unity for $t \geq z'/v_f$ and zero otherwise, $P(z')$ is the height-dependent current attenuation factor introduced by Rakov and Dulzon (1991), v_f is the upward-propagating front speed, and v is the current-wave propagation speed. An equivalent formulation in terms of the line charge density $\rho(z',t)$ expressed as the sum of transferred and deposited charge density components was proposed by Thottappillil *et al.* (1997).

At the beginning of the return-stroke stage the corona sheath expands outward from the channel core inside the leader corona sheath, and then it shrinks up to a nearly zero radius (see Fig. 1). In order to estimate the rate of expansion and shrinking of the corona sheath, we consider a closed cylindrical surface (Gaussian cylinder) dS that is coaxial with and surrounding a segment of channel core whose length is dz. According to Gauss' law,

$$\varepsilon_0 \oint_{dS} \mathbf{E} \cdot d\mathbf{S} = dQ\,, \tag{2}$$

where $\mathbf{E}$ is the electric field on closed surface dS, and dQ is the total charge inside this surface. Maslowski and Rakov (2006) showed that Eq. (1) can be rewritten in the equivalent form as follows

$$2\pi r_{out}^{+}\varepsilon_0 E_r^{+} dz = dQ^{+} + dQ^{-}, \tag{3}$$

where r_{outer}^{+} is the outer radius of the inner zone of corona sheath (Zone 1) containing positive charge deposited by the radial conduction current flowing during the return stroke stage (see Fig. 1b), E_r^{+} is the constant radial electric field on the lateral surface of radius r_{outer}^{+}. The total charge dQ enclosed by dS consists of the negative charge dQ^{-} deposited by the preceding leader and the positive charge dQ^{+} associated with the return stroke stage. In order to estimate r_{outer}^{+}, the radial electric field E_r^{+} must be chosen. We assume that the corona sheath zone with uniform ionization extends outward from the channel core until the field becomes less than the positive breakdown electric field. Note that the radial electric field cannot be established instantaneously, but we will use a constant value of breakdown field for simplicity. In this paper, we assume that the positive breakdown electric field is $E_r^{+} = 1.0$ MV/m (Kodali *et al.* 2005). The return-stroke charge dQ^{+} can be specified using return-stroke models and represented as the sum of two components (Thottappillil *et al*. 1997) as follows

$$dQ^{+} = \rho_{tran} dz + \rho_{leak} dz . \tag{4}$$

The first term of (4) is the charge transferred upward through the channel segment, and the second term represents the deposited charge that is spent to neutralize the leader charge previously deposited in the corona sheath of this segment.

Assuming a uniform radial distribution of the negative leader charge just before the return-stroke stage, one can show that dQ^{-}, which is a portion of the total negative charge stored in the corona sheath located within the radial extent, r_{out}^{+}, of positive charge dQ^{+} can be expressed for $t \geq z'/v$, as

$$dQ^{-} = dQ_1^{-} + dQ_2^{-} = k\rho_L dz' + \left(\rho_L - k\rho_L\right)\left(1 - e^{-(t - z'/v)/\tau_{CN}}\right) dz , \tag{5}$$

where $k = (r_{outer}^{+} / r_{outer}^{-})^2$, $dQ_1^{-} = k\rho_L dz'$ is the negative leader charge deposited within Zone 1 just before the return-stroke stage, dQ_2^{-} is the negative charge that penetrates Zone 1 from Zone 2, and τ_{CN} is the decay time constant describing reduction of negative charge deposited within Zone 2, and, hence, the rate of motion of the negative charge from Zone 2 to Zone 1. In fact, Williams and Heckman (1989) suggested that some slow breakdown processes (positive streamers) can develop outwards from the uniform breakdown region at fields in excess of as low as 0.2 MV/m.

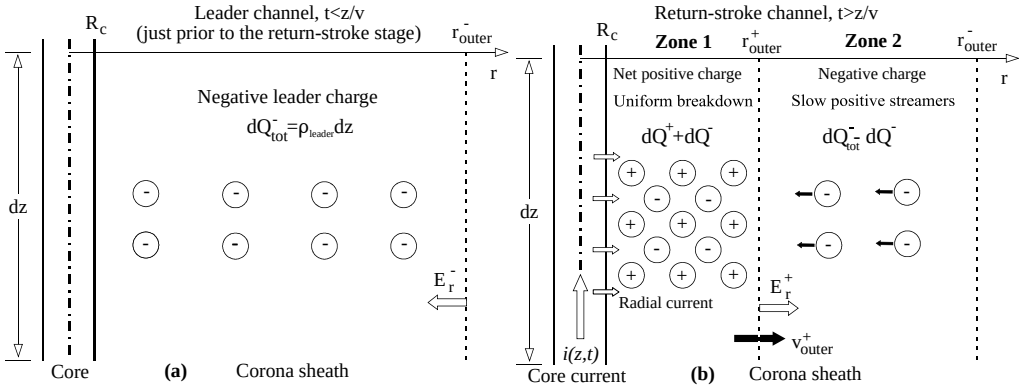

Fig. 1. (a) Leader channel composed of a narrow core of radius R_c and negatively charged corona Heath. (b) Two zones of the corona sheath during the return-stroke stage. Negative charges drift from Zone 2 to Zone 1 so that charge in Zone 2 decays exponentially, while $r_{outer}^{-} = const$.

According to Appendix B of Maslowski and Rakov (2006), dQ_1^- can be expressed as

$$dQ_1^- = \left(2\pi\varepsilon_0 r_{outer}^+ E_r^-\right)^2 dz'/\rho_L , \tag{6}$$

where E_r^- is the negative breakdown electric field which is assumed to be greater (in absolute value) than E_r^+ and equal to 1.5 MV/m (Kodali *et al*. 2005), and ρ_L is the negative charge density per unit channel length prior to the return stroke stage. Note that r_{outer}^+ is necessarily smaller than r_{outer}^-, the radial extent of the negative leader corona sheath. From (3), (4), (5), and (6) we have

$$2\pi r_{outer}^+ \varepsilon_0 E_r^+ = \rho_{tran} + \rho_{dep} + \rho_L\left(1 - e^{-(t-z'/v)/\tau_{CN}}\right) + \frac{(2\pi r_{outer}^+ \varepsilon_0 E_r^-)^2}{\rho_L} e^{-(t-z'/v)/\tau_{CN}} . \tag{7}$$

The radius of Zone 1, r_{outer}^+, is a solution of quadratic Eq. (7) which reduces to (20) of Maslowski and Rakov (2006) for $\tau_{CN} \to \infty$, in which case negative charge from Zone 2 does not penetrate Zone 1. The corona-sheath model described by (7) enables one to predict both the radial expansion of Zone 1 and its shrinkage up to a nearly zero radius, once the decay time constant τ_{CN} is specified.

3. Expansion of Zone 1 for LCS and DCS Models

We estimated τ_{CN} based on the horizontal (radial) electric field component measured in the immediate vicinity of lightning channel during the 2000 triggered-lightning experiment at Camp Blanding, Florida (Miki *et al.* 2002). Electric field waveforms at

horizontal distances from triggered lightning channel attachment point ranging from 0.1 to 1.6 m (most likely inside the corona sheath) have been measured with Pockels sensors. The horizontal electric field change measured during the leader stage was often overcompensated by the opposite-polarity electric field change during the return-stroke stage. Interestingly, the maximum horizontal electric field values during some return strokes were high enough (from 413 kV/m up to more than 520 kV/m) for starting positive breakdown. The time of field relaxation to practically zero level during the overcompensation stage is very similar for all measured waveshapes and is estimated to be approximately 2 ms. Hence, one can estimate the decay time constant to be about one-third of this value.

Evolution of Zone 1 as a function of time at height $z = 10\,\mathrm{m}$ for the three LCS return stroke models, MTLL (Modified Transmission Line model with Linear current decay with height – Rakov and Dulzon 1987), MTLP (Modified Transmission Line model with Parabolic current decay with height – Rakov and Dulzon 1991), and MTLE (Modified Transmission Line model with Exponential current decay with height – Nucci *et al.* 1988), are shown in Fig. 2. Channel base current used here is the same as that adopted by Maslowski and Rakov (2006) and is characterized by a current peak of 12 kA and maximum current rate of rise of about 40 kA/μs. As seen in Fig. 2, Zone 1 expands approximately up to about 500 μs in the case of model described by Eq. 7. After this time, Zone 1 shrinks. Note that for the model with exponential charge decay in Zone 2, one can adjust the rate of corona sheath expansion and its shrinking by changing the decay time constant.

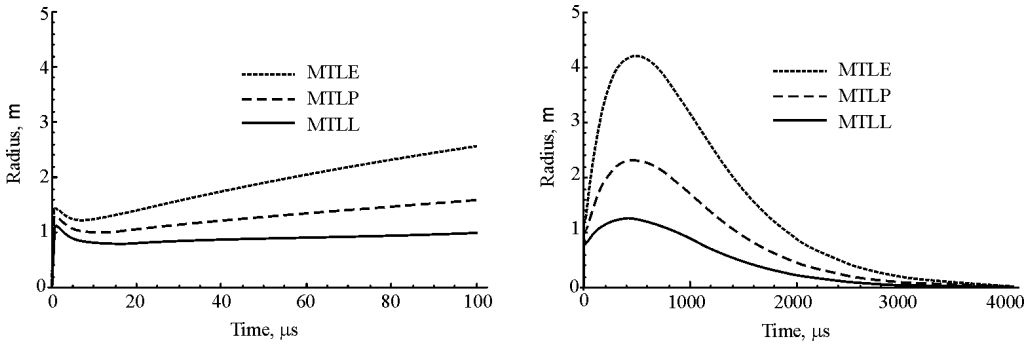

Fig. 2. Comparison of radius r_{outer}^{+} of Zone 1 versus time at a height of 10 m for three return stroke models, MTLL, MTLP, and MTLE (H = 7500 m, λ = 2000 m, v = 130 m/μs) shown on two timescales, 100 μs (left), and 4 ms (right), as predicted by (7). It was assumed in (7) that τ_{CN} = 650 μs.

According to Williams and Heckman (1989), the longitudinal return-stroke current can be decomposed into an "extension current" of tens of kiloamperes for tens of microseconds and two "corona currents", one from streamers providing kiloamperes for hundreds of microseconds and the other one from ion drift providing an ampere for seconds. Also, Diendorfer and Uman (1990) suggested that the return-stroke current can be decomposed into the "breakdown current", which corresponds to the "exten-

sion current" introduced by Williams and Heckman (1989), and "corona current". In the following, we will adopt this latter current division. The "breakdown current" is assumed to be generated at the return-stroke tip and in the central core, while the "corona current" originates in the corona sheath surrounding the central core.

Following Diendorfer and Uman (1990), one can also calculate the absolute value of the leader charge density deposited along the channel before the return-stroke stage as a function of the "breakdown" and "corona" currents (Maslowski and Rakov, 2009)

$$\left|\rho_{\mathrm{L}}(z')\right| = \frac{1}{v^*}\left\{i_{\mathrm{BD}}(0, z'/v^*) + \tau_{\mathrm{BD}}\frac{di_{\mathrm{BD}}(0, z'/v^*)}{dt}\right\} + \frac{1}{v^*}\left\{i_{\mathrm{C}}(0, z'/v^*) + \tau_{\mathrm{C}}\frac{di_{\mathrm{C}}(0, z'/v^*)}{dt}\right\}. \tag{8}$$

Charge density described by (8) is identical to the deposited charge density at the end of the return-stroke stage, which was obtained by Thottappillil *et al*. (1997). In fact, for the DU model with two discharge time constants, τ_{BD} and τ_{C}, this charge density can be expressed as

$$\rho_{\mathrm{L}}(z', t) = -\frac{i_{\mathrm{BD}}(0, t + z'/c)}{c} - \left[\frac{i_{\mathrm{BD}}(0, z'/v^*)}{v} + \frac{\tau_{\mathrm{BD}}}{v^*}\frac{di_{\mathrm{BD}}(0, z'/v^*)}{dt}\right]e^{-(t-z'/v)\tau_{\mathrm{BD}}} + \frac{1}{v^*}\left[i_{\mathrm{BD}}(0, z'/v^*) + \tau_{\mathrm{BD}}\frac{di_{\mathrm{BD}}(0, z'/v^*)}{dt}\right] - \frac{i_{\mathrm{C}}\left(0, t + \frac{z'}{c}\right)}{c} - \left[\frac{i_{\mathrm{C}}(0, z'/v^*)}{v} + \frac{\tau_{\mathrm{C}}}{v^*}\frac{di_{\mathrm{C}}(0, z'/v^*)}{dt}\right]e^{-(t-z'/v)\tau_{\mathrm{C}}}. \tag{9}$$

Note that (9) reduces to (8) for long enough time. It means that (9) represents the positive charge density during the return-stroke stage. Thottappillil *et al*. (1997) proposed division of the total charge density described by (9) into transferred and deposited charge density components. Cooray (2003) modified the original division proposed by Thottappillil *et al*. (1997). According to Cooray's division, for $t \geq z'/v$, the transferred charge density for the two time constants can be written as

$$\rho_{tran}(z', t) = -\frac{i_{\mathrm{BD}}\left(0, t + \frac{z'}{c}\right)}{c} + \frac{i_{\mathrm{BD}}(0, z'/v^*)}{c}e^{-(t-z'/v)\tau_{\mathrm{BD}}} - \frac{i_{\mathrm{C}}\left(0, t + \frac{z'}{c}\right)}{c} + \frac{i_{\mathrm{C}}(0, z'/v^*)}{c}e^{-(t-z'/v)\tau_{\mathrm{C}}}. \tag{10}$$

and the deposited charge density as

$$\rho_{dep}(z',t) = \frac{\tau_{\mathrm{BD}}}{v^*}\left\{\frac{di_{\mathrm{BD}}\left(0,\frac{z'}{v^*}\right)}{dt} + \frac{i_{\mathrm{BD}}\left(0,\frac{z'}{v^*}\right)}{\tau_{\mathrm{BD}}}\right\}\left[1 - e^{-\left(t-\frac{z'}{v}\right)/\tau_{\mathrm{BD}}}\right]$$

$$+\frac{\tau_{\mathrm{C}}}{v^*}\left\{\frac{di_{\mathrm{C}}\left(0,\frac{z'}{v^*}\right)}{dt} + \frac{i_{\mathrm{C}}\left(0,\frac{z'}{v^*}\right)}{\tau_{\mathrm{C}}}\right\}\left[1 - e^{-\left(t-\frac{z'}{v}\right)/\tau_{\mathrm{C}}}\right]. \qquad (11)$$

The deposited charge density at height z' given by (11) is zero for $t = z'/v$ and for $t > z'/v$ increases up to a value which is consistent with (8).

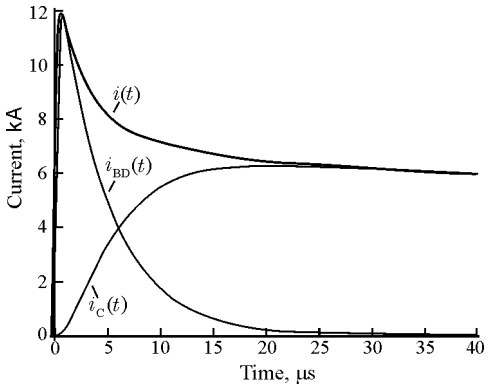

Fig. 3. Illustration of the division of the channel-base current into the "breakdown" and "corona" current components.

Now, we can use (7) to investigate dynamics of the lightning channel corona sheath predicted by DCS type models, in which ρ_{tran}, ρ_{dep}, and $\rho_{\mathrm{L}} = -\left|\rho_{\mathrm{L}}(z')\right|$ are given by (10), (11), and (8), respectively. Again, we assume the same channel base current as in Maslowski and Rakov, (2006). This current can be arbitrarily divided into two current components (see Fig. 3), this division being similar to that of Diendorfer and Uman (1990).

Using these current components one can calculate the line charge density deposited along the lightning channel at the end of the return stroke stage and radius of the corona sheath versus time for different discharge time constants. According to Fig. 4, the distribution of the total charge density strongly depends on the time constant τ_{C}. For greater τ_{C} more charge has to be deposited near the bottom of the channel in order to satisfy the specified channel-base current. In the case of the assumed division of channel-base current and relatively small τ_{C}, the maximal line charge density is predicted close to the ground surface (see curve (1) in Fig. 4a) and for greater τ_{C} the peak line charge density is at a height of about 250 m (see curves (2) and (3) in Fig 4a).

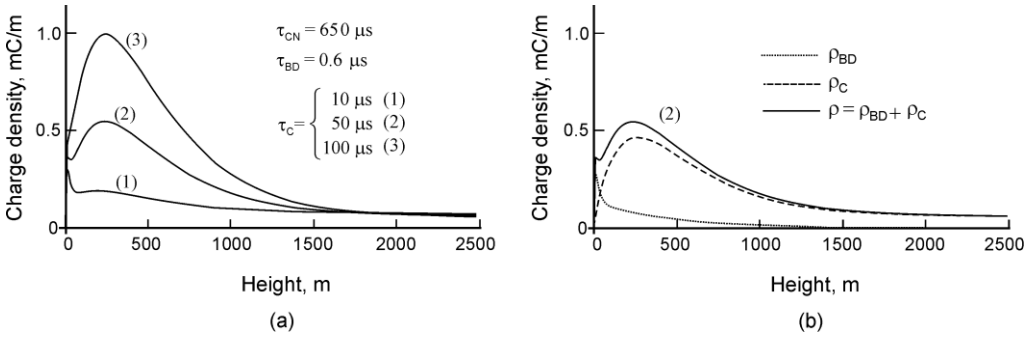

Fig. 4. (a) The leader charge density deposited along the channel before the return-stroke stage which is a function of the "breakdown" and "corona" currents for τ_{BD} = 06 μs, τ_{CN} = 650 μs, and three different τ_C. (b) The leader charge density for τ_C = 50 μs which can be viewed as the sum of "breakdown", ρ_{BD} and "corona", ρ_C components.

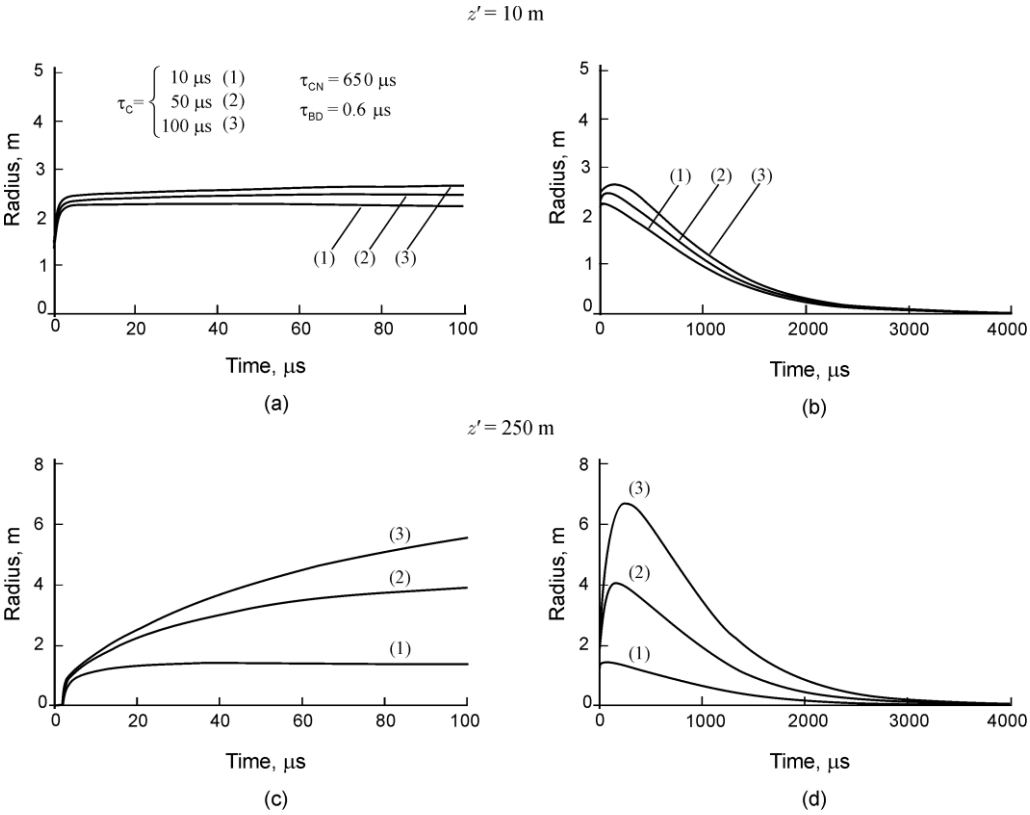

Fig. 5. Comparison of radius r^{+}_{outer} of Zone 1 versus time at a height (a)-(b) of 10 m and (c)-(d) 250 m for the DU model and three values of τ_C, as predicted by (7). Plots are shown on two timescales, 100 μs (left column), and 4 ms (right column). It was assumed in (7) that τ_{CN} = 650 μs. A small longitudinal current predicted by the DU model at the channel top has been neglected, the same as for the MTLE model.

Radii of the corona sheath at z' = 10 m and 250 m for DCS type model (DU model) and three different values of τ_C are shown on two timescales in Fig. 5. Note that small longitudinal current predicted by the DU model at the channel top has been neglected, the same as for the MTLE model. Maximal radius of the corona sheath at a height of 250 m results from the specific distribution of line charge density along the channel for grater τ_C (50 μs and 100 μs). One can see that dynamics of the corona sheath described by LCS type models (see Fig. 2) and those for the DU model are comparable on both timescales.

4. Conclusion

We examined dynamics of the lightning-channel corona sheath that is implicitly specified by lumped-current-source type and distributed-current-source type lightning return-stroke models. A relaxation model of charge motion in the corona sheath is used to investigate the rate of its expansion and shrinking. This model can be viewed as generalization of the model proposed by Maslowski and Rakov (2006) and can be applied for both LCS and DCS return-stroke models with specified longitudinal current distribution. Dynamics of the corona sheath described by LCS type models and the analysed DCS type model (DU) are comparable on both microsecond and millisecond time scales.

References

Baum, C.E., and L. Baker (1990), Analytic return-stroke transmission-line model. **In:** R.L. Gardner (ed.), *Lightning Electromagnetics*, New York: Hemisphere, pp.17-40.

Cooray, V. (2003), On the concepts used in return stroke models applied in engineering practice, *IEEE Trans. Electromagn. Compat.* **45**, 1, 101-108, DOI: 10.1109/TEMC.2002.808041.

Diendorfer, G., and M.A. Uman (1990), An improved return stroke model with specified channel-base current, *J. Geophys. Res.* **95**, D9, 13,621-13,644.

Gorin, B.N. (1985), Mathematical modeling of the lightning return stroke, *Elektrichestvo* **4**, 10-16.

Heckman, S.J., and E.R. Williams (1989), Corona envelopes and lightning currents, *J. Geophys. Res.* **94**, D11, 13,287-13,294, DOI: 10.1029/JD094iD11p13287.

Kodali, V., V.A. Rakov, M.A. Uman, K.J. Rambo, G.H. Schnetzer, J. Schoene, and J. Jerauld (2005), Triggered-lightning properties inferred from measured currents and very close electric fields, *Atmospheric Research* **76**, 1-4, 355-376, DOI: 10.1016/j.atmosres.2004.11.036.

Maslowski, G., and V.A. Rakov (2006), A study of the lightning channel corona sheath, *J. Geophys. Res*. **111**, D14110, DOI: 10.1029/2005JD006858.

Maslowski, G., and V.A. Rakov (2007), Equivalency of lightning return-stroke models employing lumped and distributed current sources, *IEEE Trans. Electromagn. Compat.* **49**, 1, 123-132, DOI: 10.1109/TEMC.2006.890170.

Maslowski, G., and V.A. Rakov (2009), New insights into lightning return-stroke models with specified longitudinal current distribution, *IEEE Trans. Electromagn. Compat*. **51**, 3, 471-478, DOI: 10.1109/TEMC.2009.2017200.

Maslowski, G., V.A. Rakov, J. Cvetic, and M. Miki (2009), An improved model for prediction of the dynamics of lightning channel corona sheath. **In:** *Proc. 20th International Symposium on Electomagnetic Compatibility*, Zurich, Switzerland.

Miki, M., V.A. Rakov, K.J. Rambo, G.H. Schnetzer, and M.A. Uman (2002), Electric fields near triggered lightning channels measured with Pockels sensors, *J. Geophys. Res.* **107**, D16, 4277, DOI: 10.1029/2001JD001087.

Nucci, C.A., C. Mazzetti, F. Rachidi, and M. Ianoz (1988), On lightning return stroke models for LEMP calculations. **In:** *Proc. 19th International Conference on Lightning Protection*, Graz, Austria.

Rakov, V.A. (1998), Some inferences on the propagation mechanisms of dart leaders and return strokes, *J. Geophys. Res.* **103**, D2, 1879-1887, DOI: 10.1029/97JD03116.

Rakov, V.A., and A.A. Dulzon (1987), Calculated electromagnetic fields of lightning return stroke, *Tekh. Elektrodin*. **1**, 87-89.

Rakov, V.A., and A.A. Dulzon (1991), A modified transmission line model for lightning return stroke field calculation. **In:** *Proc. 9th International Symposium on Electomagnetic Compatibility*, p. 44H1, Zurich, Switzerland.

Rakov, V.A., and M.A. Uman (2003), *Lightning: Physics and Effects*, Cambridge University Press, Cambridge, UK, 687 pp.

Thottappillil, R., V.A. Rakov, and M.A. Uman (1997), Distribution of charge along the lightning channel: Relation to remote electric and magnetic fields and to return-stroke models, *J. Geophys. Res.* **102**, D6, 6987-7006, DOI: 10.1029/96JD03344.

Accepted 29 October 2009

PUBLS. INST. GEOPHYS. POL. ACAD. SC., D-73 (412), 2009

Natural Lightning Channel Evolution Obtained from High-Speed Digital Video Camera Recordings

Grzegorz MASŁOWSKI[1], and Piotr BARAŃSKI[2]

[1]Rzeszow University of Technology, Rzeszów, Poland
e-mail: maslowski@prz.edu.pl

[2]Institute of Geophysics, Polish Academy of Sciences, Warszawa, Poland
e-mail: baranski@igf.edu.pl

Abstract

First Polish recordings of natural lightning channel evolution obtained from high-speed digital video camera Phantom MIRO 4 on millisecond-scale resolution are presented. The camera was mounted at the observation point on the seventh floor of a high building in Warsaw during thunderstorm condition on August 15, 2008. Three series of digital recordings of CG flashes with relatively good quality were collected, that is, (1) the fork lightning with two terminations to ground, (2) the lightning flash discharge including continuing current, and (3) the CG flash together with some preceding in-cloud discharges activities. The obtained recordings show that high-speed digital video camera with the time resolution of 1 ms and large own buffer memory (4 GB) can be used to keep track/trace of the entire lightning discharge time evolution. However, in order to investigate in greater detail the process of initial stage of return stroke, notably when its current front is traveling between ground and cloud, it would be desirable to have the camera recording possibility giving the time resolution less than ten microseconds. The optimum way of recordings of natural lightning channel time evolution requires at least two digital cameras working simultaneously with very good GPS time synchronization and having different time resolution and other optical parameter settings. This can prevent undesirable overexposures caused by very large luminosity changes/bursts associated with rapid lightning current flow during the return stroke stages. Another advantage of simultaneous using of two digital cameras viewing at different azimuth angle toward the same and possible lightning flash hitting, e.g., in a very high object, is a chance of obtaining/reconstructly the real three dimensional picture of all visible lightning branches together with its main channel for such flash event. We plan to do that experiment during our next field measuring campaign, using two separated high speed cameras, having very good time synchronization supplied by the external IRIG-B connection.

1. Introduction

At the beginning of systematic lightning study, natural lightning channel evolution has been investigated by using stationary cameras, and then, Boys-cameras having fast-moving films (Uman 1984). In fact, photographic studies of lightning discharges were started in the second half of the nineteenth century. In 1884, H. Kayser (Kayser 1884) photographed a ribbon lightning (the spatially-separated strokes of a flash by the strong wind) using a stationary camera. On the other hand, H.H. Hoffert (Hoffert 1889) and L. Weber (Weber 1889) obtained flash-resloved lightning photographs by rapidly moving their stationary camera in the horizontal plane. Due to such operation, they confirmed in 1889 occurrence of several components during a cloud to ground (CG) flash. H.H. Hoffert also raported that both short strokes and, in some cases, a continuing luminosity were detected during a single flash. At the beginning of the twentieth century, B. Walter published in Germany very valuable photographic investigations (Walter 1902). He used a clock-work mechanism which controlled motion of the camera. Hence, it was possible to measure the time between strokes with a relatively good accuracy. In 1929, C.V. Boys described his new two-lens camera having a fast-moving film, which was mounted on the inner surface of a cylindrical drum (Boys 1929). The time resolution of such a camera approached even 1 microsecond. Also, a slower, single-lens camera having moving film, commonly known as a streak camera, was constructed in order to investigate the leader process with the time resolution about 100 microseconds. Some crucial photographic investigations of CG flashes by using of Boys-cameras have been made in South Africa in the 1930s (Shonland 1956, Malan 1963). In that way, B.F.J. Shonland, H. Collens, D.J. Malan and their co-workes described whole CG flash in detail. Also, a modern lightning terminology was created in that time. Results obtained in South Africa have been confirmed by I.S. Stiekolnikow and C. Walijcew in their CIGRE report published in 1937 r. (Stiekolnikow 1937), and also by J.H. Hagengouth (Hagengouth 1947) who reported photographic results collected within the period 1935-1942 in Pittsfield, USA. A lot of photographic data have been also obtained during the Empire State Building study in New York City. There were described mainly upward lightning events (McEachron 1939, McEachron 1941, Hagenguth 1952). Other interesting photographic study has been made by American researchers in Tucson, Arizona (Evans 1963) and nearby Socorro in New Mexico, USA (Kitagawa 1962). Similarly, in the 1970s K. Berger (Berger 1967) photographed a lot of lightning discharge events in Europe. He observed upward lightning initiated by two ground-based towers situated on two tops, i.e., the Monte San Salvatore and the Monte San Carlo close to small town Lugano in Switzerland. Also, flashes striking directly to the ground close to these towers were registered. His results are very important up to now, because the lightning parameters he determined have been adopted to the current lightning protection standards.

It is to be noted that S. Szpor together with his co-workers started long-term photographic study of CG flashes in Poland, just after the Second World War, in 1945. He postulated, among other things, that the so-called lightning series are typical in the north part of Poland, while the multi-stroke flashes, which predominate in tropical climate are rather rare (Szpor 1963, 1964, 1969, 1972, 1977, 1983). It is worth to no-

tice that one of the modified Boys-camera used in Poland had three discs with flat films which were rotated with different speed. First disc with the highest speed of 8000 circle per minute enables to detect return-stroke evolution, the second one which rotated with speed of 160 circle per minute was dedicated to record leader stages, and the last one with the slowest speed registered only the order of strokes in multi-stroke flashes. Other types of modified Boys-cameras used by Polish researchers were described by Kosztaluk (1985), together with his reports of the main results obtained from the lightning photography.

Later investigations of natural lightning channel evolution, not mentioned above but thoroughly characterized in other publications (e.g., Rakov 2003), have contributed mostly to more detailed description of lightning stages distinguished in the past. Presently, more and more new digital recordings of cloud to ground (CG) flashes are analyzed in different publications (e.g., Ballarotti 2005, Saba 2007). Even though high-speed digital cameras are still very expensive, they are more accessible than Boys-cameras which have been operated mainly in scientific laboratories. In the following sections, we present the first high-speed digital video camera recordings carried out in Poland, which have shown possibilities of tracking of natural lightning channel evolution with 1 ms time resolution (see Figs. 2-4).

2. Instrumentation and measuring setup

The black/white high-speed digital video camera Phantom MIRO 4, manufactured by the Vision Research Inc. Wayne, New Jersey, USA, was used to keep track of natural lightning channel evolution in the Warsaw region. This type of digital camera is useful for applications that demand higher resolution with the ability to record at 800×600 pixels frame resolution. Additional benefits of the MIRO 4 camera include: (1) frame rates ranging from one fps to 1.000 fps; (2) minimum shutter speed of two microseconds, programmable in one microsecond increments; (3) one gigabyte of internal high-speed memory (upgradeable to two gigabytes); (4) compact flash slot for non-volatile storage; (5) touch-sensitive LCD screen for controlling features and viewing slow motion images, (6) user-replaceable, compact, rechargeable battery pack allows the camera to be used in the field without the need for a power source; (7) micro cooling system to keep internal components within optimal operating temperature range; (8) CMOS sensor which offers an ISO rating of 4,800 (monochrome, saturation-based ISO 12232 standard). The camera accepts any standard one-inch, C-mount lens. The MIRO 4 can be also triggered from external control signals allowing camera synchronization, and time-stamping according to the IRIG-B time code. Additional, more extended technical information about that camera and its possible operations is available on the web site www.visionresearch.com.

The SIGMA lens 28-135 mm with f: 3.8-5.6 and manual focus has been connected to camera (see Fig. 1) and used during our thunderstorm observations in Warsaw on 15 August 2008. All successfully obtained captures were exposed by 995 μs and were triggered manually with 1095 ms pre- and post-triggered time. Then, the total time of records was 2.19 seconds with 1 ms time resolution (1000 fps).

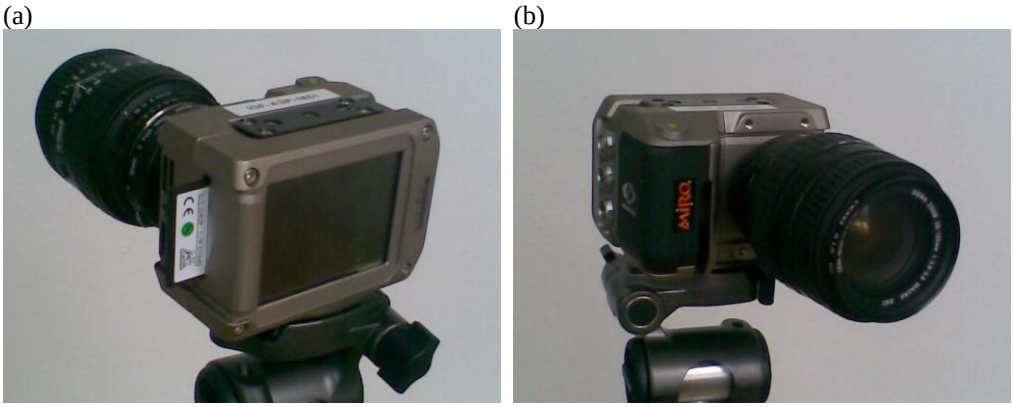

Fig. 1. General view of the high-speed digital video camera Phantom MIRO 4 with its front (a) and back (b) project, and mounted on a tripod.

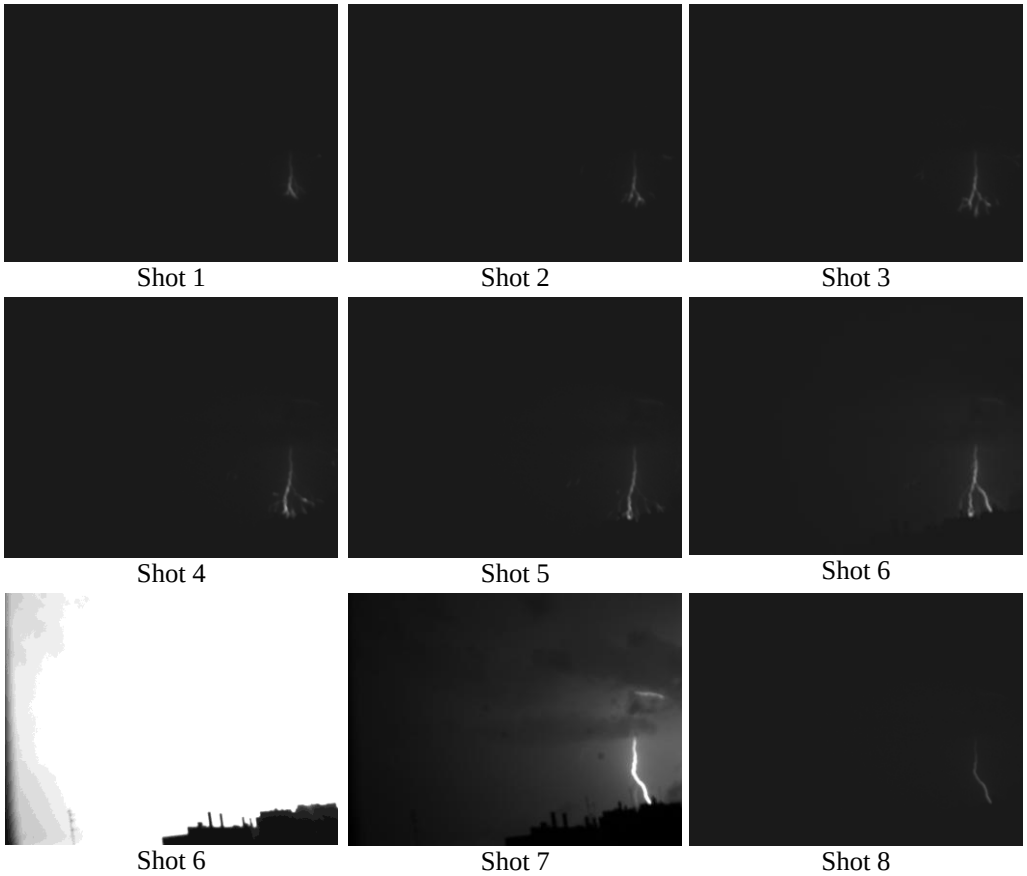

Fig. 2. Natural channel evolution of fork lightning recorded by high-speed digital video camera Phantom MIRO 4 in Warsaw, Poland, during active lightning thunderstorm evening (2008.08.15). Development of stepped leader channel is visible in Shots 1-6 and two return-stroke stages in Shots 7-9.

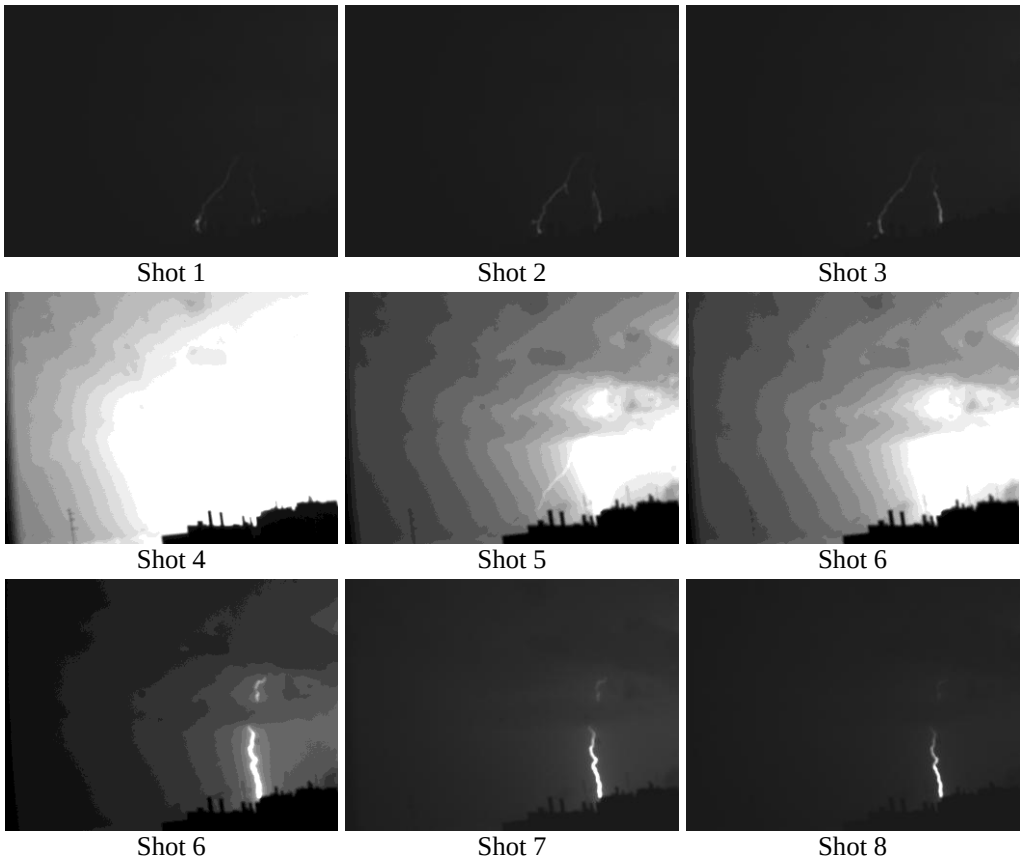

Fig. 3. Natural channel evolution of another fork lightning flash recorded by high-speed digital video camera Phantom MIRO 4 in Warsaw, Poland, during active lightning thunderstorm evening (2008.08.15).

3. Results of lightning flash photography recordings obtained from high-speed digital video camera

Some examples of different natural lightning channel evolution records obtained by using high-speed digital video camera Phantom MIRO 4 are shown in Figs. 2, 3 and 4. It was the first preliminary test done with this camera during thunderstorm conditions in Warsaw on 15 August 2008. The camera was mounted at the observation point on the seventh floor of a high building in Warsaw ($\varphi = 52°13'55''$N, $\lambda = 20°54'37''$E).

Finally, three series of digital recordings of few cloud-to-ground (CG) flashes with relatively good quality as shown in Figs. 2, 3 and 4, were collected. In Fig. 2, one can see the scenario of development of fork lightning discharge with two terminations to ground. On the other hand, the preceding channel evolution of stepped leader of such incident is presented in following sequence of six shots (Shots 1–6). It is worth to note that the time interval between shots was 1 ms and single shot exposure time had also the duration nearly 1 ms. Thus, the time span of visible observation of that lightning

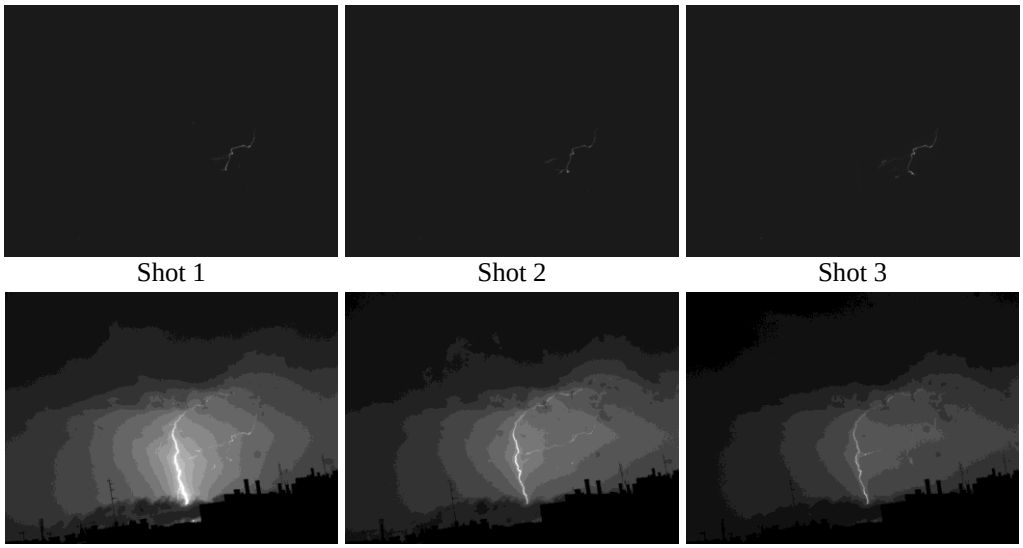

Fig. 4. Natural channel evolution of fork lightning recorded by high-speed digital video camera Phantom MIRO 4 in Warsaw, Poland, during active lightning thunderstorm evening (2008.08.15).

stage lasted 12 ms. Shot 7 presents the first stage of return stroke when the lightning current front is traveling between ground and cloud. At the end of that photo session, in shots 8 and 9, the final stage is depicted of this fork flash, that is, when also relatively small current is flowing, and therefore, luminosity of the channel is not so intensive as in shot 7, but still visible. It also should be remarked that the whole return-stroke process lasts a few milliseconds (usually it is assumed to be of the order of 3 ms, e.g., Rakov,2003, Maslowski and Rakov 2006), since such a time is needed to neutralize the entire charge deposited by preceding leader in the corona sheath.

In the first three shots in Fig. 3, another channel evolution of stepped leader is presented. This stepped leader development precedes the return-stroke stage depicted in shots 4-6 in the same figure. We can note that luminosity of lightning channel is still visible clearly in the last three (see Shots 7-9). This could mean that the continuing current was flowing just after the return-stroke stage. Again, in Fig. 4, one can see how the development of stepped leader (the sequence of first three shots: Shots 1-3) together with the associated in-cloud channel evolution was prolonged. On the other hand, the next three shots present some kind of return-stroke stage which vanishes within more than 3 ms interval and perhaps is also a result of continuing current flow in its channel.

4. Short discussion

Some results of first lightning photography by fast digital recordings carried out in Poland in 2008, presented in Figs 2, 3 and 4, have shown that a high-speed digital video camera can be used as a suitable tool to investigate natural lightning flash chan-

nel evolution. We can postulate that the time resolution of the order of 1 ms is enough to keep track of entire lightning discharge process including stepped leader, return-stroke stage, continuing current flow with its M-components, and also in-cloud discharges activity accompanying the next CG flashes. However, in order to study the return-stroke channel evolution in detail, much higher time resolution is required. Especially, the first stage of return stroke, when lightning current front is traveling between ground and cloud, should be recorded with the time resolution less than ten microseconds. On the other hand, in modern digital video cameras, increasing time resolution causes decreasing spatial resolution of recordings. Therefore, it is difficult to observe with a good quality the entire return-stroke channel when the very high time resolution is fixed at the same time. Another problem with lightning channel recordings resulting from using digital camera, as one can notice in Figs. 2 and 3, is a much higher luminosity of lightning channel during the first stage of return-stroke than the one observed during other next lightning discharge stages. In our opinion, optimum recordings of natural lightning channel evolution in real 3D space requires a set of at least three devices. Each set should consist of two high-speed digital video cameras with different optical parameters and time resolutions, and mounted at practically the same observation point.

More recordings of natural lightning channel evolution obtained by using different high-speed digital video cameras are planned in Poland in the near future. These recordings will be correlated with data from lightning location systems and electric field change measurements in order to investigate different lightning stages more thoroughly.

5. Summary

We have analyzed the first Polish recordings of natural lightning channel evolution obtained during thunderstorm conditions in Warsaw on 15 August 2008 by using high-speed digital video camera Phantom MIRO 4. The digital recordings of CG flashes on millisecond-scale, presented in the paper, have shown usefulness of such a video technology to keep track of entire lightning discharges. In order to investigate in detail return-stroke channel evolution, especially that within first few dozen microseconds, when the lightning current front is traveling between ground and cloud, it would be desirable to make these recordings with the time resolution less than ten microseconds. Similarly, as during Boys-camera recordings, optimum digital video recordings of natural lightning channel evolution require more cameras working at the same time with different time resolutions, and also, with different optical parameters, because of very high luminosity of return-stroke channel in comparison to that appearing during other lightning stages. A new video investigation of lightning discharges using different high-speed digital video cameras are planned in Poland in the near future. These recordings will be correlated with data from lightning location systems working in Poland and electric field change measurements in order to analyse longitudinal and radial lightning channel evolution.

Acknowledgments. This work was partially supported by grant No. COST/204/2006 from Polish Ministry of Science and High Education. The second

author is also grateful Mr. Paweł Dobrosielski for his helpful assistance with starting up and performing first lightning capture shots by using high-speed digital video camera Phantom MIRO 4.

References

Ballarotti, M.G., M.M.F. Saba, and O. Pinto Jr. (2005), High-speed camera observations of negative ground flashes on a millisecond-scale, *Geophys. Res. Lett.* **32**, L23802, DOI: 10.1029/2005GL023889.

Berger, K. (1967), Novel observations on lightning discharges: results of research on Mount San Salvatore, *J. Franklin Inst.* **283**, 478-525.

Boys, C.V. (1929), Progressive Lightning, *Nature* **124**, 54-55, DOI: 10.1038/124054a0.

Campos, L.Z.S., M.M.F. Saba, O. Pinto Jr., M.G. Ballarotti (2007), Waveshapes of continuing currents and properties of M-components in natural negative cloud-to-ground lightning from high-speed video observations, *Atmospheric Research* **84**, 4, 302-310, DOI: . 10.1016/j.atmosres.2006.09.002.

Ewans, W.H., and R.L. Walker (1963), High Speed Photographs of Lightning at Close Range, *J. Geophys. Res*. **68**, 4455-4461.

Hagenguth, J.H. (1947), Photographic study of lightning, *Trans. AIEE* **66**, 577-585.

Hagenguth, J.H., and J.G. Anderson (1952), Lightning to the Empire State Building – Part III, *Trans. AIEE* **71**, 1, 641-649, DOI: 10.1109/AIEEPAS.1952.4498521.

Hoffert, H.H. (1889), Intermittent Lightning Flashes, *Phil. Mag*. **18**, 106-109.

Malan, D.J. (1963), *Physics of Lightning*, London: English Universities Press, 176 pp., DOI: 10.1002/qj.49709038423.

Masłowski, G., and V.A. Rakov (2006), A study of the lightning channel corona sheath, *J. Geophys. Res*. **111**, D14110, DOI: 10.1029/2005JD006858.

McEachron, K.B. (1939), Lightning to the Empire State Building, *J. Franklin Inst*. **227**, 149-217.

McEachron, K.B. (1941), Lightning to the Empire State Building, *Trans. AIEE* **60**, 9, 885-890, DOI: 10.1109/T-AIEE.1941.5058410.

Kayser, H. (1884), *Über Blitzphotographien*, Berlin Königliche Akad. Berlin, 611-615.

Kitagawa, N., M. Brook, and E.J. Workman (1962), Continuing Currents in Cloud-to-Ground Lightning Discharges, *J. Geophys. Res.* **67**, 2, 637-647, DOI: 10.1029/JZ067i002p00637.

Kosztaluk, R., *et al*. (1985), *Technika badań wysokonapięciowych*, T.1, T.2, Warszawa, WNT.

Rakov, V.A., and M.A. Uman (2003), *Lightning: Physics and Effects*, Cambridge University Press, Cambridge, U.K., 687 pp.

Schonland, B.F.J. (1956), The Lightning Discharge, *Handbuch der Physik* **22**, 576-628, Berlin: Springer-Verlag.

Stiekolnikow, I.S., and C. Walijcew (1937), L'etude de la foudre dans un Laboratoire de campagne, CIGRE report no. 30.

Szpor, S. (1969), Comparison of Polish Versus American Lightning Records, *IEEE Trnas. on Power Apparatus and Systems* **PAS-88**, 5, 646-652, DOI: 10.1109/TPAS.1969.292353.

Szpor, S. (1977), Photographic studies on lightning by means of a stationary camera – II, *Archiwum Elektrotechniki* **26**, 1, 3-16.

Szpor, S., and J. Samuła (1983), *Ochrona odgromowa*, T. 1, Warszawa, WNT, 416 s.

Szpor, S., J. Kotłowski, and B. Zaborowski (1963), Badania nad piorunem i błyskawicą bezziemną za pomocą aparatu fotograficznego wirującego – II. W: "Piorun i ochrona odgromowa – Cześć I", *Zbiór prac z Zakładu Wysokich Energii Politechniki Gdańskiej*, Gdańsk: Gdańskie Towarzystwo Naukowe, s. 9-34.

Szpor, S., B. Zaborowski, E. Bylicki, and K. Kardacz (1972), Photographic studies on lightning by means of a rotating camera – IV, Northern Poland, *Archiwum Elektrotechniki* **20**, 1, 9-11.

Szpor, S., E. Wasilenko, J. Samula, E. Dytkowski, J. Suchocki, and B. Zaborowski (1964), *Results of lightning stroke registrations in Poland*, CIGRE Rep. 319.

Uman, M.A. (1984), *Lightning*, Dover Publications Inc., New York, 298 pp.

Walter, B. (1902), Ein photographischer Apparat zur genaueren Analyse des Blitzes, *Physik Z.* **3**, 168-172.

Weber, L. (1884), *Über Blitzphotographien*, Ber. Königliche Akad. Berlin, 781-784.

Accepted 29 October 2009

PUBLS. INST. GEOPHYS. POL. ACAD. SC., D-73 (412), 2009

Engineering Utilization of the Results of Lightning Research

Zdobysław FLISOWSKI

Warsaw University of Technology,
Department of High Voltage Engineering and Electrical Apparatus
Koszykowa 75, 00-662 Warsaw, Poland

Abstract

This paper deals with the way in which the data on lightning discharges are utilized by engineers for lightning protection. A comprehensive review of these data and their selected features, important from lightning hazard point of view, is followed by a description of the hazard assessment methods. The role of Stanisław Michnowski in lightning discharge physics is pointed out.

1. Introduction

While discussing the engineering utilization of lightning data, the achievements of Stanisław Michnowski, acknowledged expert on atmospheric electricity, as discussed in the accompanying address (Flisowski 2009, this issue), are to be pointed out. He substantially contributed to collecting the lightning discharge data and to the development of lightning discharge physics.

2. Engineering Utilisation of Lightning Data for Lightning Protection

In order to utilize the data on lightning discharges for the engineering practice, the standards on structure protection against lightning flashes have been established in international scale [1], [2], [3], [4]. According to these standards, the lightning cloud-to-ground flashes (Fig. 1) are recognized as most significant from the point of view of lightning hazard for ground-based structures, although the cloud-to-cloud discharges should not be ignored, because their number reaches 70% of all the discharges and they can cause unacceptable electromagnetic interferences (EMI) of different devices, especially electronic ones.

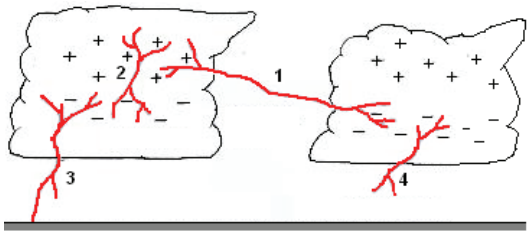

Fig. 1. Kinds of discharges: 1 – cloud-to-cloud, 2 – intercloud, 3 – cloud-to-ground (complete), 4 – cloud to-ground (partial)caption.

The following cloud-to-ground discharges (Fig. 2) may be distinguished:

- downward (types 1 and 3) and upward (types 2 and 4) discharges,
- negative (types 1 and 2) and positive (types 3 and 4) discharges,
- stopped or partial (type a) and complete (type b) discharges.

The attention is directed to the lightning discharges (or flashes) of type 1, because they create about 90% of all the flashes, as well as to flashes of type 4, because their strokes are more dangerous than those of type 1.

Flashes of type 2 and 3 are less important. First of these develop only from high structures and the other appear very rarely.

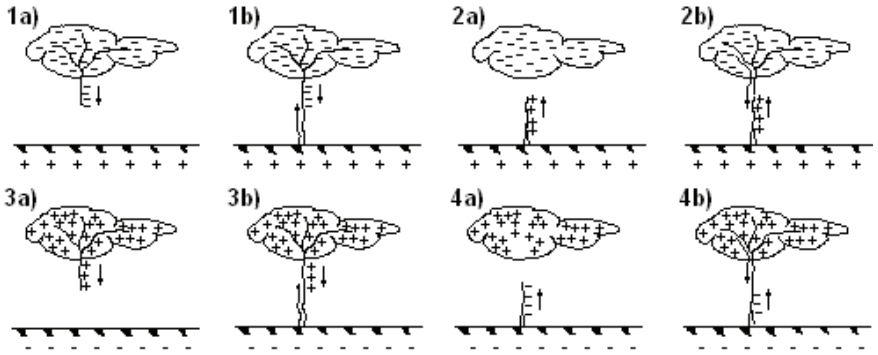

Fig. 2. Types of cloud-to-ground flashes: (1) downward negative, (2) upward negative, (3) downward positive, (4) upward positive; (a) stopped, (b) completed.

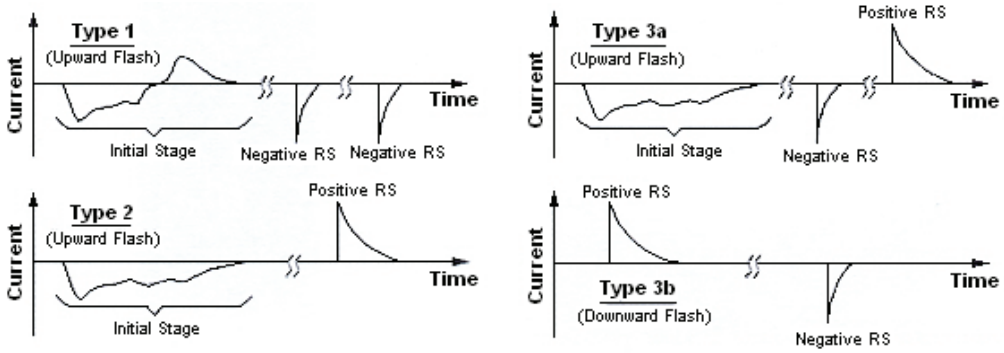

Fig. 3. Types of bipolar discharges.

The above-mentioned flashes (Fig. 2) are unipolar, but the need of considering bipolar flashes (Fig. 3) is also taken into account.

Strokes appearing in downward flashes (Fig. 4) and those of upward flashes (Fig. 5) may differently influence the hazard for structures and the devices of their equipment.

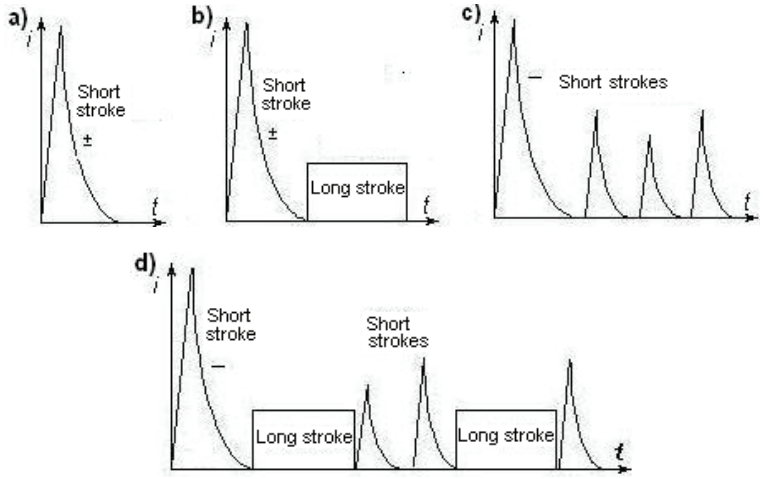

Fig. 4. Possible (in a flat country) components of downward discharges: (a) first short stroke (positive or negative), (b) long stroke after the first short one (positive or negative), (c) first negative stroke and successive ones, (d) first negative stroke and successive ones (long and short).

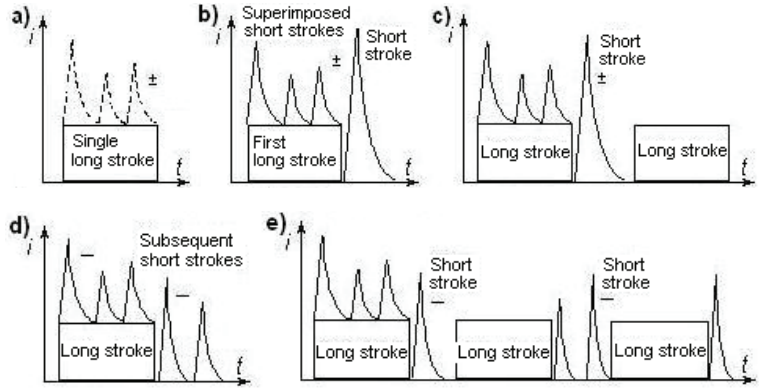

Fig. 5. Possible components of upward discharges: typical for exposed and/or higher structures.

It has been fund that:

- the first short stroke, defined as in Fig. 6a, is dangerous for the sake of its great peak value (Table 1),
- successive short strokes, defined also as in Fig. 6a, are dangerous for the sake of their great current rate of rise,
- long strokes, defined as in Fig. 6b, are dangerous for the sake of great transferred charge.

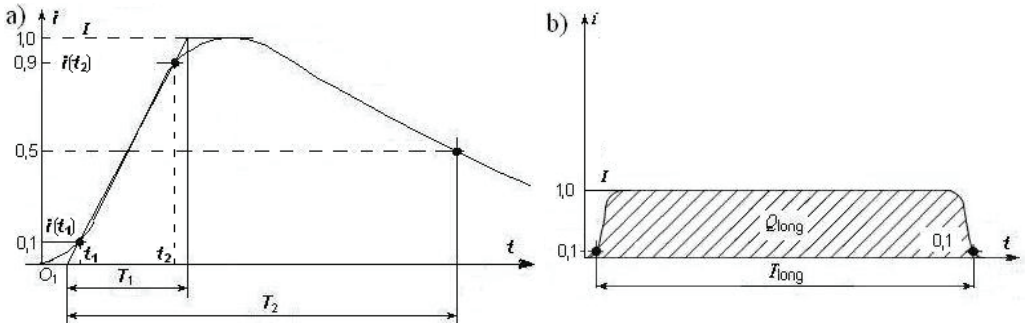

Fig. 6. Current stroke: (a) short (first and subsequent), (b) long; O_1 – virtual origin of short stroke current, I – peak value of short stroke current, T_1 – front time of short stroke current, T_2 – time to half value of short stroke current, T_{long} – duration of long stroke current, Q_{long} – long stroke charge.

With the purpose of the lightning hazard assessment due to stroke currents and entire lightning flashes, the following parameters may be distinguished:

- peak value of short stroke current I;
- maximum steepness of the front of short stroke current $S_{\max} = (di/dt)_{\max}$;
- average steepness of the front of short stroke current $S_{av} = (di/dt)_{av}$;
- front time T_1 and time to half value T_2 of short stroke current;
- flash charge $Q_{flash} = \int_0^T I dt$;
- short stroke charge $Q_{short} = \int_{T_{short}} I dt$;
- long stroke charge $Q_{long} = \int_{T_{long}} I dt$;
- specific energy dissipated in the resistance of 1 Ω (time integral of the square of the flash duration current) $W/R = \int_0^T i^2 dt$;
- number n of current strokes in a flash;
- annual density N_g of lightning flashes/km^2).

Parameters of lightning strokes as well as the phenomenon of lightning discharge itself have a random nature and are subjected to statistical evaluation. The cumulative distribution function of lightning parameters ($Z = I, S, Q, W, T_1, T_2, n$) is of log-normal nature, as shown in Fig. 7. The parameters of this distribution are presented in Tables 1 and 2 and the function of its density is expressed by the following formula

$$g(Z) = \frac{1}{\sqrt{2\pi} Z \sigma_Z} \exp\left[-\frac{\left(\ln Z - \ln Z_{50\%}\right)^2}{2\sigma_Z^2} \right], \tag{1}$$

where $Z_{50\%}$ is the average value of the variable Z, and $\sigma_Z = \ln Z_{16\%}/Z_{50\%}$ is the standard deviation of its distribution.

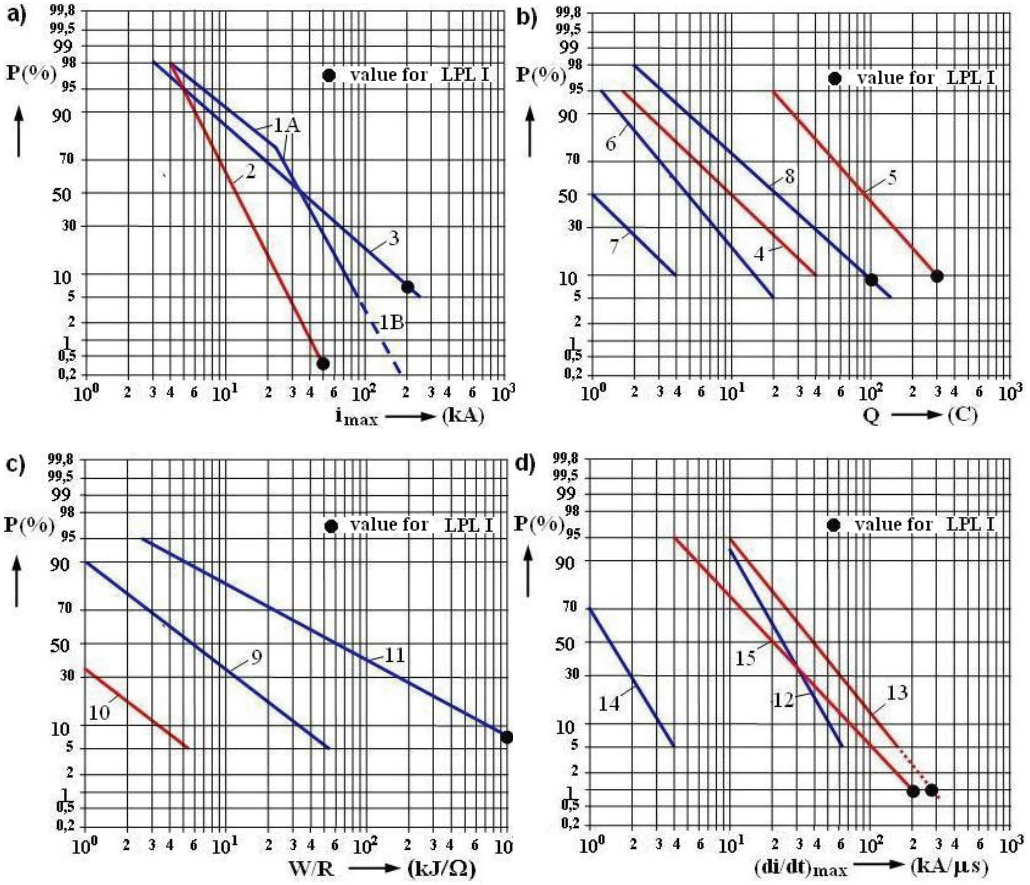

Fig. 7. Cumulated frequencies of the appearance of lightning current parameters. The numbering of curves is explained in Tables 1 and 2.

It should be explained here that one of specified lightning parameters, namely the annual density N_g of lightning flashes, is not subject to this distribution. The uniform distribution is attributed to this density and its value resulting from the formula

$$N_g = \alpha N_d^{\beta}, \tag{2}$$

where N_d is the isokeraunic level, and α, β are the coefficients depending mainly on the latitude. For practical applications the coefficients have been approximated by values $\alpha = 0{,}1$ i $\beta = 1$, which gives the formula

$$N_g = 0.1 N_d . \tag{3}$$

More upgraded approach to this number is based on the data registered by lightning location systems.

Four Lightning Protection Levels (LPL) have been distinguished and coordinated with maximum and minimum values of lightning current parameters (see Tables 3 and 4, respectively).

Table 1

Log-normal distribution of lightning current parameters – the average value μ and standard deviation σ_{log} determined on the basis of 95 % and 5 % values of CIGRE data

Parameter	Average μ	Standard deviation σ_{log}	Type of stroke	Curve in Fig. 7
I (kA)	61,1/33,3	0,576/0,263	First negative short (80 %)	1A / 1B
	11,8	0,233	Subsequent negative short	2
	33,9	0,527	First positive short	3
Q_{flash} (C)	7,21	0,452	Negative flash	4
	83,7	0,378	Positive flash	5
Q_{short} (C)	4,69	0,383	First negative short	6
	0,938	0,383	Subsequent negative short	7
	17,3	0,570	First positive short	8
W/R (kJ/Ω)	57,4	0,596	First negative short	9
	5,35	0,600	Subsequent negative short	10
	612	0,844	First positive short	11
di/dt_{max} (kA/μs)	24,3	0,260	First negative short	12
	40,0	0,369	Subsequent negative short	13
	2,53	0,670	First positive short	14
$di/dt_{30/90\%}$(kA/μs)	20,1	0,420	Subsequent negative short	15
Front time (μs)	5,69	0,304	First negative short	
	0,995	0,398	Subsequent negative short	
	26,5	0,534	First positive short	
Stroke duration (μs)	77,5	0,250	First negative short	
	30,2	0,405	Subsequent negative short	
	224	0,578	First positive short	
Flash duration (ms)	12,8	1,175	Negative flash	
	83,7	0,472	Positive flash	

Maximum values are decisive for the range of thermal, mechanical and electrical hazard for the structure and its equipment, whereas the minimum values are decisive for the interception efficiency of lightning strikes by air terminations, but in this case the following principles are applicable:

- when the efficiency should be greater, the radius r of rolling sphere (Fig. 8) should be lesser;
- the radius r providing a postulated interception efficiency of air terminations determinates the minimum value of the lightning current (Table 4);
- all lightning strikes with greater current values will be intercepted by air terminations (Fig. 8b);
- the probability of lightning strike interception is equal to the probability of appearance of the minimum peak value of the current (Table 5).

The depth of sphere penetration into area between air terminations may be obtained from the formula as follows

$$p = r - \left[r^2 - (0.5d)^2 \right]^{0.5}. \tag{4}$$

Table 2

The values of lightning current parameters accepted on the basis of CIGRE data

Parameter	Values for LPL I	Distribution values			Type of the stroke	Curve in Fig. 7
		95 %	50 %	5 %		
I (kA)	50	4(98 %)	20(80 %)	90	First negative short	1A+1B
		4,9	11,8	28,6	Subseq. negative short	2
	200	4,6	35	250	First positive short	3
Q_{flash} (C)	300	1,3	7,5	40	Negative flash	4
		20	80	350	Positive flash	5
Q_{short} (C)	100	1,1	4,5	20	First negative short	6
		0,22	0,95	4	Subseq. negative short	7
		2	16	150	First positive short	8
W/R (kJ/Ω)	10 000	6	55	550	First negative short ótki	9
		0,55	6	52	Subseq. negative short	10
		25	650	15 000	First positive short	11
di/dt_{max} (kA/µs)	20	9,1	24,3	65	First negative short	12
		9,9	39,9	161,5	Subseq. negative short	13
		0,2	2,4	32	First positive short	14
$di/dt_{30/80\,\%}$	200 (kA/µs)	4,1	20,1	98,5	Subseq. negative short	15
Q_{long} (C)	200				Long	
t_{long} (s)	0,5				Long	
Front duration (µs)		1,8	5,5	18	First negative short	
		0,22	1,1	4,5	Subseq. negative short	
		3,5	22	200	First positive short	
Stroke duration (µs)		30	75	200	First negative short	
		6,5	32	140	Subseq. negative short	
		25	230	2 000	First positive short	
Interval (ms)		7	33	150	Multiple negative	
Flash duration (ms)		0,15	13	1 100	Negative flash (all)	
		31	180	900	Negative flash(nosingle)	
		14	85	500	Positive flash	
Note: Values I = 4 kA and I = 20 kA correspond to a probability of 98 % and 80 % respectively						

Table 3

Maximum values o lightning current parameters according to distinguished levels (LPL)

Current parameters	Symbol	Unit	LPL		
First sort stroke			I	II	III – IV
Current peak value	I	kA	200	150	100
Short stroke charge	Q_{short}	C	100	75	50
Specific energy	W/R	kJ/W	10.000	5.625	2.500
Time parameters	T_1/ T_2	µs/µs	10 / 350		
Subsequent short stroke			I	II	III – IV
Current peak value	I	kA	50	37,5	25
Average steepness	di/dt	kA/µs	200	150	100
Time parameters	T_1/ T_2	µs / µs	0,25 / 100		
Long stroke			I	II	III – IV
Long stroke charge	Q_{long}	C	200	150	100
Time parameter	T_{long}	s		0,5	
Flash			I	II	III – IV
Flash charge	Q_{flash}	C	300	225	150

Table 4

Connections between LPL and minimum values of lightning current and adequate radiuses of rolling sphere (Fig. 8)

LPL ⟶	I	II	III	IV
Criteria of interception				
Minimum current peak value I kA	3	5	10	16
Minimum rolling sphere radius r m	20	30	45	60

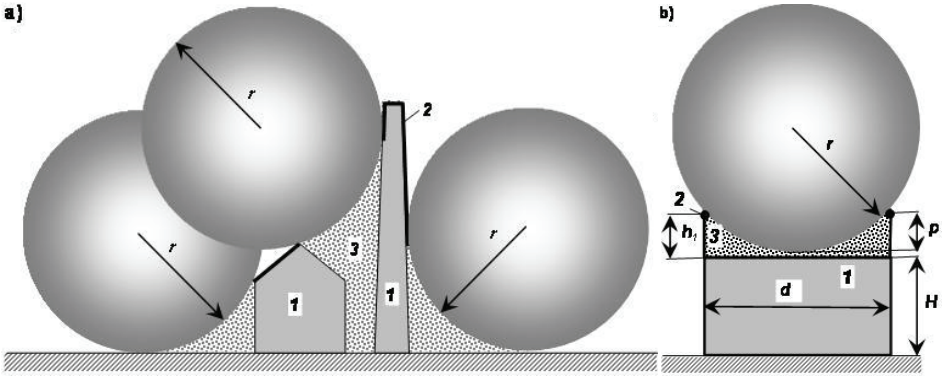

Fig. 8. Protected areas according to the rolling sphere method: (a) arrangement of two structures (high and low), (b) arrangement of horizontal air terminations on the roof; 1 – structure, 2 – air termination, 3 – protected area, H – structure height, h_1 – air termination height above the roof, d – distance between the air termination conductors, r – rolling sphere radius corresponding to protection level (LPL), p – depth of sphere penetration into area between air terminations.

Table 5

The probability of appearance of current values greater than the minimum ones for given LPL

LPL	I	II	III	IV
Probability	0,99	0,97	0,91	0,84

According to the Electro-Geometrical Model (EGM), the radius r of the rolling sphere (the length of the final jump of the lightning leader) is correlated with the current peak value of the first short stroke. This correlation may be expressed by the formula

$$r = 10 \cdot I^{0.65}, \tag{5}$$

where r is the radius of rolling sphere, in m, and I is the current peak value, in kA.

Standard current wave shapes T_1/T_2 (Fig. 6a and Table 3) of short strokes: first T_1/T_2 = 10/350 μs and subsequent T_1/T_2 = 0,25/100 μs, are obtained from the formula

$$i = \frac{I}{k} \frac{(t/\tau_1)^{10}}{(t/\tau_1)^{10}+1} \exp(-t/\tau_2), \tag{6}$$

where I is the current peak value, k is the correction factor of current peak value, t is time, τ_1 is the front time constant, and τ_2 is the tail time constant. The values of k, τ_1 and τ_2 for the current shapes distinguished above are given in Table 6.

Table 6

Values of k, τ_1 and τ_2 for current calculation in accordance with formula (6)

Parmeters in formula (6)	First short stroke (10/350 μs)			Subsequent short stroke (0,25/100 μs)		
	LPL			LPL		
	I	II	III-IV	I	II	III-IV
I_m (kA)	200	150	100	50	37,5	25
k	0,93	0,93	0,93	0,993	0,993	0,993
τ_1 (μs)	19	19	19	0,454	0,454	0,454
τ_2 (μs)	485	485	485	143	143	143

The need of protection application should be decided on the basis of calculations of the risk of lightning damage, which should be performed according to the standard method presented in [2]. The general formula of the calculation is the following

$$R(t) = 1 - \exp(-NPLt), \tag{7}$$

where R is the risk of damage, N is the number of flashes influencing the structure, P is the probability of damage appearance due to one lightning flash, L the consequent loss due to damage in a structure, and t is the hazard time under consideration.

When t = 1 year and the exponent $NPLt \ll 1$, then

$$R \approx NPL. \tag{8}$$

Eight risk components have been distinguished as follows:

- three components (R_A, R_B, R_C) connected with direct flashes to the structure,
- three components (R_U, R_V, R_W) connected with direct flashes to the incoming line,
- one component (R_M) connected with flashes striking near to the structure,
- one component (R_Z) connected with flashes striking near to the incoming line.

Their values enable, respectively, to assess the risk of:

- the shock of living beings outside the structure (R_A) and inside it (R_U),
- physical damages – burst, fire, explosion (R_B, R_V),
- damages due to overvoltages (R_C, R_M, R_W, R_Z).

In order to evaluate a selected component R_X, the following formula may be used

$$R_X \approx N_X P_X L_X, \tag{9}$$

where X = A, B, C, M, U, V, W, Z.

The number of flashes N_X for relevant component X is expressed by the product

$$N_X \approx N_g A_X C_d , \tag{10}$$

where: N_g is the annual stroke density, in km^{-2}, A_X is the equivalent area dependent on structure dimensions, in km^2, C_d is the structure location coefficient.

Probability P_X is the product

$$P_X \approx P_X^* K_S , \tag{11}$$

where $P_X^* = 1$ represents the damage probability of unprotected structure, K_S the damage probability reduction factor representing the efficiency of protection measures (its values are determined in [2]).

The value of consequent loss L_X is evaluated taking in account:

- destination of the structure and its equipment;
- presence of the people inside and outside the structure;
- kind of public services;
- expenses for loss reduction.

At the approximated assessment of the entire risk of damages, the sum of values of relevant risk components should be evaluated from the following formula

$$R \approx \sum_{X=A}^{X=Z} N_X P_X L_X . \tag{12}$$

In general approach, different combinations of components may be considered. They are explained graphically in Fig. 9.

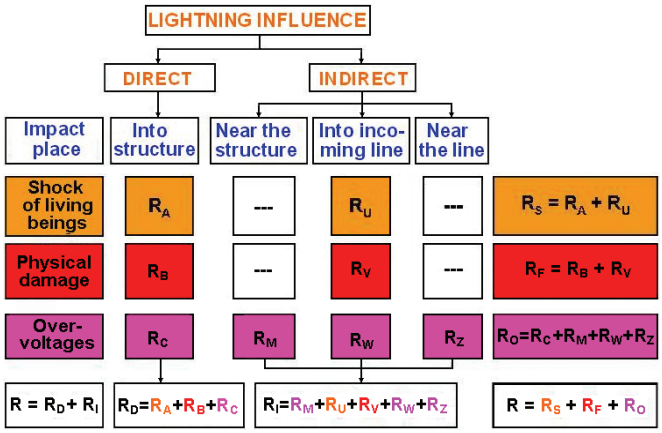

Fig. 9. Combinations of risk components.

When the calculated value of risk R is greater than its tolerable value R_T, then adequate protection measure should be selected and installed. The condition to be fulfilled is

$$R < R_T . \tag{13}$$

If not, the next protection measure should be selected and the condition (13) should be checked again, and so on. For this aim, the procedure presented in Fig. 10 should be applied.

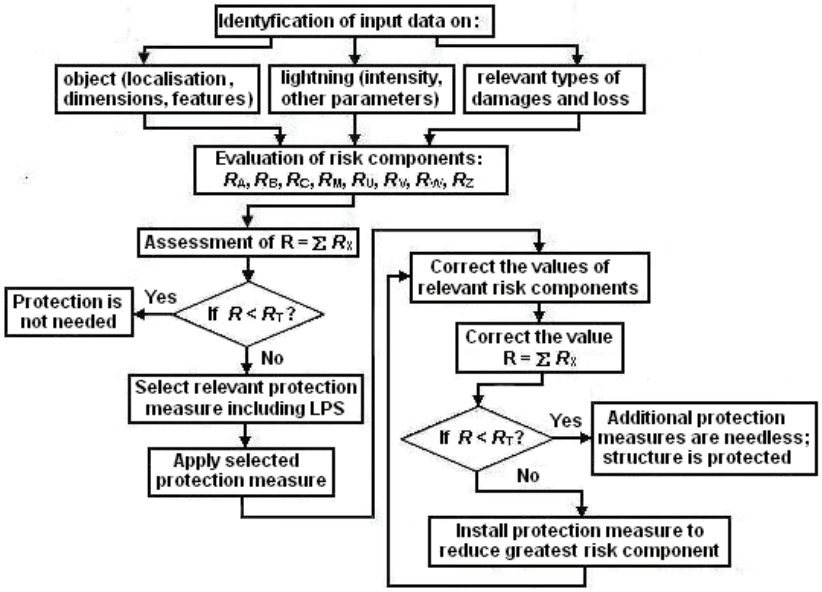

Fig. 10. Procedure of selection of lightning protection measures.

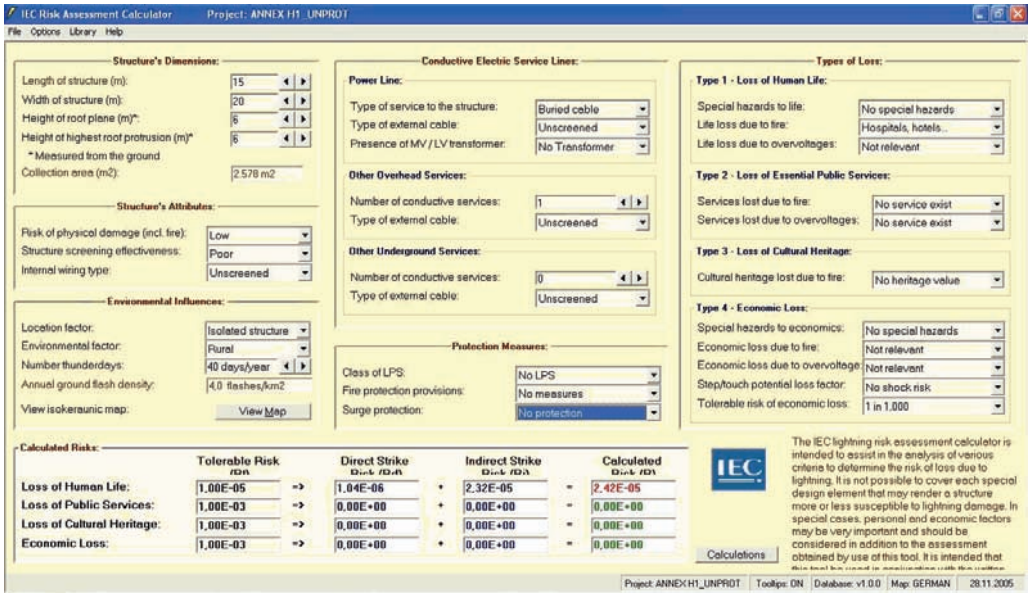

Fig. 11. Printout of the RAC page.

In order to reduce the risk to tolerable level, adequate protection measure and its efficiency must be selected. Relevant protective efficiency is attributed to the protection measure by the reduction factor, which – according to relation (11) – limits the probability of damage and which in this way reduces the risk component. The selected protection measure should influence the risk component having the greatest value.

The value of tolerable risk is usually accepted on the level of $R_T = 10^{-5}$, when the loss of people life is endangered, and on the level of $R_T = 10^{-3}$, when other losses are taken in account. The condition (13) may be checked according to the procedure based on the special computer programs. One of them is the computer program RAC (Risk Assessment Calculator) prepared in frames of IEC TC81 together with the standard IEC 62305-2 [2]. Printout of the page of this program is shown in Fig 11.

3. Final Remarks

- The data on lightning discharges cumulated for many years create a good and reliable basis for lightning hazard evaluation.
- The risk calculation method involved to the selection of lightning protection measures enables avoiding damages of the structure and its equipment in efficient and optimum way.

References

Flisowski, Z. (2009), Recollections, congratulations and wishes on the occasion of Stanisław Michnowski's Jubilee, *Publs. Inst. Geophys. Pol. Acad. Sci*. **D-73**, 412 (this issue).

[1] EN 62305-1:2006. Protection Against Lightning – Part 1: General principles.

[2] EN 62305-2:2006. Protection Against Lightning – Part 2: Risk management.

[3] EN 62305-3:2006. Protection Against Lightning – Part 3: Physical damage to structures and life hazard.

[4] EN 62305-4:2006. Protection Against Lightning – Part 4: Electrical and electronic systems within structures.

Received March 12, 2009

PUBLS. INST. GEOPHYS. POL. ACAD. SC., D-73 (412), 2009

Preliminary Assessment of Ions Distribution in the Atmospheric Mixed Layer Based on a Single Column Model

Marek KUBICKI

Institute of Geophysics, Polish Academy of Sciences
Księcia Janusza 64, 01-452, Warszawa, Poland

Abstract

The distribution of ions in the convective boundary layer (CBL) is investigated based on a non-local closure model. The obtained results show that the ion fluxes are not linear and exhibit distinct maxima. The fluxes of small ions, large ions, and aerosol particles strongly differ from each other. Vertical profiles of small ion concentrations are less variable with height than those of large ions. The lifetime of ions versus the eddy turnover time of the CBL is of decisive influence for shaping their fluxes and vertical profiles. The resulting vertical profiles of ions are used for estimating the electrical convective current.

1. Introduction

In the global electric circuit over the so-called fair-weather areas, the Maxwell current between the ionosphere and the Earth is dominated by the conductivity current

$$J_{con} = E\lambda,$$

where E is the electric field strength, and λ is the electrical conductivity of air (Israel 1973). Under certain meteorological situations, notably in the presence of a negative temperature gradient near the Earth's surface and strong turbulent mixing, the values of the convective current $J_{cov} = w\rho$ (where w is the vertical component of wind velocity, and ρ is the space charge) may be large. This current is directed upwards, opposite to J_{con}, violating the budget of the Maxwell current and vertical profiles of ion density and field E. The effect of turbulent mixing on E and λ near the Earth's surface is considered as a local factor that contaminates the measurement of global variations of atmospheric electricity parameters.

The present paper deals with the determination of ion and space charge profiles in the planetary convective layer. In the presence of thermals, the excess of the positive electric charge gathered near the Earth's surface is transported upward, and subsequently it drifts downwards. The processes that take place during the transport are: generation, annihilation, and conversion of small and large ions in the presence of aerosol. The lifetime of ions varies depending upon the CBL turnover time, which leads to electrical charge separation and different patterns of vertical profiles of concentration and fluxes of ions and aerosol particles. These ions are related to the flow of the electric current in the atmosphere. In the windless atmosphere, the ions flow along the lines of the electric field *E*, and their velocity depends on *E*. Under the fair-weather conditions (absence of cloud cover and precipitation), the average value of *E* is 100 V/m, the velocity of small ions is 1.2-1.4 cm/s, while that of large ions is by three orders lower (Chalmers 1967).

Earlier work (e.g., Hoppel and Getman 1971) was focused on the determination of vertical profiles of *E* and ions in the surface layer using the K-theory approach. Willet (1975) modeled the space charge resulting from charge collected on small ions using Large Eddy Simulation (LES), with no account for the presence of aerosol. He presents relations between the heat flux, which reaches maximum in early afternoon hours, and the behavior of field *E* measured in the surface layer at the same time. The heat flux growth is correlated with the decrease of the field *E*. Willet's model does not directly account for the effect of aerosol, which – under the conditions of strong convection and large mixed layer height – may substantially influence the vertical ion concentration profiles in the convective layer (CBL).

The main objective of this paper is to evaluate and analyze the vertical concentrations of ion fluxes in the presence of a large amount of aerosol, as a function of parameters of the CBL.

2. Model

The CBL model applies the single-column (one-dimensional) equations of the form:

$$\frac{\partial u}{\partial t} = f(v - v_g) - \frac{\partial R_x}{\partial z}, \qquad \frac{\partial v}{\partial t} = -f(u - u_g) - \frac{\partial R_y}{\partial z}, \qquad \frac{\partial \Theta}{\partial t} = -\frac{\partial H}{\partial z},$$

$$\frac{\partial n_i}{\partial t} = -\frac{\partial F n_i}{\partial z} + f_{ni}, \qquad \frac{\partial N_i}{\partial t} = -\frac{\partial F N_i}{\partial z} + f_{Ni}, \tag{1}$$

where u and v are the components of the wind vector, u_g and v_g are the components of the geostrophic wind, f is the Coriolis parameter, Θ is the potential temperature, n_i and N_i are the concentration of the i-th ion and aerosol (i = 0, 1, 2), R_x, R_y, H, Fn_i, and FN_i are the turbulent fluxes for momentum, heat, ions/aerosol, f_{ni} and f_{Ni} are the ion/aerosol source and sink functions.

The first two equations of the above system are the momentum equations, while the third fourth and fifth equation are the budgets for the potential temperature and the ion/aerosol concentrations. Making use of the atmospheric electricity notation, n_1 is the positive small ion concentration, n_2 is the negative small ion concentration, N_1 is

the positive large ion concentration, N_2 is the negative large ion concentration, *No* is the large aerosol concentration, and n_0 is the small aerosol (nuclei) concentration. The source and sink functions, f_{ni} and f_{Ni}, express the ion transformations and are of the form:

$$f_{n1} = q_0 - \alpha_r n_1(z) n_2(z) - \beta_0 n_1(z) N_0(z) - \beta_1 n_1(z) N_2(z)$$

$$f_{n2} = q_0 - \alpha_r n_1(z) n_2(z) - \beta_0 n_2(z) N_0(z) - \beta_1 n_2(z) N_1(z)$$

$$f_{N1} = \beta_0 N_0(z) n_1(z) - \beta_1 n_2(z) N_1(z)$$

$$f_{N2} = \beta_0 N_0(z) n_2(z) - \beta_1 n_1(z) N_2(z)$$

$$f_{No} = \beta_1 N_2(z) n_1(z) + \beta_1 N_1(z) n_2(z) - \beta_0 n_1(z) N_0(z) - \beta_0 n_2(z) N_0(z)$$

$$f_{no} = \alpha_r n_1(z) n_2(z) - q_o \tag{2}$$

where q_0, α_r, β_0, β_1 are the ionization rate, recombination coefficient, attachment coefficient between small ions and uncharged aerosols, and attachment coefficient between small ions and large ions.

The system (1) is augmented by the boundary conditions in the form:

$$\text{at } z = z_o: \quad u = 0, \quad v = 0, \quad \Theta = \Theta_o, \quad n_i = n_{io}, \quad N_i = N_{io}$$

$$\text{at } z = D: \quad u = u_g, \quad v = v_g, \quad d\Theta/dz = \Gamma, \quad dFn_i/dz = g_{ni}, \quad dFN_i/dz = g_{Ni} \tag{3}$$

where z_o is the roughness parameter, D is the upper limit of the computational domain, Θ_o, n_{io}, and N_{io} are the surface values of the temperature and small ion/aerosol, large ion/aerosol concentration, Γ, g_{ni}, and g_{Ni} are the gradients of temperature and small, large ion/aerosol concentration in the free atmosphere. The values of z_o, Γ, g_{ni}, and g_{Ni} are specified, while Θ_o, n_{io}, and N_{io} are evaluated iteratively using the Monin-Obukhov similarity theory, based on given values of surface fluxes H_o, Fn_{io}, and F_{Nio}. During the simulation, the surface fluxes H_o, Fn_{io}, and F_{Nio} were kept constant with time, which takes place in the atmosphere around noon (mid-day quasi-steady conditions). At the beginning of the simulation (initial condition), the functions u, v, Θ, n_i, and N_i were specified as given functions of height.

In convective conditions, the turbulent fluxes, i.e., those of momentum, heat, humidity and ions/aerosols, consist of the three components: the local terms, the counter-gradient (non-local) terms which represent the large-eddy contributions, and entrainment terms. The calculations of fluxes were based on the modified K-theory (Sorbjan 2008, 2009a) and its further modifications, not yet published, kindly provided to the author (Sorbjan 2009b, private communication). Equations (1) are solved numerically by three-step Runge-Kutta scheme.

3. Results

The vertical profiles of ions and ion fluxes are calculated under the assumption that the values of fluxes in the surface layer are constant and the initial values of all ions

concentration are zero, and using the adopted aerosol profile. The assumption that the flux is constant enables us to use the Monin-Obukhov theory for calculating the temperature, humidity, ion concentrations at the ground in near-noon hours, during the occurrence of the CBL. The values of ions surface flux for particular types of those ions were determined in so as to be in accordance with the ground ion distributions forced by the external electric field *E*.

The profiles of virtual temperature, humidity, and wind components *u* and *v*, as well as fluxes of momentum, heat and humidity, as obtained from the model simulations, are characteristic for the convective layer (Fig. 1). The profiles are constant with height, and the fluxes are linear in the mixed layer (Sorbjan 2005).

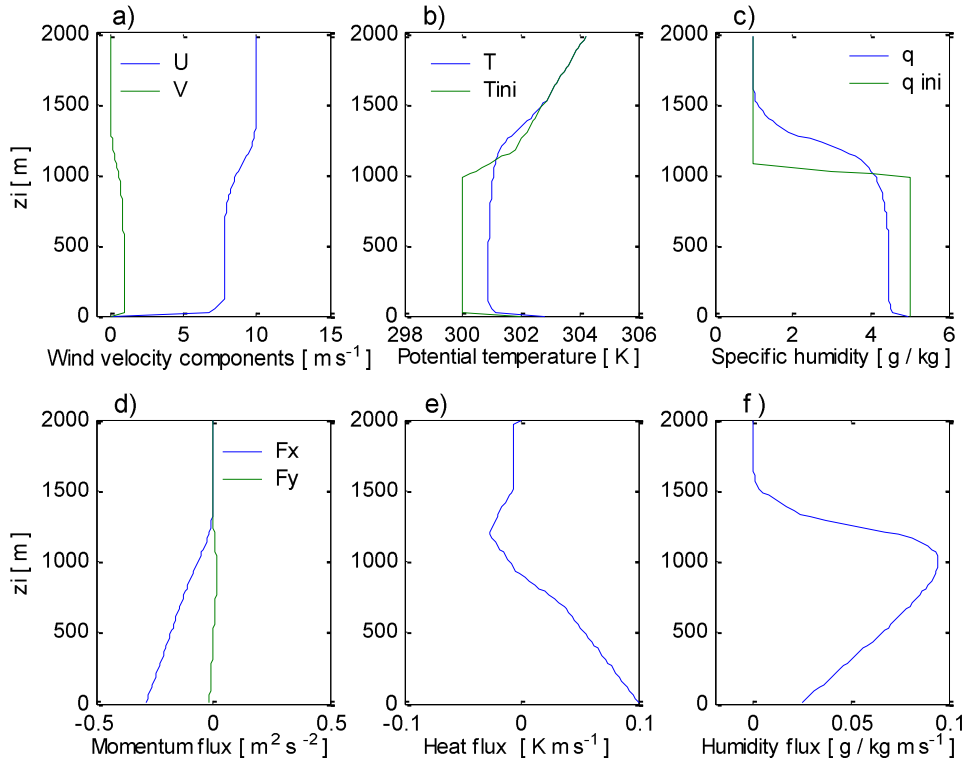

Fig. 1. Profiles of (a) wind velocity components u and v, (b) potential temperature, (c) specific humidity, (d) momentum flux, (e) heat flux, and (f) humidity flux. The parameters: convective velocity scale $w_* = 1.62$ m s^{-1}, geostrophic wind $G = 10$ m s^{-1}, surface heat flux $H_o = 0.1$ K m s^{-1}, mixing height $z_i = 1333$ m, time simulations 2.08 hours. T_{ini}, g_{ini} are the initial conditions of temperature and humidity.

The heat flux varies with depth and is negative in the entrainment layer, owing to the downward heat influx from the free atmosphere. Above the mixed layer, the wind changes into the geostrophic wind.

Figure 2 presents the ion concentration profiles. The profiles have large gradients near the surface, which results from the emission of ions.

In the mixed layer, the concentration of small ions exhibits less variability than that of large ions. This may be related to better mixing of small ions due to the fact that their life-time is much shorter than the turbulent mixing time. The life-times of small and large ions strongly depend on the aerosol concentration, so we can expect to observe changes in the vertical ion profiles resulting from changes in the aerosol concentrations. The resultant electric charge collected on all ions is shown in Fig. 2e. We see a distinct maximum near the Earth's surface. Owing to the bottom-up transport of ions in the mixed layer, its course is nearly linear.

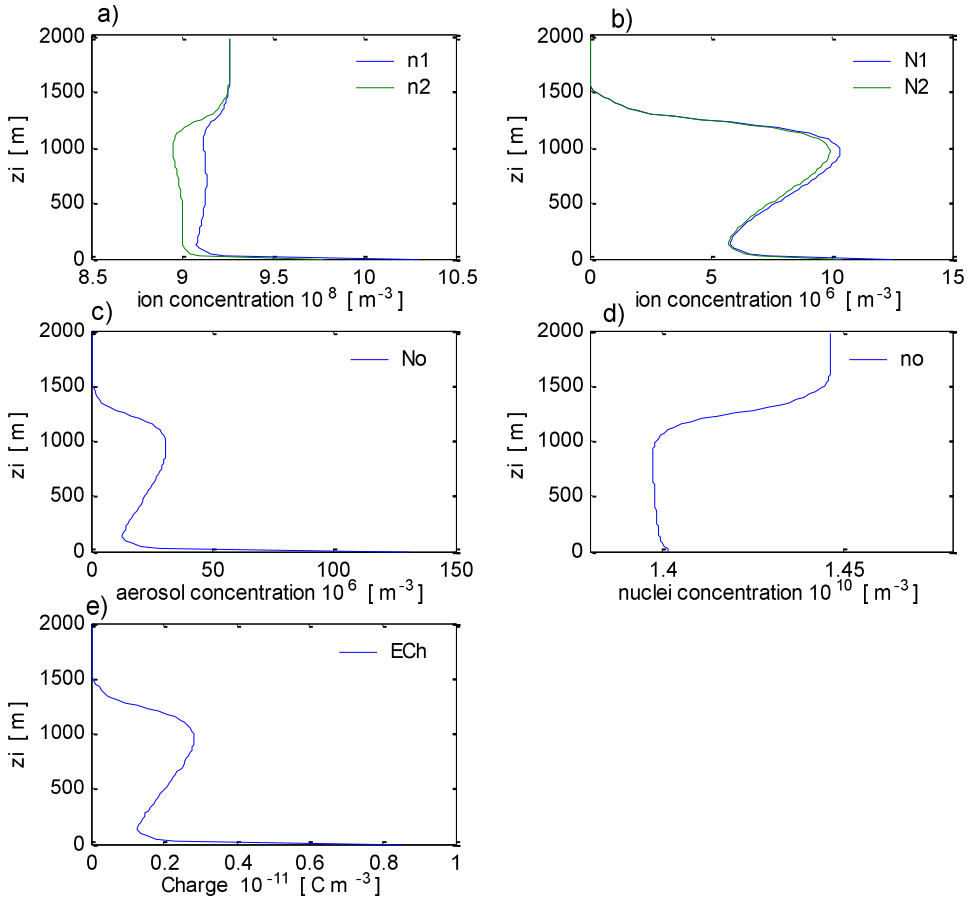

Fig. 2. Vertical profiles of ions concentrations: (a) small positive and small negative ions, (b) large positive and large negative ions, (c) aerosol concentration, (d) nuclei concentration, and (e) electric charge density.

The ion concentration maxima occur near the surface and at the top of the mixed layer. The ion fluxes are shown in Fig. 3. They are not linear and are strongly variable near the surface (Vinuesa 2007). This is a result of conversion of ions in the presence of aerosol. The flux maxima occur at the heights where the concentration gradient is large. Negative values of the large ion fluxes, both positive and negative, at a height of about 500 m, can be related to the deposition process (Ebel 2007).

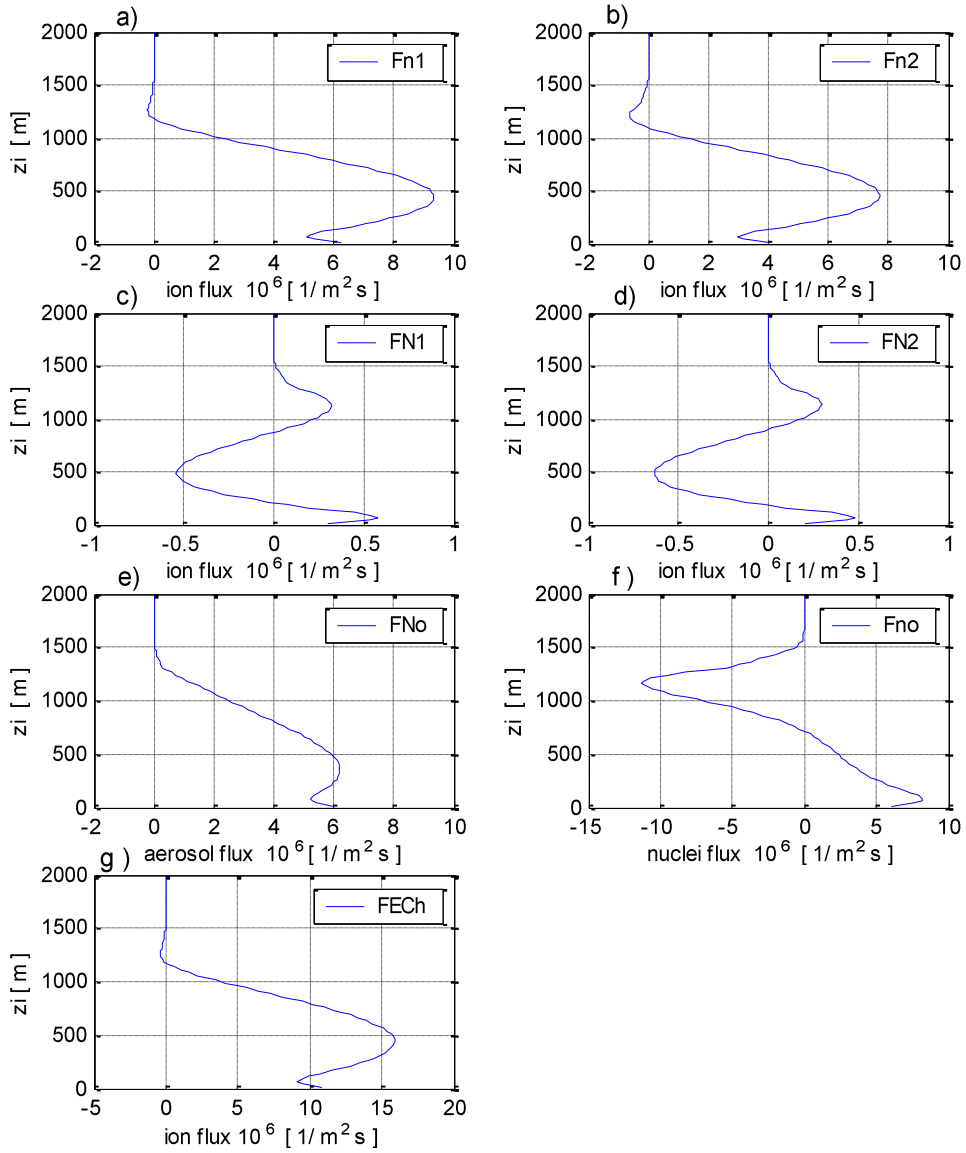

Fig. 3. Vertical profiles of the fluxes of: (a) small positive ions, (b)small negative ions, (c) large positive ions, (d) large negative ions, (e) aerosols, (f) nuclei, and (g) electric charge.

The effect of entrainment layer is also marked in the behavior of fluxes. In the case of small ions, it produces the negative flux, while for large ions the positive flux; this is a result of greater concentration of ions in the free atmosphere as compared to that in the mixed layer. At the same time, the changes of ion concentration in time cause an adequate change in the ion fluxes with height.

In the convective boundary layer, there exists a force related to the vertical mass exchanges; the velocity of this exchange may be by two orders greater than the velocity of ions in the electric field. This gives rise to the convection current. Its density,

J_{cov}, can be described by the relations $J_{cov} = Kd\rho/dz$, where K is the eddy diffusivity, ρ is the space charge (resultant electric charge on all ions), and z is the vertical coordinate. The occurrence of this current affects the budget of electric currents in the surface layer and modifies the vertical profiles of the atmospheric electricity parameters: electric field E and electric conductivity of the air λ. The convection current determined from the model has large fluctuations up to a height of 400 m. The reason may be sought in the physics of the upward ion transport up to a height they attain during their life span. This height will grow with growing aerosol concentration.

4. Conclusions

The model enables us to analyze temporal and spatial changes of ion and aerosol concentrations for quasi-steady state, depending upon the parameters of the CBL. The eddy diffusivity parameter used in the model takes into account the local, non-local, and entrainment factors, rendering it possible to separate these factors in the main ion flux and the electric currents corresponding to them.

The effect of convection and turbulence in the boundary layer on atmospheric electricity parameters may be considerable, as confirmed by preliminary model results. Ions traveling in the electric field are also carried upwards by thermals to reach the top of the mixed layer, and then transported back to the surface by the downdrafts fluxes. This process generates the convective electric current whose value, under certain conditions, can be large as compared to the conduction current $J_{con} = \lambda E$ related to the motion of ions in the field E alone (Markson 1981).

The preliminary results show considerable variations of the ion profiles near the surface, and in the mixed layer (large ions). The ion fluxes are non-linear and have distinct maxima near the surface and in the mixing layer (large ions). This may be the effect of conversion of ions during their fast bottom-up transport, processes in the entrainment layer, and their slower top-down transport.

With this model, it will be also possible to draw conclusions about the magnitude of local effects evoked by the convective layer onto the atmospheric electricity parameters measured near the Earth surface.

The former models have been assuming a linear coefficient K and have not accounted for the large aerosol concentrations and temperature gradient which limited their applicability in case of polar and marine situations. From interpretation of atmospheric electricity parameters E, λ, and J_{con} in surface stations it follows that these are the situations in which the values of convective electric current are expected to be large and difficult to be directly measured, as a function of height in particular.

The model presented here enables us to study and analyze the impact of convective layer on the atmospheric electricity parameters. Further investigations will be focused on the interpretation of these relationships as a function of the mixing height, surface heat flux, geostrophic wind, and aerosol concentration.

Acknowledgements: The author is grateful to Professor Zbigniew Sorbjan from the Institute of Geophysics, Polish Academy of Sciences, for providing his unpublished modifications of the K-theory, and his help.

References

Chalmers, J.A. (1967), *Atmospheric Electricity*, Pergamon Press, pp. 515.

Ebel, A., M. Memmesheimer, H.J. Jakobs (2007), Chemical perturbations in the planetary boundary layer and their relevance for chemistry transport modelling, *Bound.-Layer Meteor*. **125**, 2, 265-278, DOI: 10.1007/s10546-007-9157-x.

Hoppel, W.A., S.G. Gathman (1971), Determination of eddy diffusion coefficients from atmospheric electrical measurements, *J. Geophys. Res*. **76**, 6, 1467-1477, DOI: 10.1029/JC076i006p01467.

Israel, H. (1973), *Atmospheric Electricity*, vol. II, Jerusalem, pp. 796.

Marksom, R., J. Sedlacek, W. Fairall (1981), Turbulent transport of electric charge in the marine atmospheric boundary layer, *J. Geophys. Res*. **86**, C12, 12.115-12.121.

Sorbjan, Z. (2005), Statistics of scalar fields in the atmospheric boundary layer based on large-eddy simulations. Part I: Free convection, *Bound.-Layer Meteor*. **116**, 3, 467-486.

Sorbjan, Z. (2008), Gradient-based similarity in the atmospheric boundary layer, *Acta Geophys*. **56**, 1, 220-233, DOI: 10.2478/s11600-007-0036-0.

Sorbjan, Z. (2009a), Improving non-local parameterization of the convective boundary layer, *Bound.-Layer Meteor*. **130**, 57-69, DOI: 10.1007/s10546-008-9331-9.

Sorbjan, Z. (2009b), Private communication.

Vinuesa, J.F., S. Galmarini (2007), Characterization of the ^{222}Rn family turbulent transport in the convective atmospheric boundary layer, *Atmos. Chem. Phys*. **7**, 697-712.

Willett, J.C. (1979), Fair weather electric charge transfer by convection in an unstable planetary boundary layer, *J. Geophys. Res*. **84**, C2, 703-718, DOI: 10.1029/JC084iC02p00703.

Accepted 10 November 2009

PUBLS. INST. GEOPHYS. POL. ACAD. SC., D-73 (412), 2009

Ground-Level Electric Field and Current Variations in Polar and Mid-Latitude Regions, in Relation to Solar Wind Changes

Extended Abstract[1]

Stanisław MICHNOWSKI[1], Marek KUBICKI[1], Zbigniew KŁOS[2], Natalia KLEIMENOVA[3], Olga KOZYREVA[3], Ninel NIKIFOROVA[3], Sven ISRAELSSON[4]

[1]Institute of Geophysics P.A.Sci., Ks. Janusza 64, 01 452, Warszawa, Poland

[2]Space Research Centre P.A.Sci., Bartycka 18a, 00 715 Warszawa, Poland

[3]Institute of Earth's Physics, R.A.S., Gruzinskaya 10, 123 810 Moscow, Russia

[4]Meteorology Geocentrum, Uppsala University, Villavaegen 16, 752 36 Uppsala, Sweden

Researches on a relationship between the lower atmosphere electricity and solar wind (SW) changes are still meager and delayed in comparison to impressive advances in investigations of the magnetosphere and ionosphere (M-I) dependence on these changes. Remarkable increase of the knowledge on the SW−M-I coupling seems to open new possibilities for a more effective study of the SW effects on the vertical component of electric field (Ez) and electric current (Jz) monitored near the Earth surface. These effects are still not much known and understood in spite of their potential utility in studies of physical processes involved in weather and climate changes in the lower atmosphere. Although some correlations between the SW−M-I and the corresponding atmospheric electricity parameters have been established, on the basis of station observations in the Antarctida, as statistically significant, the number of data on direct physical dependences between them in individual cases is still very scarce. The shortage of systematic atmospheric electricity observations is particularly drastic in the Arctic, despite the fact that at high latitude regions of Northern Hemisphere the modern M-I investigation facilities have been implemented and are in service for a long time.

[1] The full text is prepared for publication

This paper presents the results of investigation of ground-based electric field, Ez, and current, Jz, response to solar wind changes in the Arctic and in middle latitudes on the basis of the recordings at Hornsund (Spitsbergen) and atmospheric electricity observations at Świder (Poland). Individual events were demonstrated in considerable number for selected coincidences with various M-I states and configurations that were actually imposed by solar wind. Also, cases of average and individual daily Ez and Jz variations for fair-weather in coincidence with quiet magnetic conditions were used, mainly for comparison. The electric ground-level recordings were presented on the background of data on corresponding concurrent solar wind and M-I changes obtained by internet from satellite missions, the magnetic station networks, coherent polar radars, riometer nets and other sources. This approach allowed to discern and show some features of the possible polar and middle latitude Ez and Jz responses to characteristic SW−M-I changes. (Few fragments from subtropical Vietnamese-Polish atmospheric electricity recordings at Sa-Pa in Vietnam are supplementarily used, although they were with limited background of geophysical conditions. It is to be noted that long-term continuous recordings at Sa-Pa and Phu-Lien are waiting to be accessible from Vietnamese Institute of Oceanology in Hanoi, Vietnam.)

Various repeatedly occurring solar wind effects on Ez and Jz variations were revealed by their comparison with corresponding ones in undisturbed, fair-weather and magnetically quiet conditions. The Ez variation events were preceded by changes mainly in solar wind, interplanetary magnetic field intensity and in its orientation, in solar wind pressure, solar wind electric field intensity and its orientation, and in solar wind velocity and density. The recorded effects extend previous observations largely, not only in number and diversity of their signatures, but first of all in pointing out their relations to solar wind and corresponding M-I configuration changes. In some examined cases, the solar wind changes might be compared in an extent with the changes in ionosphere potential distribution estimated by the known empirical models, and by conductivity changes in and below the ionosphere, produced by energetic particle precipitation, partly shown by the riometer indications. All these factors affect the Ez values. In the polar region, most of the presented Ez effects were found for the first time during the main and recovery phases of geomagnetic substorms, during sudden enhancement of geomagnetic storms, and even at quiet magnetic conditions. The first-time detected occurrences at mid latitudes of the impressive individual Ez responses to the main phase of magnetic storms are especially remarkable. Their striking large amplitudes, sometimes comparable to the total ground-level values in the global electric circuit, and quite long duration, up to one or two hours, have to be taken into account in extension of present models of the global electric current circuit (GECC) in the lower atmosphere.

The findings gathered in this study show that the ground-level electric measurements are able to bring very interesting data on the lower atmosphere dependence on solar wind changes, most often via magnetosphere-ionosphere effects. On the other hand, they allow to increase significantly our knowledge on global electric current circuit in the lower atmosphere. Since the GECC in the lower atmosphere and the solar wind imposed magnetosphere current circuits are closed by common ionosphere medium, a joint treatment of them is justified, at least in the studies of electrical coupl-

ings of the lower atmosphere with the SW−M-I system. A suggestion of preliminary, very simplified but common model of the global electric current circuit in lower atmosphere and the general model of electric current circuit in the near geospace was put forward.

PUBLS. INST. GEOPHYS. POL. ACAD. SC., D-73 (412), 2009

Bibliography of Stanisław Michnowski's Publications in Chronological Order (1955-2009)

Compiled by Zofia Okrasińska

Michnowski S., 1955. Wpływ wyładowań z ostrzy na wartość natężenia pola elektrycznego przy powierzchni Ziemi [The influence of point discharge currents on the Earth's electric field], Acta Geophys. Pol. 3 (3), 115-130.

Michnowski S., 1955. Główny problem elektryczności atmosferycznej w Międzynarodowym Roku Geofizycznym 1957/1958, Post. Fizyki 8 (5), 567-593.

Michnowski S., 1957. Point discharges in the interchange of electric charge between the Earth and the atmosphere, Acta Geophys. Pol. 5 (2), 123-134.

Michnowski S., Stefanicki K., 1958. Pomiary elementów elektryczności atmosferycznej prowadzone w Cha-Pa. Acta Geophys. Pol. 6 (3), 303-306.

Michnowski S., 1960. Introduction into problems of atmospheric electricity [So Luoc w Nhung von de Dien Khi Quyen] (in Vietnamese).

Michnowski S., 1960. O pomiarach z zakresu elektryczności atmosferycznej prowadzonych w Cha-Pa. [On the atmospheric electricity measurements in Cha-Pa], Biul. Inf. Komitetu Współpracy Geofizycznej 1960, 14-19.

Michnowski S., 1960. Stacja elektryczno-atmosferyczna w Cha-Pa (Wietnam) [The atmospheric electricity station at Cha-Pa (Vietnam)], Acta Geophys. Pol. 8 (2), 164-171.

Michnowski S., 1962. Problematyka badań elektryczności atmosferycznej w strefie polarnej [On the program of research in the field of atmospheric electricity in the polar regions], Biul. Inf. Komitetu Współpracy Geofizycznej 1962, 2 (28), 12-16.

Michnowski S., 1963. Obserwacje wyłądowań piorunowych w chmurze ciepłej [Observations of lightning in warm clouds], Acta Geophys. Pol. 11 (3), 213-217.

Michnowski S., 1963. On the observations of lightning in warm clouds, Ind. Journ. Meteor. Geophys. 14 (3), 320-322.

Michnowski S., Nguyen Manh Duc, 1964. Pomiary zanieczyszczeń promieniotwórczych powietrza i opadów w Cha-Pa w latach 1960-1961 [Measurements of the

radioactive contaminations of the air and rainwater at Cha-Pa in the years 1960-1961], Biul. Inf. Komitetu Współpracy Geofizycznej 3 (38), 23-47.

Michnowski S., 1965. Comments concerning the results of atmospheric electric and radioactive measurements at Cha-Pa, [in:] Problems of Atmospheric and Space Electricity, Elsevier Publishing Company, Amsterdam, 241 pp.

Michnowski S., Nguyen Manh Duc, 1965. On the values and the variations of the atmospheric electric field at Cha-Pa, Mater. Prace Zakł. Geofizyki nr 7, 107-123.

Michnowski S., Nguyen Tac Nhan, 1965. Remarks on preliminary electrical observations of fog and clouds at Cha-Pa, Mater. Prace Zakł. Geofizyki nr 7, 144-152.

Michnowski S., Nguyen Manh Duc, Nguyen Tac Nhan, 1965. The seasonal and short duration variations of fallout at Cha-Pa 1958-1961. Mater. Prace Zakł. Geofizyki nr 7, 125-134.

Michnowski S., 1967. Electric field variations following lightning discharges measured in Warsaw and Świder [Zmiany pola elektrycznego po wyładowaniach atmosferycznych obserwowanych w Warszawie i Świdrze], Acta Geophys. Pol. 15 (4), 315-334.

Michnowski S., 1968. Zmiany pola elektrycznego chmur burzowych w warstwie przyziemnej powietrza w Świdrze i w Warszawie [Electric field variations of thunderclouds in Swider and Warsaw], Mater. Prace Zakł. Geofizyki nr 25, 23-52 (in English and Polish).

Michnowski S, 1969. Comments on monitoring of global thunderstorm activity [in:] Planetary Electrodynamics, Coroniti S.C. and Hughes J. (editors), Gordon and Breach, Science Publishers New York, vol. 2, 17-18.

Michnowski S., 1969. Observations of electric field variations following lightning discharges [Obserwacje zmian pola elektrycznego po wyładowanuach atmosferycznych], Acta Geophys. Pol. 17 (3), 241-252.

Michnowski S., 1969, Some observations of electric field variations following lightning discharges, [in:] Planetary Electrodynamics, Coroniti S.C. and Hughes J. (editors), Gordon and Breach, Science Publishers New York, vol. 2, 51-54.

Nguyen Manh Duc, Michnowski S., 1969. Some results of lightning frequency investigation in Poland during 1966-1967 [Wstępne wyniki badań częstości wyłądowań piorunowych w Polsce w latach 1966-1967], Acta Geophys. Pol. 17 (2), 189-196.

Michnowski S., 1969. Z prac Międzynarodowej Konferencji Elektryczności Atmosferycznej, Tokio 12-18. V. 1968 [The International Conference on Atmospheric Electricity, Tokyo], Przegl. Geofiz. 14 (22), 109-111.

Michnowski S., 1969. Najnowsze osiągnięcia nauki i techniki [Newest Achievements of Science and Technology], R. Colborna (editor), PWN Warszawa, 1969, 676-690.

Michnowski S., 1973. Electric field variations in a medium with variable conductivity, produced by a point charge above a conductive plane [Zmiany pola elektrycznego w ośrodku o zmiennym przewodnictwie w przypadku rozładowywania bieguna położonego ponad płaszczyzną przewodzącą], Acta Geophys. Pol. 21 (4), 306-324.

Michnowski S., 1974. Transient variation of electric field in nonhomogeneous medium, produced by a point charge above a conductive plane, Arch. Meteor. Geophys. Biokl. Ser. A. 23 (3-4), 333-347.

Michnowski S., 1974. Badania zmian pola elektrycznego po wyładowaniach atmosferycznych [An analysis of electric field variation following lightning discharges], Mater. Prace Inst. Geofiz. nr 81, pp. 104.

Michnowski S., 1974. O badaniach elektryczności atmosferycznej w Polsce [On the research of atmospheric electricity in Poland], Przegl. Geofiz. 19 (27), 95-100.

Michnowski S., 1974. Wacław Kowalski 16 III 1915 – 5 VIII 1974 (Obituary), Mater. Prace Inst. Geofiz. nr 83, 97-99.

Michnowski S., 1976. Atmospheric electricity and its application to meteorology [Elektryczność atmosfery i jej zastosowania w meteorologii], Publs. Inst. Geophys. Pol. Acad. Sc. D-1 (99), 3-15.

Michnowski S., 1976. Atmospheric electricity research in the Institute of Geophysics of the Polish Academy of Sciences [Badania elektryczności atmosfery w Instytucie Geofizyki Polskiej Akademii Nauk], Acta Geophys. Pol. 24 (4), 283-287.

Peńsko J., Michnowski S., Warzecha S., Gwiazdowski B., 1976. Pomiary elementów elektrycznych, radioaktywnych i meteorologicznych w Obserwatorium Geofizycznym PAN w Świdrze [Radioactivity, atmospheric electricity and meteorological elements measurements at Swider Geophysical Observatory], Przegl. Geofiz. 21 (29), 281-286.

Michnowski S., Peńsko J., Gwiazdowski B., 1976. Some results on the measurements of radioactive, atmospheric electricity and meteorological parameters at the Geophysical Observatory at Swider [Wstępne wyniki pomiarów radioaktywnych, atmosferyczno-elektrycznych i meteorologicznych prowadzonych w Obserwatorium Geofizycznym w Świdrze], Publs. Inst. Geophys. Pol. Acad. Sc. D-1 (99), 53-63.

Nikiforova N., Michnowski S., 1977. Some geomagnetic and atmospheric-electric variations observed at Świder and Belsk Observatories [in:] Electrical Processes in Atmosphere, Proceedings of the Fifth International Conference at Atmospheric Electricity held at Garmisch-Partenkirchen, Germany, 2-7 September 1974, eds. H. Doleżalek and R. Reiter, Verlag Dr Dietrich Steinkopff, Darmstadt 1977, 728-735.

Berliński J., Gierasimowicz A., Michnowski S., 1978. A new radiosonde for measurements of vertical component of electric field, air-earth current and conductivity, [in:] University of Wyoming, Department of Physics and Astronomy, Report 19778??.

Michnowski S., 1978. On the thundersorm electricity and lightning research in Institute of Geophysics of the Polish Academy of Sciences. Lecture in Cloud Physics Center, University of Missouri, Rolla, August 13, 1978 (preprint pp.5).

Rosen J.M., Hofman D.J., Gringel W., Michnowski S., Morita J., Ogawa T., Olson D., 1980. Balloon borne atmospherical measurements to 33 km. Part I. Small ion mobility, air-earth current density, conductivity, ionization and electric field. [in:] Proceedings of the 6-th International Conference on Atmospheric Electricity held in Manchester, 1980; (preprint pp. 20).

Michnowski S., Warzecha S., Wajdwicz A., 1980. Wpływ rozwiązań materiałowo-konstrukcyjnych na jonizację powietrza pomieszczeń mieszkalnych [Effect of building materials and structures upon air-ionization in flats] [in:] Wpływ Rozwiązań Materiałowo-Konstrukcyjnych w Budownictwie na Zdrowie Człowieka, I Krajowe Sympozjum Naukowe, Warszawa 18-19 listopada 1980 r. Pr. Nauk. Inst. Techn. Budowl. 1980, 35, 173-184.

Korniewicz W., Kowalski J.M., Michnowski S., 1980. Wpływ rozwiązań materiałowo-konstrukcyjnych na zagrożenie zdrowia przez elektryczność statyczną [Effect of building materials and structures upon health hazard from static electricity] [in:] Wpływ Rozwiązań Materiałowo-Konstrukcyjnych w Budownictwie na Zdrowie Człowieka, I Krajowe Sympozjum Naukowe, Warszawa 18-19 listopada 1980 r. Pr. Nauk. Inst. Techn. Budowl. 1980, 35, 186-195.

Berliński J., Michnowski S., 1981. An antenna for electric field and air-earth current measurement in the free atmosphere, [in:] University of Wyoming, Department of Physics and Astronomy, Report AP-67, p.23.

Rosen J.M., Hofmann D.J., Gringel W., Berliński J., Michnowski S., Morita J., Ogawa T., Olson D., 1982. Results of an international workshop on atmospheric electrical measurements., J. Geophys. Res. 87, no C2, 1219-1227.

Michnowski S., Enayatollah M.A., 1983. On the estimation of random error for the LLP System. Publs. Inst. High Volt. Res., Uppsala Univ., 14 pp.

Israelson S., Enayatollah M.A., Pisler E., Michnowski S., Adebokoun I., 1983. On the occurrence of cloud-to-ground flashes in southern Sweden., Publs. Inst. High Volt. Res., Uppsala Univ., 37 pp.

Michnowski S., Corray V., Koszewski I., 1983. On the system of recording of fast and slow electric field variations produced by lightning, Publs. Inst. High Volt. Res., Uppsala Univ.

Michnowski S., Parfiniewicz J., Israelson S., Enayatollah A., Pisler E., 1984. Distribution of to ground lightning discharges and their polarity during thunderstorms observed in Sweden on May 18, 1982. Presented at: VII International Conference on Atmospheric Electricity at Alabama, USA (preprint).

Michnowski S., Israelson S., Parfiniewicz J., Enayatollah A., Pisler E., 1987. A case of thunderstorm system development inferred from lightning distribution. [Analiza mezoskalowego układu burz na podstawie wyładowań atmosferycznych]. Publs. Inst. Geophys. Pol. Acad. Sc. D-26 (198), 3-57.

Astrom E., Michnowski S., 1987. On the applicatiom of the dynamical method for recording of electric fields by a dual field-mill [O stosowaniu metody dynamicznej do rejestracji pól elektrycznych za pomocą podwójnego młynka], Publs. Inst. Geophys. Pol. Acad. Sc. D-26 (198), 181-200.

Warzecha S., Michnowski S., 1987. On the effect of insolation on aerosol and atmospheric ions density at Swider [O wpływie insolacji na koncentrację aerosolu i jonów atmosferycznych w Świdrze], Publs. Inst. Geophys. Pol. Acad. Sc. D-26 (198), 155-180.

Berliński J., Michnowski S., 1987. Partly insulated wire antenna for electric field and air-earth current in the free atmosphere [Częściowo izolowana antena do pomiaru natężenia pola elektrycznego i gęstości prądu pionowego w wolnej atmosferze], Publs. Inst. Geophys. Pol. Acad. Sc. D-26 (198), 215-238.

Barański P., Michnowski S., 1987. Variations of the electric field and precipitation measured under thunderclouds in Warsaw [Zmiany pola elektrycznego mierzone pod chmurami burzowymi w Warszawie], Publs. Inst. Geophys. Pol. Acad. Sc. D-26 (198), 59-74.

Barański P., Michnowski S., 1988. Estimation of the field-dependent currents from the electric field variation following lightning discharges [in:] Proceedings of the 8th International Conference on Atmospheric Electricity, June 13-16, 1988. Uppsala, Sweden, Inst. High Volt. Research Uppsala Univ., 1988, 833-840.

Nikiforova N.N., Michnowski S., Marianiuk J., 1987. Sopostavlenie variatsii geomagnitnogo i atmosferno-elektricheskikh poley po materialam Observatorii Świder i Belsk [in:] Estestvennoye Elektromagnitnoe Pole Ziemli, Izd. Nauka, Moskva, 88-97.

Michnowski S., Warzecha S., Israelsson S., 1989. Variations of atmospheric ion concentrations and conductivity related to air pollution and radioactive debrises [in:] 14th General Assembly of the European Geophysical Society, Barcelona, Spain, March 12-19, 1989.

Michnowski S., Szymański A., Nikiforova N.N., Kozyreva O.V., Ermolenko D.Yu., 1991. Analysis of synchronous geomagnetic and atmospheric electric field observations at Polish Station Hornsund, Spitsbergen [in:] XX Assembly IUGG, Vienna, 11-24 August 1991, IASPEI, Program and Abstracts, p. 266.

Michnowski S., 1991. Concluding remarks on the Mądralin Workshop. Publs. Inst. Geophys. Pol. Acad. Sc. D-35 (238), 249-256.

Michnowski S., Szymański A., Nikiforova N.N., Kozyreva O.V., Ermolenko D., Zielkowski K., 1991. On simultaneous observations of geomagnetic and atmospheric-

electric field changes at Arctic Station, Hornsund, Spitsbergen [in:] Proceedings of the International Workshop on Global Atmospheric Electricity Measurements, Mądralin, Poland, 10-16 September 1989, Publs. Inst. Geophys. Pol. Acad. Sc. D-35 (238), 83-95.

Barański P., Michnowski S., 1992. The field-dependent currents derived from electric field variation following lightning discharges observed at the earth surface. Acta Geophys. Pol., 39 (3), 335-348.

Kleimonova N.G., Kozyreva O.V., Michnowski S., Szymański A., Ermolenko D.Yu., 1992. Vysokoshirotnye dlinnoperiodnye pulsatsii v geomagnitnom pole i atmosfernom elektrichestve po nablyudenii na Arch. Shpitsbergen., Geom. Aeron. 32 (2), 41-48.

Kleimonova N.G., Michnowski S., Nikiforowa N.N., Kozyreva O.V., 1995. Dlinnoperiodnye pulsacii i fluktuacii napriazennosti elektricheskogo pola atmosfery na szirotach poliarnego kapsa, Geom. Aeron., 35, 4, 38-48.

Michnowski S., 1996. O zastosowaniu obserwacji atmosferyczno-elektrycznych w Hornsundzie w badaniach oddziaływań wiatru słonecznego na atmosferę ziemską [Atmospheric-electric and geomagnetic observations at Hornsund in the studies of solar wind effects on the atmosphere], Przegl. Geofiz., 41, 1-2, 1-2.

Michnowski S., 1996. Potrzeby udziału Polskiej Stacji Polarnej Hornsund w badaniach relacji Słońce-Ziemia na tle dotychczasowych prac i planów w tym zakresie [On possibile participation of Polish Polar Station Hornsund in Sun-Earth relations research], Przegl. Geofiz. 41, 1-2, 7-10.

Michnowski S., 1996. Remarks on observations of the solar wind influences on the electric field at the earth's surface in Polar Regions, [in:] Proceedings of the 10th International Conference on Atmospheric Electricity, June 10-14, Osaka, Japan 1996, 516-519.

Michnowski S., Nikiforova N.N., 1996. Długookresowe fluktuacje pola geomagnetycznego i atmosferycznego pola elektrycznego podczas subburz i innych zaburzeń magnetycznych w Hornsundzie [Long-period fluctuations of geomagnetic and atmospheric-electric field at Hornsund during substorms and other magnetic disturbances], Przegl. Geofiz. 41, 1-2, 57-65.

Michnowski S., Nikiforova N.N., Kleimenova N.G., 1996. The response of ground atmospheric-electric field at Hornsund to magnetospheric-ionospheric events, [in:] Proceedings of the 10th International Conference on Atmospheric Electricity, June 10-14, Osaka, Japan 1996, 520-523.

Michnowski S., 1996, On the observation of the solar wind influence on the electric field and current measured at the earth's surface in the high latitude regions [in:] Seminars in Atmospheric Electricity, Institute of High Voltage Research, Uppsala University, November 6, 1996.

Kleimenova N.G., Michnowski S., Nikiforova N.N., Kozyreva O.V., 1998. Variatsii vertikalnoy sostavlayushchey atmosfernogo elektricheskogo pola v viechernom sektore polarnykh shirot (Obs. Hornsund), Geomagn. Aeronomy 38 (6), 149-156.

Michnowski S., 1998. Solar wind influences on atmospheric electricity variables in polar regions, J. Geophys. Res. 103, D12, p. 13,939-13,948.

Michnowski S., Barański P., 1998. In memory of Andrzej Łosakiewicz, Newslett. Atmos. Electr. 9, 1, p. 1.

Michnowski S., Barański P., 1998. Research activity by Institute of Geophysics, Polish Academy of Sciences, (Warsaw, Poland), Newslett. Atmos. Electr., 9, 1, p. 5.

Michnowski S., 1999. Obituary Reinhold Reiter (1920-1998), Bull. Am. Meteor. Soc. 80, 9, 1927-1931.

Michnowski S., Barański P., 1999. Research activity by Laboratory of Atmospheric Electricity in Institute of Geophysics, Polish Academy of Sciences (Warsaw, Poland), Newslett. Atmos. Electr., 10, 1, 13-14.

Michnowski S., Barański P., 2000. Research activity by atmospheric electricity group at the Institute of Geophysics, Polish Academy of Sciences (Warsaw, Poland), Newslett. Atmos. Electr., 11, 2, p. 18.

Nikiforova N.N., Kleimenova N.G., Kozyreva O.V., Michnowski S., Kubicki M., 2000. Atmospheric electric field variations in polar cap as a response to substorm ionosphere disturbances, [in:] International Conference on Problems of Geophysics (poster).

Barański P., Kubicki M., Michnowski S., 2002. Research activity of the atmospheric electricity research group at the Institute of Geophysics Polish Academy of Sciences, Newslett. Atmos. Electr., 13, 2, 21-22.

Kobyliński Z., Michnowski S., 2002. On correlations of tropospheric dynamics with solar activity during a presence of volcanic aerosols in stratosphere, [in:] EGS XXVII General Assembly, Nice, France, Geophys. Res. Abstr., 4 (CD-ROM), p. EGS02-A-02541.

Nikiforova N.N., Kleimenova N.G., Kozyreva O.V., Kubicki M., Michnowski S., 2002. Polar cap atmospheric electric field response to the sudden commencement of the Bastille day magnetic storm, [in:] Book of Abstracts - International Conference on Problems of Geocosmos, St. Petersburg State University, St. Petersburg, Russia, p. 58.

Barański P., Kubicki M., Michnowski S., 2003. Research activity of the atmospheric electricity group at the Institute of Geophysics, PAS, Newslett. Atmos. Electr., 14 (2), 13-14.

Kobyliński Z., Michnowski S., 2003. On the atmospheric response to solar cosmic ray events, [in:] Proc. 12-th ICAE Conference, 9-13 June 2003, Versailles, France, 1, 381-382.

Kubicki M., Michnowski S., Mysłek-Laurikainen B., Warzecha S., 2003. Long term variations of some atmospheric electricity, aerosol, and extraterrestrial parameters at świder Observatory, [in:] Proc. 12-th ICAE Conference, 9-13 June 2003, Versailles, France, 1, 291-294.

Michnowski S., Kubicki M., Drzewiecki J., Israelsson S., Kleimenova N., Nikiforova N., Kozyreva O., 2003. Variations of atmospheric electricity elements in polar regions related to the solar wind changes, [in:] Proc. 12-th ICAE Conference, 9-13 June 2003, Versailles, France, 1, 295-296.

Nikiforova N., Kleimenova N., Kozyreva O., Kubicki M., Michnowski S., 2003. Influence of high energy electrons on global electric network (in Russian), [in:] V Russian Conference on Atmospheric Electricity, 21-26 September 2003, Vladimir, Russia, Sbornik nauchnykh trudov, vol. 1, p. 35.

Nikiforova N., Kubicki M., Michnowski S., 2003. Analysis of relations between changes of magnetic and electric fields of the Earth basing on data from Świder Observatory and Polar Station Hornsund (in Russian), [in:] I Russian School of Electromagnetic Sounding of the Earth, 10-15 November 2003, Moskva, MAKS Press, p. 19.

Nikiforova N.N., Kleimonova N.G., Kozyreva O.V., Kubicki M., Michnowski S., 2003. Influence of auroral-latitude precipitation of energetic electrons on variations in the atmospheric electric field at polar latitudes (Spitsbergen Archipelago), Geom. Aeron., 43 (1), 29-35.

Barański P., Kubicki M., Michnowski S., 2004. Research activity by atmospheric electricity group at the Institute of Geophysics, Polish Academy of Sciences (Warsaw, Poland), Newslett. Atmos. Electr., 15 (2), 19-20.

Nikiforova N., Kozyreva O.V., Kleimenova N., Kubicki M., Michnowski S., 2004. Mid-latitude atmosphere electric field (*Ez*) variations during main phase of the 30 October magnetic storm, [in:] International Symposium on Solar Extreme Events of 2003, July 12-14, 2004. Moscow, Russia, Moscow State University, Programme and Abstract Book, poster C16, p. 54.

Nikiforova N., Kubicki M., Michnowski S., 2004. Influence of the magnetospheric-ionospheric generators on the atmospheric electricity of high latitudes, [in:] Book of Abstracts 5th International Conference “Problems of Geocosmos”, May 24-28, 2004, St. Petersburg, Russia, 259-261.

Nikiforova N.N., Kleimenova N.G., Kozyreva O.V., Kubicki M., Michnowski S., 2005. Unusual variations in the atmospheric electric field during the main phase of the strong magnetic storm of October 30, 2003, at Świder Polish midlatitude Observatory, Geom. Aeron., 45 (1), 140-144.

Barański P., Kubicki M., Michnowski S., 2005. Research activity by atmospheric electricity group at the Institute of Geophysics, Polish Academy of Sciences (Warsaw, Poland), Newsletter Atm. Electr., 16 (2), p. 17.

Michnowski S., 2005. Nguyen Manh Duc (1935-2004) – In Memoriam, Publs. Inst. Geophys. Pol. Acad. Sc., D-68 (383), 73-76.

Nikiforowa N.N., Kubicki M., Michnowski S., 2006. The research on atmospheric electric field anomaly as an index for short-impending prediction of earthquakes, [in:] The 6-th International Conference on Problems of Geocosmos, St. Petersburg, 23-27 May 2006, 131-132.

Kozyreva O.V., Nikiforowa N.N., Kleimenova N.G., Kubicki M., Michnowski S., 2006. Case study on the pulsations in the atmospheric electric current and polar cap substorms, [in:] The 6-th International Conference on Problems of Geocosmos, St. Petersburg, 23-27 May 2006, 226-227.

Kleimenova N.G., Kozyreva O.V., Nikiforowa N.N., Michnowski S., Kubicki M., 2006. Atmospheric electric field variations at polar latitudes (obs. Hornsund, Spitsbergen), [in:] The 3rd International Conference Geophysical Research in Spitsbergen Archipelago, Murmansk-Barensburg, 03-05 October, 11-18.

Barański P., Kubicki M., Michnowski S., 2006. Research activity by atmospheric electricity group at the Institute of Geophysics, Polish Academy of Sciences (Warsaw Poland), Newslett. Atmos. Electr., 17, No. 2, 8-9 (13).

Nikiforova N.N., Teisseyre K.P., Michnowski S., Kubicki M., 2007. On atmospheric electricity field anomaly before the Carpathian earthquake of 30.08.1986 at the Polish Observatory Świder, [in:] 13 Conference on Atmospheric Electricity, Beijing, China, I, 37-40.

Kubicki M., Michnowski S., Mysłek-Laurikainen B., 2007. Seasonal and daily variations of atmospheric electricity parameters registered at the Geophysical Observatory at Świder (Poland) during 1965-2000, [in:] 13 Conference on Atmospheric Electricity, Beijing, China, I, 50-54.

Nieckarz Z., Kułak A., Kubicki M., Michnowski S., Barański P., 2007. Calculating global storm activity rate on the basis of Schumann resonance background component, [in:] 13 Conference on Atmospheric Electricity, Beijing, China, I, 72-76.

Michnowski S., Kubicki M., Kleimenova N., Nikiforova N., Kozyreva O., Israelsson S., 2007. The polar ground-level electric field and current variations in relation to solar wind changes, [in:] 13 Conference on Atmospheric Electricity, Beijing, China, I, 9-12

Kozyreva O., Nikiforova N., Kleimenova N., Michnowski S., Kubicki M., 2007. Electric air-earth vertical current pulsations at Hornsund during polar substorms. Case studies, [in:] 13 Conference on Atmospheric Electricity, Beijing, China, I, 29-33.

Barański P., Michnowski S., Masłowski G., Gajda W., 2007. Signatures of electric field changes associated with the continuing current stage of cloud-to-ground flashes, [in:] 13 Conference on Atmospheric Electricity, Beijing, China, I, (poster).

Nieckarz Z., Kułak A., Kubicki M., Michnowski S., Barański P., 2007. Calculating global storm activity rate on the basis of Schumann resonance background component, [in:] 13 Conference on Atmospheric Electricity, Beijing, China, I, 491-492.

Masłowski G., Barański P., Michnowski S., 2007. Analysis of electric field spectrograms of lightning discharge components, [in:] Abstracts of 2-nd International Symposium on Lightning Physics and Effects, Vienna, Austria, p. 41.

Barański P., Kubicki M., Michnowski S., 2007. Research activity by atmospheric electricity group at the Institute of Geophysics, Polish Academy of Sciences (Warsaw, Poland), Newslett. Atmos. Electr., 18 (2), 21-22.

Kleimenova N.G., Kozyreva O.V., Michnowski S., Kubicki M., 2008. Effect of magnetic storms in the atmospheric electric field at midlatitudes, Geomagn. Aeronomy 48 (5), 622-630.

Nieckarz Z., Kułak A., Zięba S., Kubicki M., Michnowski S., Barański P., 2009. Comparison of global storm activity rate from Schumann resonance background components to electric field intensity *Ez*, Atmos. Res., doi: 10.1016/j.atmos.2008.06.006.

Kleimenova N.G., Kozyreva O., Kubicki M., Michnowski S., 2009. Variations of the mid-latitude atmospheric electric field (*Ez*) associated with geomagnetic disturbances and Forbush decreases of cosmic rays, Publs. Inst. Geophys. Pol. Acad. Sc., D-73 (412).

Michnowski S., Kubicki M., Kłos Z., Kleimenova N., Kozyreva O., Nikiforova N., Israelsson S., 2009, Ground-Level Electric Field and Current Variations in Polar and Mid-Latitude Regions, in Relation to Solar Wind Changes (Extended Abstract), Publs. Inst. Geophys. Pol. Acad. Sc., D-73 (412).